2006

Green Organic Solar Cells from a Water Soluble Polymer and Nancrystalline TiO2

Qiquan Qiao
Virginia Commonwealth University

GREEN ORGANIC SOLAR CELLS FROM A WATER SOLUBLE POLYMER AND

NANOCRYSTALLINE TiO_2

A disseration submitted in partial fulfillment of the requirements for the degree of Doctor of Philosophy in Engineering at Virginia Commonwealth University.

by

QIQUAN QIAO

Master in Optics, Shanghai Institute of Optics and Fine Mechanics, China, 2003
Bachelor in Engineering, Hefei University of Technology, China, 1999

Director: JAMES T. MCLESKEY, JR.
PH.D. DEPARTMENT OF MECHANICAL ENGINEERING

Virginia Commonwealth University
Richmond, Virginia
December 2006

Acknowledgement

I would like to thank my advisor, Dr. James T. McLeskey, Jr. for his help and advice during the last three years. I could not have asked for a better advisor. His generous support makes it possible for me to spend most of my time in the research on organic photovoltaics. Dr. McLeskey has provided all of the benefits not only about research but also general life including offering research facilities, inspiring me to do the original work, sending me to conferences, sharpening my presentation skills, providing me the chances to teach, helping me to improve my teaching, encouraging me to apply for awards, preparing me for future career, and teaching me the living styles in US. Dr. McLeskey served as a model for a perfect advisor.

I am very grateful to Dr. Kenneth J. Wynne in Department of Chemical Engineering at VCU and Dr. My T. Nguyen from American Dye Source, Inc. for the valuable discussions regarding the redshift in absorption spectra for the lower molecular weight PTEBS. The authors also would like to thank Dr. Hadis Morkoç, Dr. Ümit Özgür and Yi Fu from Microelectronics Materials & Device Laboratory (MMDL) in Electrical and Computer Engineering at VCU for the assistantance with the PL and the SEM. The authors also thank Dr. Fred M. Hawkridge in Chemistry Department at VCU for his help with the cyclic voltammogram measurement.

I want to thank Dr. Hadis Morkoç, Dr. Randy Heflin, Dr. Gregory Tait and Dr. Gary Tepper to serve as the members on my Ph.D. examining committee for their suggestions and discussions on this thesis.

I want to thank my labmates for the time we spent together. Srirupa Ganguly, Justinian Koca, Eddie McCumiskey, Ian Mohlie, James Beck, Jake Pretko, Ryan Lumpkin, William C. Kerr, Jr., Eric Corrigan, and Mike Aust have to be mentioned here.

I would like to thank my parents, sisters and brothers for their love, help, support, encouragement and financial support for me to study at VCU.

Especially, I want to thank my wife, Jia You, for her love and support in the final stage of my Ph.D. study.

Table of Contents

List of Figures

List of Tables

Abstract

GREEN ORGANIC SOLAR CELLS FROM A WATER SOLUBLE POLYMER AND NANOCRYSTALLINE TiO_2

By Qiquan Qiao, Ph.D.

A dissertation submitted in partial fulfillment of the requirements for the degree of Doctor of Philosophy in Engineering at Virginia Commonwealth University.

Virginia Commonwealth University, 2006

Major Director: James T. McLeskey, Jr.
Ph.D. Department of Mechanical Engineering

The cost of the present generation of inorganic silicon solar cells is very high and further breakthroughs in cost and efficiency using traditional materials are becoming less and less likely after over 50 years of development. Next generation organic solar cells offer a solution to the limitations of silicon through the vision of low-cost, liquid-based, large area fabrication technology based on polymer and nanomaterials at room temperature. However, most polymers used in solar cells are dissolved in organic solvents such as xylene, toluene, chloroform, and chlorobenzene. Such solvents are

harmful to people and environments, leading to higher costs due to complicated waste disposal processing. This is in conflict with the low cost, green, and renewable energy for which we are aiming. To realize a green organic solar cell, a novel solar cell has been created using an environmentally friendly water-soluble thiophene polymer [(Sodium poly[2-(3-thienyl)-ethoxy-4-butylsulfonate])] (PTEBS) and nanocrystalline TiO_2. This novel system has shown great potential in photovoltaics the work has garnered the attention of the international community.

In our innovative solar cells, the water-soluble polythiophene (PTEBS) is used as electron donor. Nanoparticle TiO_2 acts as electron acceptor. PTEBS/TiO_2 solar cells with various structures including bilayer heterojunctions, bulk heterojunctions and a hybrid of bilayer and bulk heterojunctions have been developed and explored. These results are comparable to the best polymer/metal-oxide solar cells reported by other groups using organic solvents.

In summary, this is the first time that green solar cells have been fabricated from environmentally friendly water-soluble polymers. By using water as the solvent and utilizing liquid-based processing, the cost of the energy generated by this type of solar cell will be further lowered. In addition, the flexible polymer offers the ease of fabrication and integration into different devices.

Chapter 1 Introduction and Outline

1.1 Introduction and motivation

The development of renewable clean energy sources is very important to meet the future energy needs of the world. Currently, eighty-seven percent of energy is produced from traditional non-renewable resources including coal, nuclear, oil and gas, etc.[1] However, these sources are limited and will be depleted. In addition, the process of power generation often produces pollution in the environment.

Solar energy is a promising alternative for the fossil fuel energy currently widely used. Photovoltaics have attracted much attention and are being investigated extensively. Presently, three kinds of photovoltaic devices have been developed: silicon solar cells, solar cells based on thin film polycrystalline semiconductor materials ($CuInSe_2$, CIGS and CdTe), and organic solar cells made from conjugated polymers, small molecules, dyes and inorganic-organic hybrids. Silicon solar cells cannot generate energy at low cost due to the high temperature fabrication process and large amounts of pure (costly) semiconductor silicon[2]. Thin film solar cells are also expensive because of high temperature processing.

Since polyacetylene was reported in 1977[3], conjugated polymers with alternating single and double bonds have been explored widely in photovoltaics[4], light-emitting diodes[5], photodetectors[6], transistors[7], and sensors[8]. Polymer photovoltaic devices have recently attracted much attention and have shown great promise in the ongoing effort to lower the cost of solar cells. Conjugated polymers are typically used as donor materials in organic solar cells. These polymer materials are

usually soluble in common solvents. This leads to the possibility of making large area thin film solar cells using inexpensive liquid based processing techniques such as spin coating[9], doctor blading, ink jet printing, screen printing[10] and reel-to-reel processing[11]. Often, the band gap and ionization potential can be tuned to the desired energies by modifying the chemical structure[12] and solar cells made from polymers are commonly lightweight and flexible.

However, photo-generated excitons are strongly bound and resist dissociation into separate charges in polymers. Furthermore, these materials suffer from low charge mobility and short exciton diffusion length[13]. Therefore, the performance of the solar cells made from homogenous polymer layers has been limited. This problem has been resolved in part by building bilayer and bulk heterojunction structures with phase separation between the polymer and certain inorganic nano-particles such as TiO_2[14-18] and CdSe[19].

Solvent-based polymers such as poly(2-methoxy-5-(2-ethyl-hexyloxy)-*p*-phenylenevinylene) [MEH-PPV][20], poly(3-hexylthiophene) [P3HT][21], poly(3-octylthiophene) [P3OT][17], and poly(2-methoxy-5-(3,7-dimethyl-octyloxy)-*p*-phenylenevinylene) [MDMO-PPV][22] have been reported as electron donors in the TiO_2 based solar cells. The solvents typically used include toluene, chloroform, chlorobenzene, Tetrahydrofuran (THF), xylene, and dichloromethane. Such solvents are harmful to people and environments, leading to the high cost, complicated waste disposal processing. The use of such organic solvents is in conflict with the prospect of developing a clean low cost energy source.

1.2 Objectives

The primary objective of this investigation is to determine whether solar cells made using water-soluble polymers can achieve efficiencies equal to or even better than those made with conventional polymers without the negative environmental consequences. No one has previously studied the use of environmentally friendly water-soluble polymers in organic solar cells. In this work, a water-soluble thiophene polymer, sodium poly[2-(3-thienyl)-ethoxy-4-butylsulfonate] [PTEBSNa], was used to build photovoltaics by incorporating nanoparticles to create heterojunctions with high interfacial areas. The devices have achieved efficiencies similar to corresponding devices from conventional polymer as well as remarkably high fill factors.

The water solubility is also compatible with a number of distinctive processing techniques that allows the fabrication of unique device structures that offer the potential for even higher efficiencies and a secondary objective was to investigate some possible new structures. Devices were first fabricated in a bilayer configuration and a significant photovoltaic effect was observed. Afterwards, devices in bulk heterojunction and a hybrid of bilayer and bulk heterojunction configurations were also fabricated and improved results were achieved.

Many properties of the subject polymer are reported (including the tunability of the absorption spectrum). By taking advantage of the processibility and tunabilty of the polymer, there is the potential for achieving even higher efficiencies in the future. Finally, it is shown that the characteristics of the devices can be analyzed using standard device models.

1.3 Outline

Chapter 2 gives a description of the background of organic solar cells and a review of literature. Information on solar radiation and air mass are introduced. A basic explanation of the characteristics of organic solar cells is then reviewed. Electrical and optical properties of semiconducting conjugated polymers are described and the chemical structures of a few widely used polymers are explained. The device architectures and the principles of operation are discussed in detail for the following three structures: metal-insulator-metal, bilayer, and composite. Finally, several techniques used to fabricate organic solar cells are presented.

In Chapter 3, the material characteristics of PTEBS, TiO_2 and the electrodes are described. The self-doping and dedoping mechanisms of PTEBS are given. Its optical properties such as the absorption and photoluminescence spectra are presented. In addition, LUMO and HOMO levels are determined from cyclic voltammetry experiments. TiO_2 nanocrystalline films are also characterized by UV-Vis, XRD and Scanning Electron Micrograghs (SEM). A brief introduction of the typical electrodes is also given.

Chapter 4 and 5 present the results from bilayer structure devices and the optimization of these devices by altering the TiO_2 thickness is considered. An optimum thickness is given from the experimental research. An efficiency of 0.15% has been achieved. It is shown that this is comparable to similar devices made using solvent-based polymers.

In chapter 6, the characteristics of a PTEBS:TiO_2 composite and its application to solar cells is described. It is observed that the UV-visible absorption spectrum of low

molecular weight PTEBS is redshifted possibly due to the formation of aggregates. The photoluminescence (PL) quenching indicates that the exciton dissociation and charge separation occurs successfully at the PTEBS:TiO_2 (1:1 by weight) interface. This enhances the possibility that the separated charges will reach the electrodes before recombining. SEM images show how the PTEBS and TiO_2 are interconnected and form paths to the electrodes to improve charge transport. One of the reasons for the low efficiencies of the devices is that the water solution of PTEBS is not viscous enough to form a homogeneous film on a smooth FTO substrate.

Chapter 7 shows a new structure with a hybrid of bilayer and heterojunction. A neat layer of TiO_2 is deposited as a buffer layer between FTO and the blended film. The buffer layer provides a rough surface, which helps to form a uniform film and also acts as a hole blocking layer. An external energy conversion efficiency of 0.17% is achieved. Chapter 8 describes the analytical work done to explain the open circuit voltage and the high fill factor. Chapter 9 concludes with a summary of this work. In addition, future research is suggested for the water-soluble polymer solar cells.

Chapter 2 Background and Literature review

2.1 Solar radiation and air mass

The sun generates a wide spectrum of wavelengths from gamma rays to radio waves with the peak around 500 nm. The percentages of the ultraviolet, visible and infrared solar radiation are shown in Table 1[23]:

Table 1. The energy distribution in different wavelength bands.

Ultraviolet (< 380 nm)	Visible (380 ~ 780 nm)	Infrared (>780 nm)
7%	47%	46%

The solar radiation from the sun is attenuated in several ways. Some of the light is reflected back to space by the clouds. During its passage through the atmosphere, the infrared part of the solar spectrum is largely absorbed or scattered by carbon dioxide, water vapor, and dust. For the ultraviolet region of sunlight, ozone absorption and Raleigh scattering are the main reasons for attenuation. The absorption and scattering is shown in detail in Table 2. After being scattered or absorbed on a clear day, roughly 75% of the extraterrestrial vertical radiation reaches the earth surface (shown in Table 2).

Table 2. Absorption and scattering of direct vertical radiation under typical clear sky conditions[23]:

Absorption and scattering under typical clear sky conditions			
Factor	Percent absorbed	Percent scattered	Percent of total passing through the atmosphere
Ozone	2%	0%	
Water vapor	8%	4%	
Dry air	2%	7%	
Upper dust	2%	3%	
Lower dust	0%	0%	
Total absorbed or scattered	14%	14%	75%

Air mass (AM), also known as optical air mass, is a measure of the length of the atmospheric path to the solar converter through which the sunlight passes. The solar radiation outside the atmosphere is called AM0 (1365 W/m^2). When the sun is directly overhead with a vertical line normal to the Earth's surface (zenith), the sunlight goes through a minimum distance to the surface and the radiation is designated by AM 1. An actual AM value is defined as:

$$AM(number) = \frac{1}{\cos\theta}$$

where θ is the angle measured with the reference to the zenith line. A typical radiation spectrum on the surface is AM 1.5 (θ=48°) and is shown in Figure 1. This value is used as a standard spectrum for solar cell efficiency measurements. The AM 1.5 and its angle is showed in Figure 2. Part of the scattered sunlight reaching back to the surface of the Earth and added to the direct irradiance is called diffuse radiation. A range of 800 - 1000 W/m^2 radiation from solar simulators with AM 1.5 filters is used in solar cell research.

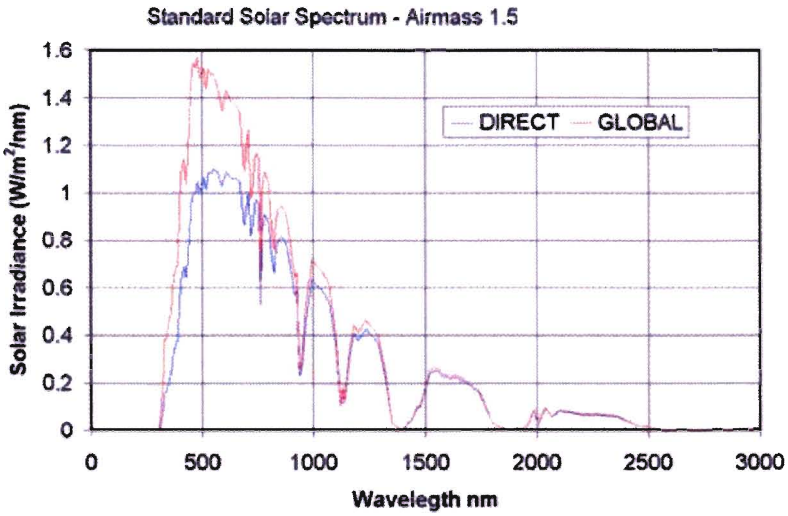

Figure 1 The solar radiation spectrum of AM 1.5 direct (lower curve) and AM 1.5 global (upper curve). The global AM 1.5 is the sum of direct and the diffuse radiation[23].

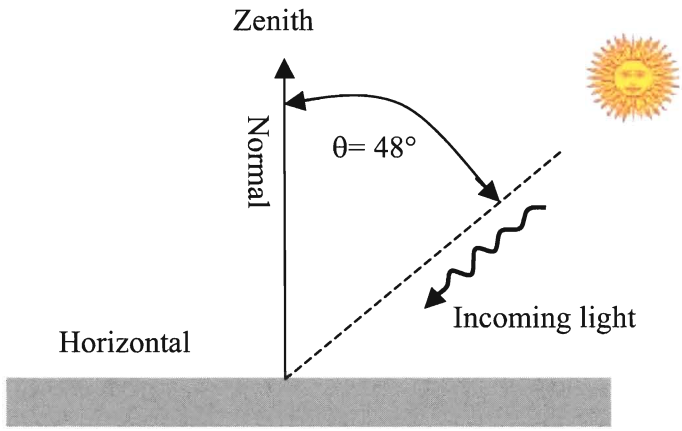

Figure 2 The geometry that defines the standard for the terrestrial solar radiation at AM 1.5.

2.2 Characteristics of solar cells

Solar cells are photodiodes and are generally characterized using current density – voltage (J-V) curves. A typical J-V curve is shown in Figure 3. The parameters of the devices such as short circuit current density (J_{SC}), open circuit voltage (V_{OC}), fill factor (FF) and power conversion efficiency (η) are all derived from Figure 3.

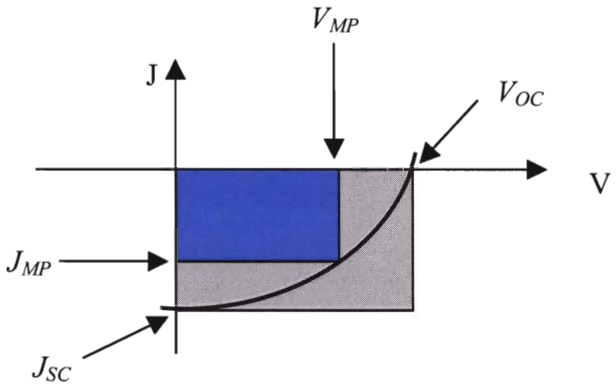

Figure 3 Current density–voltage characteristics of solar cells under illumination.

2.2.1 Open circuit voltage and short circuit current

The short circuit current density (J_{SC}) and the open circuit voltage (V_{OC}) are the maximum current and voltage the devices can generate under the white light illumination, which can be measured using a multimeter. The J_{SC} is the current produced when the device is connected to a load with zero resistance. The V_{OC} is the voltage produced when the device is connected to a load with infinite resistance. When no external voltage is applied to the solar cells, the built-in potential forces the photogenerated charges to drift and produce the short circuit current[24]. In addition, it is known that the short circuit

current can be compensated to zero if a voltage equal to open circuit voltage is applied[24]. Therefore, the intersection of the J-V curve and the y-axis is regarded as J_{SC} and the meeting point of the curve and x-axis is referred as V_{OC}.

2.2.2 Fill factor

The fill factor represents a measure of the quality of the J-V characteristic and is given by the ratio between the maximum electrical power generated and the product of J_{SC} and V_{OC}, a ratio of dark shaped area to light shaped area (Figure 2), which is defined as[25]:

$$FF = \frac{J_{MP}V_{MP}}{J_{SC}V_{OC}}$$

where J_{MP} and V_{MP} are the current density and voltage when the power is the highest. Higher fill factors mean that more electric power can be extracted at a constant current source with a maximum voltage. The theoretical FF values are between 0.25 and 1. However, it may drop below 0.25 if a blocking contact is formed at the electrodes[26].

2.2.3 Energy conversion efficiency

The energy conversion efficiency is defined as the ratio of the electrical power output of the cell at the maximum power point to the incident optical power, which can also be expressed in terms of J_{SC}, V_{OC} and FF as[27]:

$$\eta = \frac{(FF)V_{OC}J_{SC}}{P_{light}}$$

2.2.4 External quantum efficiency

The external quantum efficiency (*EQE*), also called as the incident photon-to-current conversion efficiency (*IPCE*), is another important characteristic to be explored. *EQE* is defined as the number of electrons produced per incident photon:

$$EQE(\lambda) = \frac{n_e}{n_{ph}} = \frac{I_{SC}(\lambda)/e}{P_{in}(\lambda)/(hc/\lambda)} = \frac{I_{SC}(\lambda)}{P_{in}(\lambda)}\frac{hc}{\lambda e}$$

where h is Planck's constant, c is the speed of light, λ is the wavelength of the illumination, e is the charge of the electron, $I_{SC}(\lambda)$ is the photocurrent generated in short circuit mode, and P_{in} is the incident light power at wavelength of λ. *EQE* can also be calculated from the spectral response (*SR*) and $SR(\lambda)$ is defined as:

$$SR(\lambda) = \frac{I_{SC}(\lambda)}{P_{in}(\lambda)}$$

Therefore, *EQE* is also derived as:

$$EQE(\lambda) = \frac{SR(\lambda)}{\lambda}\frac{hc}{e}$$

Because $\frac{hc}{e} = 1240(\frac{W}{A}\cdot nm)$, the formula of $EQE(\lambda)$ can be simplified as:

$$EQE(\lambda) = \frac{1240SR(\lambda)}{\lambda} = \frac{1240I_{SC}}{P_{in}\lambda}$$

EQE normally follows the absorption of the active materials in solar cells. The internal quantum efficiency (or called photocurrent action spectrum) is defined as the photocurrent divided by the absorbed photon power.

2.3 Conjugated polymers

2.3.1 Commonly used polymers

Three classes of conjugated polymers including poly(*p*-phenylenevinylene) (PPV) and its derivatives (CN-PPV[28], MEH-PPV[29], MEH-CN-PPV[30], MDMO-PPV[31]), polythiophene (PT) and its derivatives (P3HT[32], P3OT[17]), and the polyanilines (PAn[33]) have attracted attention and are being investigated widely for use in solar cells. The chemical structures of PPV and PT and their derivatives are shown in Figure 4 and Figure 5 respectively. The chemical structure of PAn is shown in Figure 6. In the research described in this dissertation, a new water-soluble polythiophene known as sodium poly[2-(3-thienyl)-ethoxy-4-butylsulfonate] or PTEBS[14-16, 18] (Figure 4) has been used to fabricate solar cells.

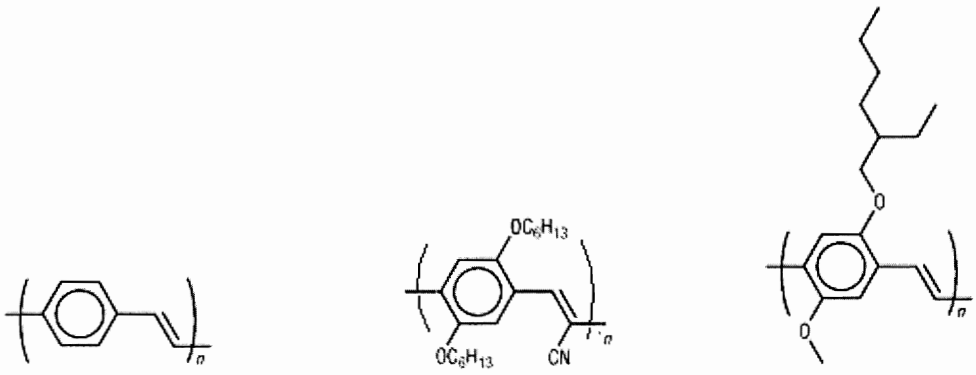

PPV CN-PPV MEH-PPV

Figure 4 Chemical structures of PPV and its derivatives.

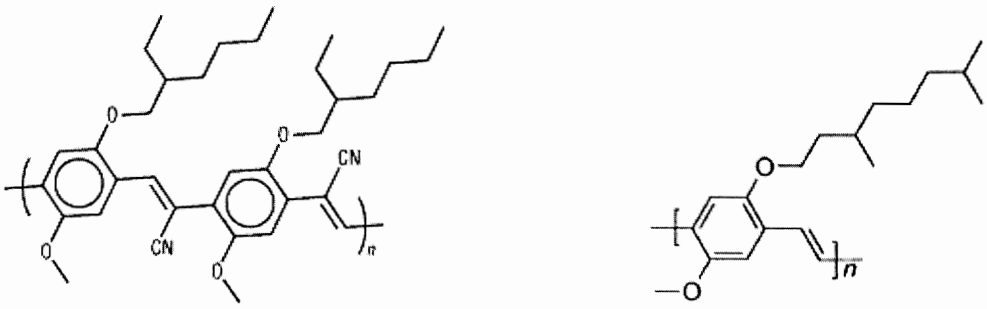

MEH–CN–PPV MDMO-PPV

Figure 5 (continued) Chemical structures of PPV and its derivatives.

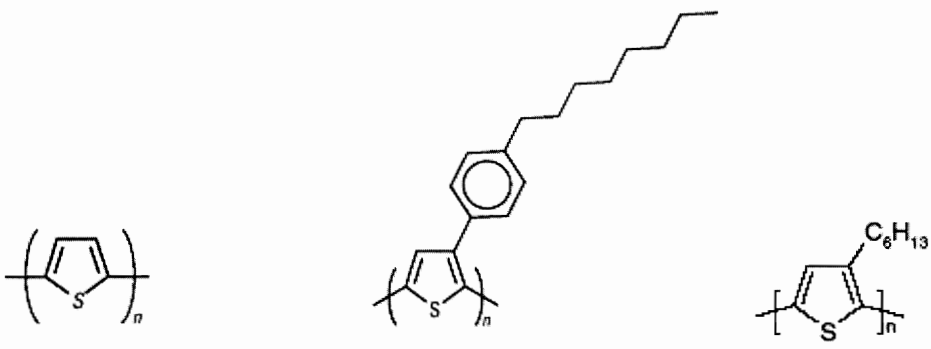

PT POPT P3HT

Figure 6 Chemical structures of Polythiophene and its derivatives.

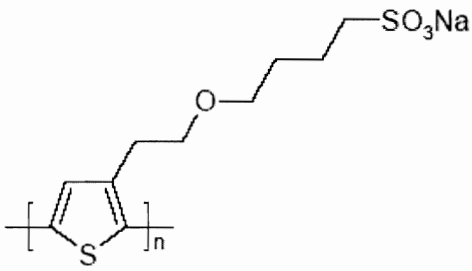

PTEBS

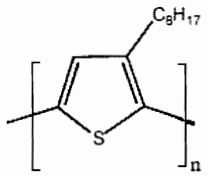

P3OT

Figure 7 (continued) Chemical structures of Polythiophene and its derivatives.

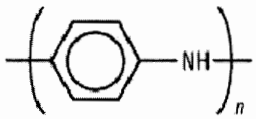

PAn

Figure 8 Chemical structure of polyaniline[34].

Conjugated polymers are semiconducting due to their framework of alternating single and double carbon–carbon bonds. Single bonds are called σ-bonds, and double bonds include a σ-bond and a π-bond. The σ-bonds can be found in all conjugated polymers. However, the π-bonds are formed from the remaining out-of-plane p_z orbitals on the carbon atoms overlapping with neighboring p_z orbitals. The π-bonds are the source of the semiconducting properties of these polymers. First, the π-bonds are delocalized over the entire molecule; and then, the overlap of p_z orbitals actually produces two orbitals, a bonding (π) orbital and an antibonding (π*) orbital. The lower energy π-orbital serves as the highest occupied molecular orbitals (HOMO), while the higher energy π*-orbital forms the lowest unoccupied molecular orbitals (LUMO). The

difference in energy between the two levels produces the band gap that determines the optical properties of the material such as photon absorption and emission.

Most conjugated polymers have a band gap between HOMO and LUMO in the range of 1.5–3 eV and a high absorption coefficient of ~ 10^5 cm^{-1}. Therefore, an incident visible-light photon has sufficient energy to excite an electron from HOMO to LUMO of the conjugated polymers. This makes them well suited to absorb the visible light for photovoltaic devices. However, the optical absorption range is relatively narrow across the solar spectrum because most conjugated polymers only absorb light in the blue and green and absorption in the red is difficult to accomplish. The incomplete light absorption in the solar spectrum limits the photocurrent generation.

2.3.2 Recently developed low band gap polymers

As stated above, most conjugated polymers have a band gap larger than 1.9 eV and accordingly only absorb light with wavelengths less than 650 nm. Recently, low band gap polymers (E_g < 1.8 eV) have been reported as an alternative for better light harvesting of solar spectrum[35, 36]. Research has been done to synthesize low band gap polymers such as poly[5,7-bis-(3-octylthiophen-2-yl)thieno[37]pyrazine] (PB3OTP)[36], poly-N-dodecyl-2,5,-bis(2'-thienyl)pyrrole,2,1,3-benzothiadiazole (PTPTB)[38], side-chain substituted poly(di-2-thienylthienopyrazine)s (PBEHTT and PTBEHT)[39], polymers based on alternating electron-donating 3,4,3',4'-tetrakis[2-ethylhexyloxy]-2,2'-bithiophene and electron-deficient 2,1,3-benzothidiazole units along the chain (PBEHTB), and alternating polyfluorene copolymers with a green color (APFO-Green 1

or APFO Green 2)[35, 40, 41]. Some of these low band polymers have been reported to absorb from 300 nm to 850 nm[40].

2.3.3 HOMO/LUMO levels and band gaps for typical polymers

The HOMO/LUMO levels and band gaps of various polymers including PPV, PT, and recently developed low band gap polymers are summarized in Table 3.

Table 3 HOMO/LUMO levels and band gaps of various polymers

Conjugated polymers	LUMO (eV)	HOMO (eV)	Band gap (eV)	Reference
P3OT	-2.85	-5.25	2.4	[9, 42]
MEH-PPV	-3	-5.3	2.3	[20]
MDMO-PPV	-2.8	-5.0	2.2	[43]
PTEBS	-2.8	-5	2.2	[14-16, 18]
P3HT	-3.2	-5.2	2.0	[44]
PPE-PPV(DE21)	-3.6	-5.6	2.0	[2]
APFO Green 2	-3.6	-5.6	2.0	[41]
PPE-PPV(DE69)	-3.56	-5.46	1.9	[2]
PTBTB	-3.73	-5.5	1.77	[38, 45]
P3DDT	-3.55	-5.29	1.74	[2]
PBEHTB	-3.6	-5.3	1.7	[46]
PB3OTP	-2.75	-4.2	1.45	[36]
PBEHTT	-3.6	-5.0	1.4	[39]
APFO Green 1	-3.9	-5.14	1.24	[35, 40]
PTBEHT	-4.0	-5.2	1.2	[39]

2.3.4 Properties of polymers for use in photovoltaics

A singlet exciton is a bound electron-hole pair generated by photoexcitation. When illuminated under the light, electrons are pumped to the LUMO level by the absorbed photons, leaving the corresponding holes in the HOMO. However, electrostatic attraction keeps them together. The exciton binding energy of the conjugated polymers

has been the subject of debate in the literature over the past decades. Reporters have proposed the values between a few k_bT (k_bT in the order of 10^{-5} eV) and 1 eV for the binding energy[47-49]. It seems that people accept that most conjugated polymers have an exciton binding energy of about 0.3 eV – 0.4 eV[50, 51]. This means strong driving forces such as an electric field are needed to dissociate the photogenerated excitons into separate electrons and holes. These excitons need to be dissociated before the carriers can be transported and then collected at the electrodes. The diffusion range of singlet excitons of conjugated polymers is approximately 5 ~ 15 nm and their radiative or nonradiative decays take place in the time of 100 ~1000 picoseconds[12].

Compared to those in the inorganic semiconductors, the charge mobilities are low (0.01 - 0.001 cm^2-V^{-1}-s^{-1})[52] because charge transport takes place through hopping between the localized states in the polymer. In addition, the photocurrent is susceptible to temperature variation through hopping transport. This limits the useful thickness of the devices. Most conjugated polymers are vulnerable to degradation in the air with the presence of oxygen or moisture. For this reason, glove boxes are generally needed to make polymer solar cells[53].

The conjugated polymers described here are mainly p-type semiconductors in the sense that they can be partially oxidized to become p-doped[34]. A corresponding reduction or n-doping will destabilise the polymers[43]. Figure 7 shows an example for the oxidation and reduction of a polythiophene[54]. N-type polymer semiconductors are also available[55, 56], however less effort has been gone into synthesizing and characterizing them.

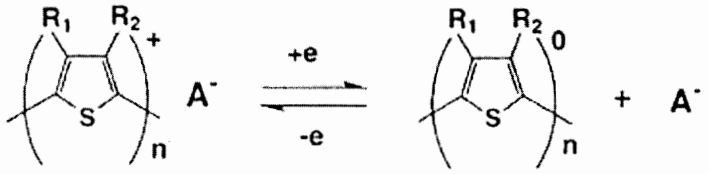

Figure 9 the oxidation and reduction of a polythiophene

2.4 Device concepts and architecture

2.4.1 Single layer devices

The simplest design for polymer solar cells uses the metal-insulator-metal (MIM) structure, a homogeneous layer of organic semiconductor sandwiched between two electrodes, as shown in Figure 8. Conjugated polymers such as polyacetylene in 1981 [43, 57], polythiophene in 1984 [58] and poly(para-phenylenevinylene) (PPV) in 1994 [48] were originally used to fabricate the solar cells and the most success has been realized by using PPVs in MIM photovoltaic devices. However, as described below, MIM devices give inefficient photogenerated charge generation and the performance of such photovoltaic devices is limited. Open circuit voltages of about 1.7 V and quantum efficiencies of approximately 1% were obtained in the ITO/PPV/Ca devices[48]. External energy conversion efficiencies are less than 0.1%[59].

In photovoltaic applications, the electric field in MIM device is caused by the difference between the work functions of the electrodes when no external voltage is applied under the short-circuit condition. The electric field causes the separated photogenerated charges to be transported to their corresponding contacts. However, the photogenerated excitons are strongly bound by the Coulomb attraction in conjugated

polymers. An exciton binding energy of roughly 0.4 eV in PPV was estimated by Marks[48]. The electric field due to the work function difference of the electrodes is not high enough to dissociate them. The excitons need to diffuse to the organic-metal interface to be dissociated by charge transfer. Since the exciton diffusion lengths in most organic semiconductors are between 5 nm and 15 nm[60, 61], most excitons will decay radiatively or non-radiatively before they reach the electrodes. This limits the thickness (and therefore the absorption) of the devices. It is also reported that exciton quenching at metal–electrode interface reduces photocurrents[62].

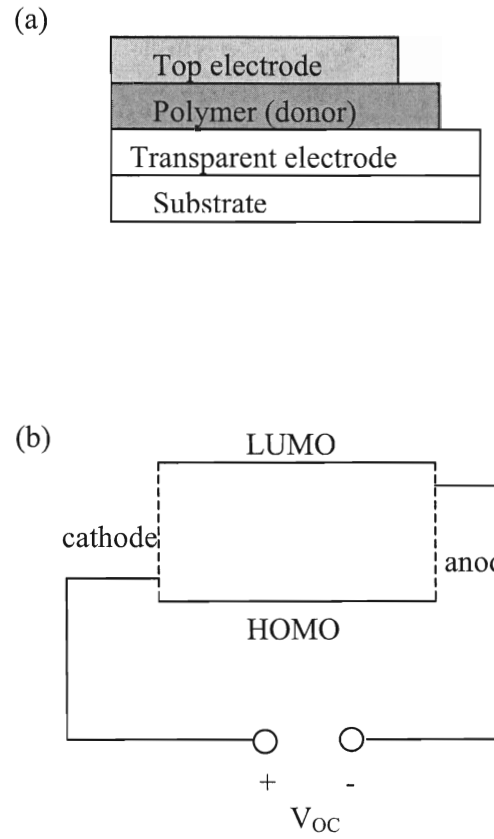

Figure 10 Schematic illustration of (a) MIM structure devices, (b) band diagram in the open circuit mode, and (c) band diagram at the short circuit mode.

2.4.2 Bilayer heterojunction devices

Improved organic solar cells are based on the charge separation at the interface between two different materials in donor/acceptor heterojunctions. The differences in potential energy between two materials, if larger than the exciton binding energy, causes the exciton dissociation and charge transfer. Initial efforts to develop organic hetero-junction solar cells were based on two different organic molecular semiconductors. Early bilayer photovoltaic devices were fabricated from the addition of an electron-transporting dye such as rhodamine and a hole-transporting dye such as phthalocyanine[2]. Tang[63] reported a breakthrough in the energy conversion efficiency (0.95%) in organic solar cells based on the bilayer concept. Tang's cell was made by evaporating a first layer of 30-nm thick copper phthalocyanine and then a second layer of 50-nm thick perylenetetracarboxylic derivative (PV) on a indium tin oxide (ITO) glass.

The bilayer concept has also been applied in polymer solar cells. In the polymer solar cells, the bilayer consists of a p-type polymer donor layer (e.g., MEH-CN-PPV [64], MEH-PPV [65], P3HT [66], MDMO-PPV[22]) and a subsequent n-type polymer or inorganic semiconductor (acceptor) layer (e.g., TiO_2[67, 68], CdSe[69], CdS[69], carbon nanotubes[70-72], fullerenes[73, 74]) (Figure 9). When the p-type polymer absorbs a photon, a bound exciton is created and dissociates at the interface. The electron will be transferred to the n-type polymer or inorganic semiconductor. This increases the free charge generation and reduces the possibility of recombination of singlet excitons. Energy conversion efficiencies have increased to a value between 0.1% and 1%[18] and external quantum efficiencies of 15%[75] have been achieved in the bilayer devices. However, charge photogeneration only takes place at the interface between the two layers

or within the exciton diffusion length, limiting active light absorption and charge generating regions.

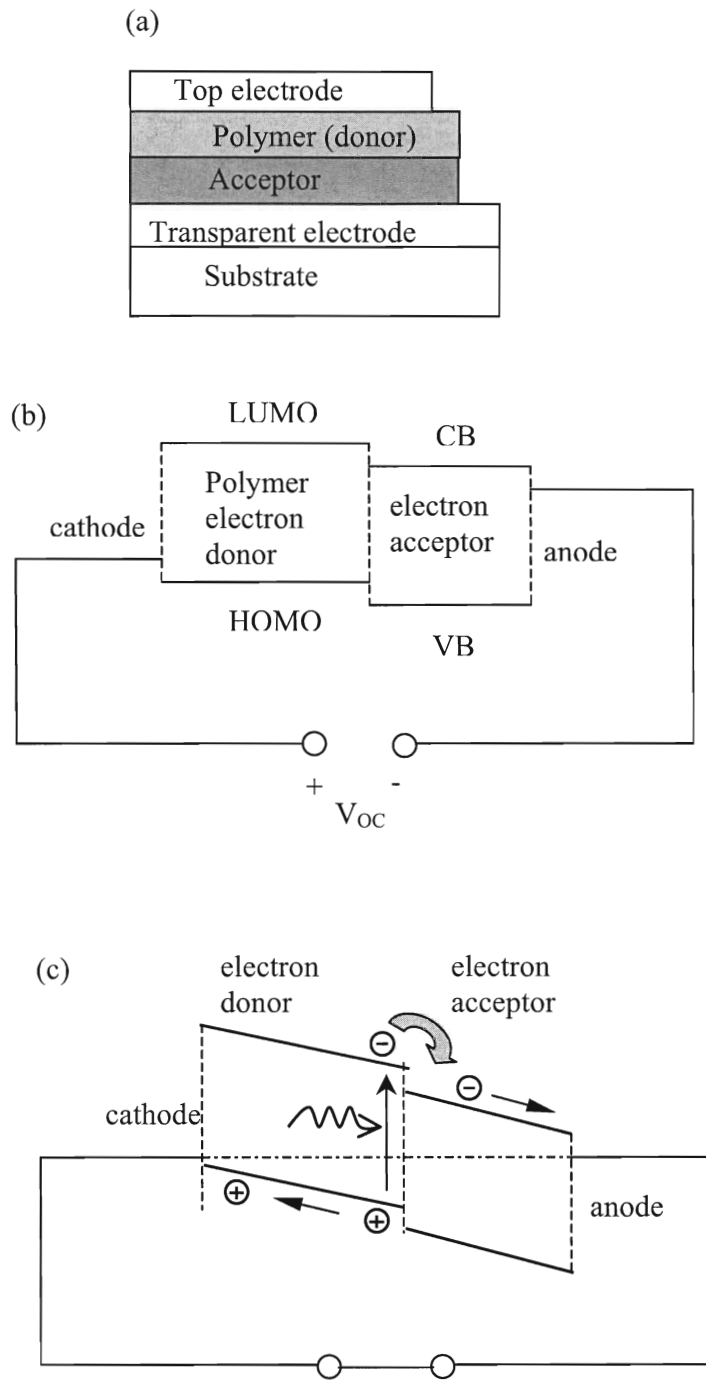

Figure 11 Schematic illustration of (a) bilayer structure devices, (b) band diagram in the open circuit mode, and (c) band diagram at the short circuit mode.

2.4.3 Bulk heterojunction devices

Interpenetrating network composites of phase separated electron donors and acceptors have been developed as an approach to overcome the limitations to the MIM and bilayer devices. A schematic description of the bulk heterojunction is shown in Figure 10. Yu et al.[74] reported that interpenetrating donor/acceptor (D/A) network heterojunctions increase the external conversion efficiency resulting from enhanced exciton dissociation and charge transfer. By blending a p-type (electron donor) and an n-type (electron acceptor) material together in the solution and controlling the morphology of the devices, a high interface area throughout the bulk can be achieved.

If the domain size of either material is not larger than the exciton diffusion length, any point in the composite is within the exciton diffusion length of an interface. All the excitons photogenerated in the composite are expected to diffuse successfully to an interface and break up into electrons and holes. However, in order to produce a useful current, these carriers must then move to the electrodes before recombining. Due to the long chain in polymers as donors, continuous paths for holes seem to be easily produced. If the electron transporting materials (acceptors) do not form a continuous path to the electrode, then the electrons may be stuck or must pass through the hole transporting polymers (donor) before reaching the electrode. Because the donor polymer materials suffer from low electron mobility and short exciton diffusion lengths[13], the likelihood of recombination is greatly increased when the electron re-enters the polymer[69]. Therefore, of great importance is to form continuous paths from the interfaces to the electrodes in both the donor and acceptor materials.

The derivatives of buckminsterfullerence (C_{60})[74], dyes[76], carbon nanotubes[9, 42, 72], inorganic semiconductors[12, 21, 44, 69, 77] and n-type polymers[28, 78] have been reported as electron acceptors to blend with polymers in bulk heterojunction solar cells. The challenge exists in the forming of the continuous paths for separated electrons. Nanorods[19, 79] appear to be an approach to solving this problem and an external power conversion of 1.7%[19] has been reported. In addition, aligned carbon nanotubes[80] have also been tried but the results so far have not been promising. To date, the highest power conversion efficiency is 5% under AM1.5 illumination and an external quantum efficiency of 90% has been reported for polymer-fullerene bulk heterojunction solar cells[81, 82].

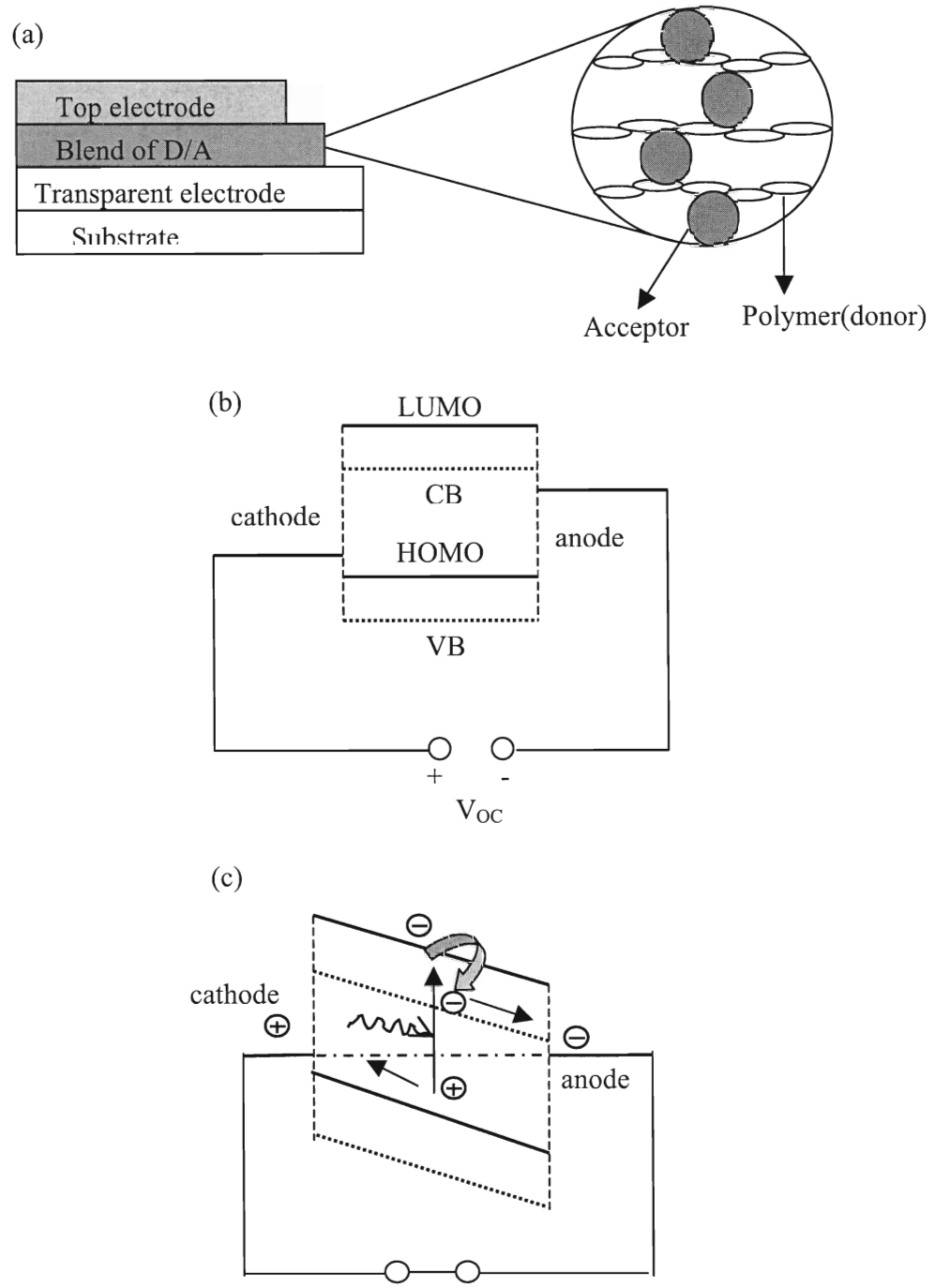

Figure 12 Schematic illustration of (a) bulk heterojunction structure devices, (b) band diagram in the open circuit mode, and (c) band diagram at the short circuit mode.

2.5 Nanoscale materials

As described above, thanks to the development of nanotechnology and various nanoscale materials, polymer solar cells have evolved from a single layer structure (homojunction) to a heterojunction geometry including bilayer and bulk heterojunctions.

2.5.1 Types of nanomaterials

Depending on their shapes, there are three kinds of nanomaterials: nanoparticles, nanorods, and nanotubes. Nanoparticles include TiO_2[14-16, 18, 21, 29, 44, 61], ZnO[4, 83, 84], fullerene and its derivatives[31, 38, 39, 46, 85-97], etc. Nanorods such as CdSe[19, 69, 79] and ZnO[98] have shown promise as electron acceptors. Single-wall carbon nanotubes (SWNTs)[9, 42, 70] and multi-wall carbon nanotubes (MWNTs)[72] are also under investigation as electron acceptors and transport materials.

2.5.2 Properties of nanomaterials for use in photovoltaics

For heterojunction solar cell applications, nanomaterials need to have a higher electron affinity than the polymer. In other words, the conductance and valence bands of most semiconductor nanoparticle materials lie well below the related HOMO and LUMO of various polymers, making them energetically favorable for exciton dissociation and charge transfer at the interfaces. In addition, a high electron accepting ability is also required for nanomaterials to be used in solar cells. For example, buckminsterfullerene is capable of taking up to six electrons[99]. Another property is high electron mobility, which works as a "speed limit" for electron transport.

2.5.3 Conductance and valence bands and band gaps for typical nanomaterials

The conductance bands, valence bands and band gaps of nanomaterials commonly used as electron acceptors are shown in Table 4.

Table 4 The conductance bands, valence bands and band gaps of nanomaterials commonly used as electron acceptors

Nanoscale materials	Conductance band (eV)	Valence band (eV)	Band gap (eV)	Reference
C60	-3.83	-6.1	2.27	[2]
PCBM - C61	-3.75	-6.1	2.35	[2]
SWNT	-4.5			[9, 42]
BM-C60	-3.51	-6.1	2.59	[2]
TiO_2	-4.2	-7.4	3.2	[14-16, 18, 20]
CdS	-4.2	-6.45	2.25	[2]
CdSe	–4.4 eV	–6.1 eV	1.7	[12, 19, 69, 100, 101]
CdTe	–4.12 eV	–5.85 eV	1.73	[102]
SiC	-3.0	-6.0	3	[100]
SnO_2	-4.95	-8.75	3.8	[100]
WO_3	-4.6	-7.2	2.6	[100]
GaAs	-4.2	-5.6	1.4	[100]
GaP	-3.6	-5.85	2.25	[100]
ZnO	-4.4	-7.6	3.2	[4]
Fe_2O_3	-4.85	-6.95	2.1	[100]

2.5.4 Energy matching for polymers and nanomaterials

In heterojunction solar cells, the polymers work as p-type semiconductors and nanomaterials serve as n-type semiconductors. However, their energy structures must be energetically favorably matched to form an effective heterojunction. Figure 11 shows how a polymer and a nanomaterial match based on energy band structure, in which most of the common polymers and nanomaterials have been included.

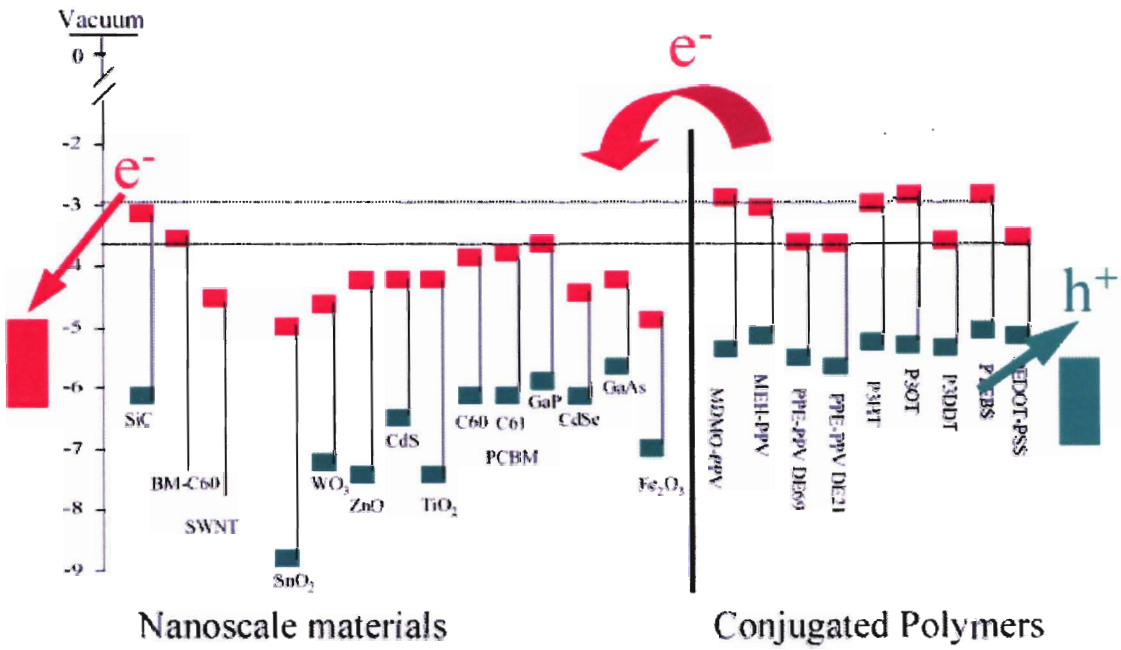

Figure 13 Matching of nanomaterials and polymer for use in solar cells based on energy band. The red squares ( ) for the polymers and nanomaterials represent the LUMO and conductance bands and the green squares ( ) for the polymers and nanomaterials represent the HOMO and valence bands. The typical electrodes shown on the right are ITO and gold, those shown on the left are FTO and aluminum.

2.6 Polymer - TiO_2 solar cells

Due to their low cost, chemically stability and non-toxicity, metal oxides such as titanium dioxide (TiO_2), zinc oxide (ZnO), and tin dioxide (SnO_2) are promising for use as electron acceptor materials in solar cells[103]. TiO_2 has been widely used to make highly efficient dye sensitized solar cells (DSSC) and unsurprisingly this has led to exploration of organic-inorganic photovoltaic devices by using polymers and TiO_2. Successful charge generation and separation at the interfaces in films consisting of TiO_2 and polymers has been demonstrated by a number of groups[20, 104-106].

Generally, there are two configurations for heterojunctions using TiO_2 and a photoconducting polymer[2]. The first is a blended heterojunction and is made by preparing a blended solution containing the polymer and nanoparticle TiO_2, and then casting the solution onto a substrate[13, 14, 44]. The other configuration is a bilayer heterojunction and is prepared by making a nanocrystalline TiO_2 film and then filling the pores by spin coating or drop casting the polymer on the top [18, 106-108].

The first configuration is easy of fabricate, but hard to control for ideal device morphology. If the polymer and TiO_2 are not in contact, they will not form interfaces for exciton dissociation. In addition, if the TiO_2 nanoparticles do not produce a continuous path to the electrode, the electrons will be trapped in the films. Huisman et al.[14] reported a solar cell from a poly(3-octyl)thiophene and TiO_2, and obtained a power conversion efficiency of 0.06%. However, by optimizing the TiO_2 concentrations in the blended solution, Kwong et al.[44] have achieved an external quantum efficiency of 15% and an energy conversion efficiency of 0.42% in a Poly(3-hexylthiophene) (P3HT):TiO_2 solar cell by using the first configuration. In their experiments, they used anatase/rutile

solid spherical TiO_2 nanoparticles with diameters between 20 nm and 40 nm. A 30-nm layer of PEDOT:PSS was first spin-coated onto a ITO glass substrate to act as an electron blocking layer, followed by a 100-nm thick P3HT:TiO_2 layer. The TiO_2 concentration is about 50% - 60% in the blend. Aluminum was evaporated as the top electrode.

In a bilayer configuration the highest measured energy conversion efficiency before the year of 2001 was 0.18% with a quantum efficiency of 6%, reported by Breeze et al.[29]. Initially, the low power conversion efficiency was believed to be the result of incomplete polymer infiltration into the porous TiO_2, leading to insufficient polymer to absorb the light. Several recent studies[103] have shown that deep polymer/TiO_2 infiltration can be obtained by various approaches such as in-situ growth of TiO_2 from an organic precursor[22], spin coating on ultrathin dip-coated TiO_2 films[109], and dip coating of mesoporous TiO_2[110]. It is generally agreed that the penetrating depth of polymer is dependent on the pore size. The pore size is in turn determined by the nanoparticle size. In addition, the infiltration depth has also been found to be a function of the polymer type. For example, the regioregular P3HT has been found to oppose infiltration into mesoporous TiO_2 due to the coiling of the polymer chains[106]. Coakley et al.[106] and Liu et al.[111] have reported that other techniques such as melting the polymer and electropolymerization can be used to fill mesoporous TiO_2 films with polymers. Their group used x-ray photoelectron spectroscopy to measure the penetration depth of polymers. The performance parameters of their solar cells under 33 mW/cm^2 514 nm monochromatic illumination are V_{OC} = 0.72 V, J_{SC} = 1.4 mA/cm^2, FF= 0.51 and an energy efficiency of 1.5 %.

Huisman et al.[107] investigated the penetrating depth by measuring the current-voltage (I-V) characteristics of a heated P3OT polymer spin coated onto a porous TiO_2 film. They found that the I-V is symmetrical if P3OT penetrates all the way to the bottom of TiO_2 and makes an ohmic contact to both the top and bottom electrodes. In further research, these curves are linear when the films are heated in hot air at about 60 °C. However, the I-V curve shows desired diode-type behavior if P3OT does not reach the bottom of TiO_2.

Ravirajan et al.[103] reported that dip-coating before spin-coating the polymer could lead to a better polymer penetration into TiO_2 pores and therefore improve the device performance. Their optimized devices produced a short circuit current of 1 mA/cm^2, a open circuit voltage of 0.86 V, a fill factor of 0.50, and a power conversion efficiency of 0.41% under a AM 1.5 solar simulated illumination (about 100 mW/cm^2). The photovoltaic parameters for the best reported TiO_2 devices with different polymers are shown in Table.5.

Table 5 Photovoltaic parameters for the best reported TiO_2 devices with different polymers

Polymer	J_{SC} **[mA cm^{-2}]**	V_{OC} **[V]**	***FF***	η **[%]**	**Reference**
P3UBT	0.45	0.67	0.29	0.10	[112]
MEH-PPV	0.40	1.1	0.42	0.18	[29]
TPD(4M)-MEH-M3EH-PPV	0.96	0.86	0.50	0.41	[103]
P3HT	2.76	0.44	0.36	0.42	[44]

2.7 Device fabrication techniques

Small molecules and polymers have been investigated extensively in organic photovoltaics. The difference between the small molecules and polymer photovoltaics is the type of materials and the manufacturing methods. Vacuum evaporation and organic vapor phase deposition (OVPD) are used to deposit the successive layers of small molecular materials, where OVPD seems to be the less expensive because it does not require the high vacuum techniques.

Polymer based devices are prepared by solution processing and offer an alternative approach to lower the cost of the fabrication. Most of the conjugated polymers are soluble in standard solvents and provide a possibility to deposit large area thin films on flexible plastic substrates. Depositing thin films by printing processes from solution is easy and robust in comparison with vacuum based gas phase deposition techniques. Spin coating is widely used in research laboratories, but will not be competitive for commercial production. New deposition techniques such as doctor blading, screen printing, inkjet printing and roll-to-roll processing technology are available[59]. Nanosolar, Inc.[113] and Konarka[114] have claimed to have developed process technology innovations in the production of printed thin-film solar cells by utilizing the roll-to-roll technique. Setups of several processing techniques[59] are shown in Figure 12.

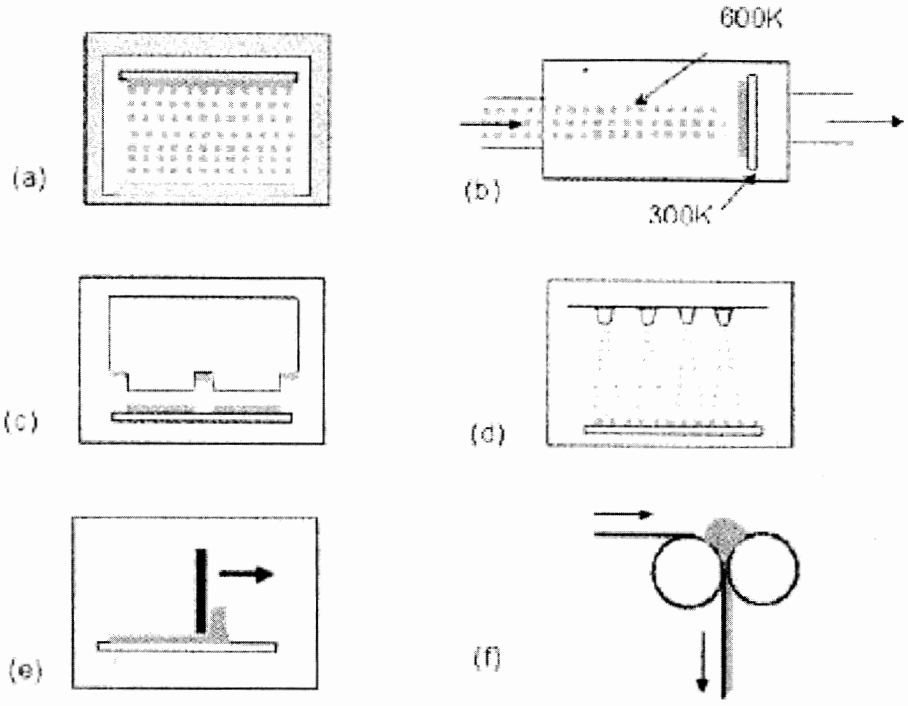

Figure 14 Setups of several processing techniques[59]

a) Molecular deposition in high vacuum (~10^{-6} torr)
b) Organic vapor phase deposition
c) Screen printing: fine mesh screen loaded with polymer solution temporally contacting substrates
d) Inkjet printing: fine jet of polymer solution sprayed onto substrates
e) Doctor blading: a rod/blade is drawn over the polymer solution
f) Roll to roll processing

Chapter 3 Material Characteristics

In this chapter, the characteristics of the specific materials used in this research will be presented. In particular, solar cells have been fabricated using the water-soluble PTEBS polymer and titanium dioxide. The optical properties such as the absorption and photoluminescence of the polymer will be presented. The mechanisms of self doping and dedoping for PTEBS will also be discussed. In addition, the semiconducting properties will be discussed by investigating the LUMO/HOMO levels and band gaps. TiO_2 will be characterized by UV-Vis absorption, Scanning Electron Micrograph (SEM) and X-ray diffraction. Finally, electrode materials including the top and bottom electrodes are summarized.

3.1 PTEBS polymer

Presently, most polymers used in organic solar cells are based on organic solvents such as xylene, toluene, chloroform, and chlorobenzene, etc. Such solutions are harmful to people and environments, leading to the high cost, complicated waste disposal processing. Water-soluble conjugated polymers with polar groups such as sodium poly(3-thiophene-β-ethanesulfonate) [P3-ETSNa], sodium poly(3-thiophene-δ-butanesulfonate) [P3-BTSNa] and their respective acids forms P3-ETSH and P3-BTSH have been reported[115] as an alternative to the widely used solvent based polymers. Recently, sodium poly[2-(3-thienyl)-ethoxy-4-butylsulfonate]) [PTEBSNa] and its acid PTEBSH have also been developed[116]. This novel environmentally friendly water-soluble thiophene polymer (Sodium poly[2-(3-thienyl)-ethoxy-4-butylsulfonate])

[PTEBS] will be used to fabricate solar cells in this dissertation. This is the first time that solar cells have been made using a water-soluble polymer. PTEBS was obtained from American Dye Source[117]. The chemical structure of the thiophene polymer is shown in Figure 13.

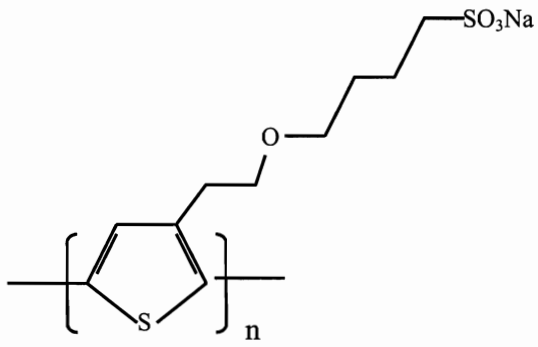

Figure 15 Chemical structure of the water-soluble polythiophene (Sodium poly[2-(3-thienyl)-ethoxy-4-butylsulfonate]).

3.1.1 UV-Vis absorption

The UV-Vis spectra for PTEBS films are shown in Figure 14. PTEBS is commercially available from American Dye Source (ADS). During the course of this investigation, it was observed that the UV-Vis absorption spectra for samples ordered at different times were slightly different. Further investigation revealed that over the course of this research, the molecular weight (MW) of the PTEBS supplied by ADS has increased. The samples (sample A) obtained early in the investigation have a lower MW compared to those (sample B) obtained more recently.

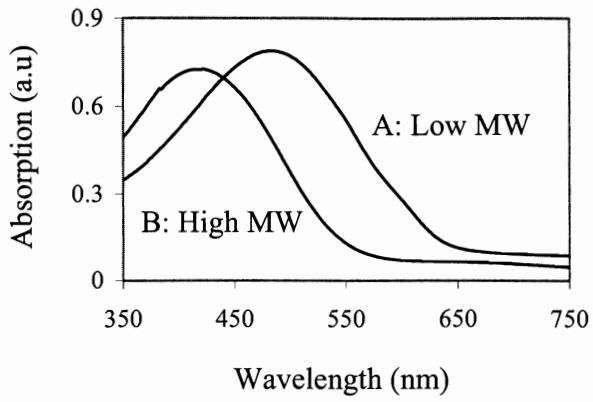

Figure 16 The absorption spectra for drop cast film from low and high molecular weight PTEBS.

As shown in Figure 14, both the absorption maximum and the onset (sample A) have shifted significantly to shorter wavelengths (sample B): from approximately 480 nm and 620 nm to 415 nm and 560 nm, respectively. In solution, the high MW PTEBS may form coils whereas the low MW PTEBS forms rod-like shapes[118]. The absorption shift may occur because the interactions between the polymer chains in a rod-like conformation are stronger than between those in a coiled conformation[119]. As the polymer concentration is increased, the polymer chains come closer together and the interchain attraction forces become stronger. These interactions are maximized when the solutions are dried into solid-state films[120]. Therefore, the more rod-like conformation solution leads to more aggregates in the films than the coil conformation. As discussed above, the aggregates in the lower MW polymer films lead to redshift in the absorption spectra. However, more research needs to be done to verify why the significant change in the absorption occurs.

The band gap of the semiconducting PTEBS can be determined from the onset of UV-Vis absorption. For low MW PTEBS, the onset of the absorption occurred at 620 nm, from which the band gap was estimated to be approximately 2.0 eV. Based on cyclic voltamperometry measurements made by Tran-Van et al. [116] in PTEBS thin films, the oxidation onset occurs at ~+0.3–+0.4 V vs. saturated calomel electrode (SCE). The HOMO level of the polymer can be estimated at the onset point. Typically, an adjustment factor of 4.4 to 4.7 eV is used in converting the energy values versus SCE into energy values versus vacuum. Therefore, the HOMO level is estimated to be between -4.7 eV and -5.1 eV. The optical gap of 2 eV results in a LUMO level between -2.7 eV and -3.1 eV.

Unless otherwise mentioned, for the remainder of this work, all PTEBS refers to high MW samples because the low MW samples are no longer available from ADS. The LUMO, HOMO and band gap of high MW PTEBS will be stated in detail in the following section.

3.1.2 LUMO and HOMO of high MW PTEBS

Figure 15 shows the electrochemical characterization of a cast film of high MW PTEBS deposited on a Fluorinated Tin Oxide (FTO) substrate. FTO glass was used the working electrode. Platinum (Pt) mesh and Ag/AgCl electrodes were used as counter and reference electrodes, respectively. A BAS 100B electrochemical analyzer was used for electrochemical study. The electrochemical measurements were carried out with the scan rate of 100 mV/s in an electrolytic solution of $CH_3CN/LiClO_4$ 0.1M in a glass cell. All the measurements were done at room temperature. As is shown in Figure 15, the

oxidation onset occurs at ~+0.6 V vs. saturated calomel electrode (SCE). The HOMO level of PTEBS can be estimated at the onset point. Typically, an adjustment factor of 4.4 to 4.7 eV is used in converting the energy values versus SCE into energy values versus vacuum. Therefore, the HOMO level is estimated to be between –5.0 eV and -5.3 eV. The energy band gap of around 2.2 eV for the high MW PTEBS is obtained from the absorption onset (560 nm, shown in Figure 14), which results in a LUMO level between -2.8 eV and -3.1 eV.

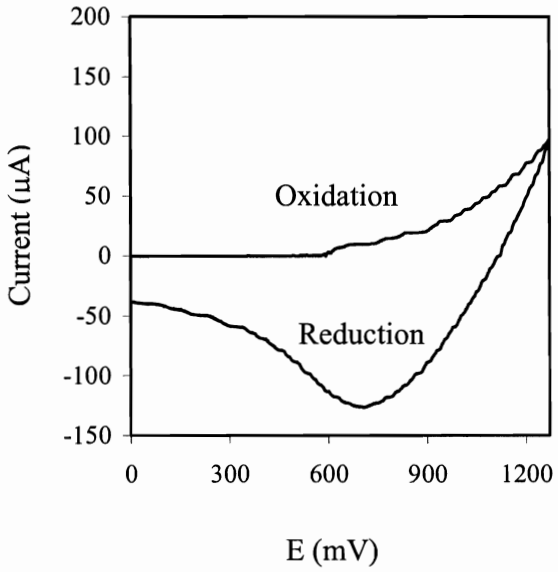

Figure 17 Cyclic voltammogram of cast thin film of PTEBS on FTO substrate in $CH_3CN/LiClO_4$ 0.1M

3.1.3 Photoluminescence and absorption coefficient

The absorbance and fluorescence spectra of PTEBS films are shown in Figure 16. The UV-Vis absorption spectrum shows an absorption onset at ~ 560 nm. The absorption peak occurs at 422 nm with an optical density (OD) of 0.097. The PTEBS film used to conduct the absorbance measurement is 23 nm thick. From the thickness of the PTEBS film and its optical density, the absorption coefficient $\alpha(\lambda)$ can be determined through the equation of $OD = \alpha d \cdot \log(e)$. The absorption coefficient of PTEBS was found to be 9.7 $\times$ 10^4 cm^{-1} at 422 nm. The fluorescence is redshifted relative to the UV-Vis absorption and the peak is at 600 nm.

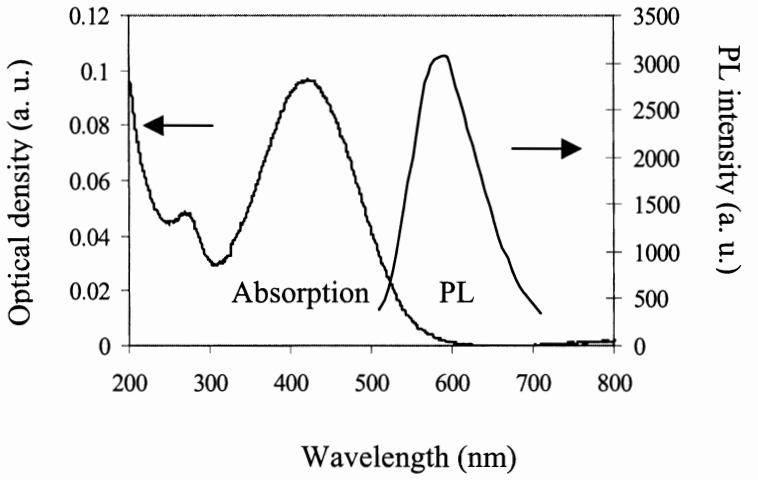

Figure 18 UV-Vis and photoluminescence spectra of PTEBS in basic films.

3.1.4 Doping and dedoping properties

An interesting feature of PTEBS is that it changes its color and UV-Vis absorption in the solutions with different pH values. Films cast from these solutions show similar phenomena. The pH values are altered by adding a base (e.g. ammonium hydroxide) or acid (e.g. hydrochloric acid). The change of colors and absorption spectra accounts for that PTEBS is doped in an acidic solution and then dedoped in a basic solution or water. Details of these properties are discussed in detail below.

3.1.4.1 Solutions

In the experiment, three solutions with 1% PTEBSNa by weight were prepared: a basic solution (pH > 7), a fresh acidic solution (pH ~ 1), and an acidic solution that was left exposed to the air for a few days. The basic solution was made by adding a few drops of ammonium hydroxide to the 1% PTEBS solution dissolved in deionized water. For acidic solutions, PTEBSNa (again, 1% by weight) was dissolved in a 3:1 volume ratio solution of hydrochloric acid (HCl, 35%) and deionized (DI) water. For acidic solutions, PTEBSNa was dissolved in a 3:1 volume ratio solution of hydrochloric acid (HCl, 35%) and deionized (DI) water. Afterwards, both the basic and acidic solutions were stirred for three days and centrifuged for 5 minutes at 13200 RPM to allow any large undissolved particles to settle out. The third solution was left exposed to the atmosphere for an additional 72 hours forming the exposed acidic solution. In order to compare the appearance of the three solutions, the basic solution was diluted with DI water, while the fresh acidic one was diluted with HCl. The fresh acidic solution changed its color from green to yellow-green when diluted. After being in the open air

for several days, the color of exposed solution changed to orange, a color very similar to that of basic solution. Figure 17 shows the appearance of the fresh acidic, the exposed acidic and basic solutions, which are yellow-green, orange and dark orange respectively. The three solutions were then diluted again and the absorption was measured using a Lambda 40 UV-Vis spectrometer. The absorption spectra are shown in Figure 18. The red-IR absorption band of the acid doped solution disappeared after staying in the air for some days, while the UV band showed little change. The absorption spectrum for the basic solution did not change after being exposed to the air for a few days.

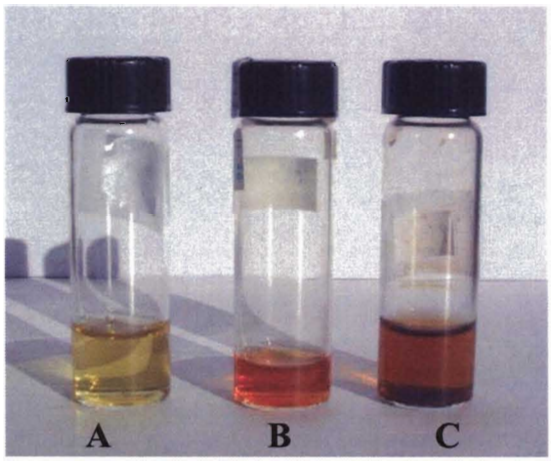

Figure 19 The appearance of the fresh acidic (A: yellow-green), exposed acidic (B: orange), and basic (C: dark orange) solution

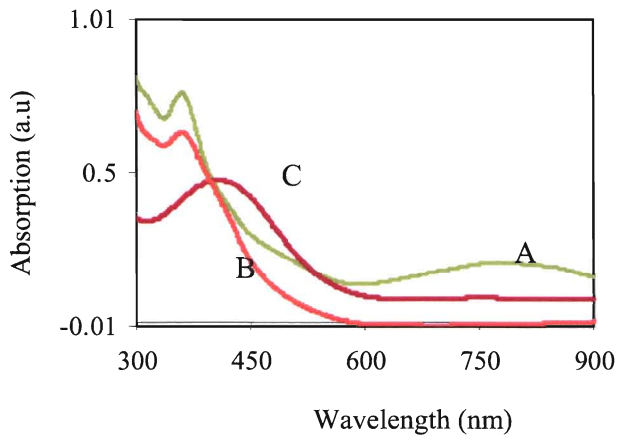

Figure 20 The absorption spectra of the fresh acidic (A), exposed acidic (B) and basic (C) solutions.

3.1.4.2 Thin films

Thin films of PTEBS made from HCl and basic solutions were also investigated. Three types of films have been made from: fresh acidic, fresh acidic films exposed to the air for a few days and basic films. Figure 19 shows that the films have an appearance similar to their respective solutions (green, orange and dark orange). Thinner films were prepared for absorption measurement by the Lambda 40 UV-Vis spectrometer. After being exposed to the air for three weeks, the ultraviolet and red-near IR absorption bands in the acidic films had weakened somewhat, but were still stronger than the films made from the basic solution. In addition, the absorption peak in the blue range broadened to include both the ultraviolet and yellow bands, which increases the total light absorption. Interestingly, we observed that the orange exposed acidic film changed its appearance back to green when exposed to HCl vapor. However, it turns orange again after staying in the air for a few days.

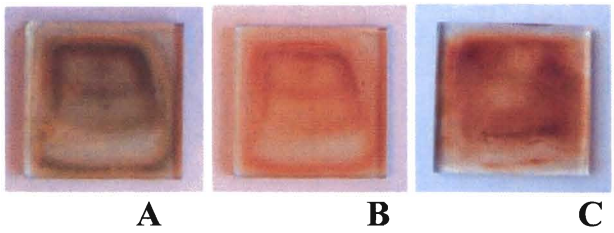

Figure 21 The appearance of fresh acidic (A: green), exposed acidic (B: orange) and basic (C: dark orange) films.

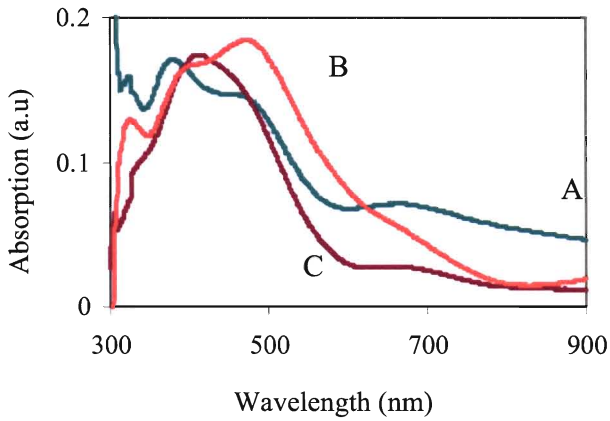

Figure 22 The absorption spectra of the fresh acidic (A), exposed acidic (B) and basic (C) films.

3.1.4.3 Acidification

The proton salt (acid from) of poly[2-(3-thienyl)-ethoxy-4-butylsulfonate acid]) [PTEBSH] was obtained via ion-exchange treatment by adding hydrochloric acid into a

PTEBSNa solution. In the acidification process an equilibrium reaction occurs between sodium salt and proton salt of PTEBS, as depicted in the scheme[117] below:

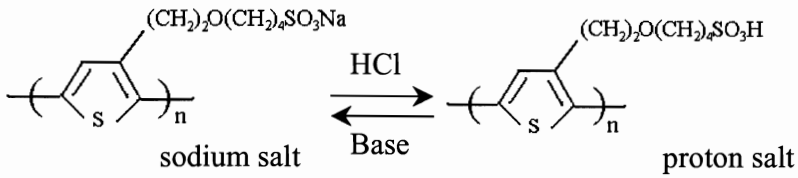

In addition to the cation exchange between the sodium and hydrogen shown in the scheme above, self-doping has also been proposed to occur in the acidification process[121, 122]. The author believes the same mechanism causes the changes in the PTEBS solutions because they have the similar chemical structures. The self-doping mechanism is shown in Figure 21. Following the removal of the cation, the counterion binds covalently to the polymer backbone chain simultaneously with electron loss in the doping and oxidation, which is different from the normal doping mechanism by the incorporation of a new anion[121, 122]. The self-doped polymers showed an increased conductivity and changes in the optical and infrared absorption after acidification[116]. These new absorption bands may lead to increased device efficiency. As is shown in Figure 21, the self-doped form of PTEBS appears green and can been dedoped by basic solution or water. The dedoped form of PTEBS returns to the orange color.

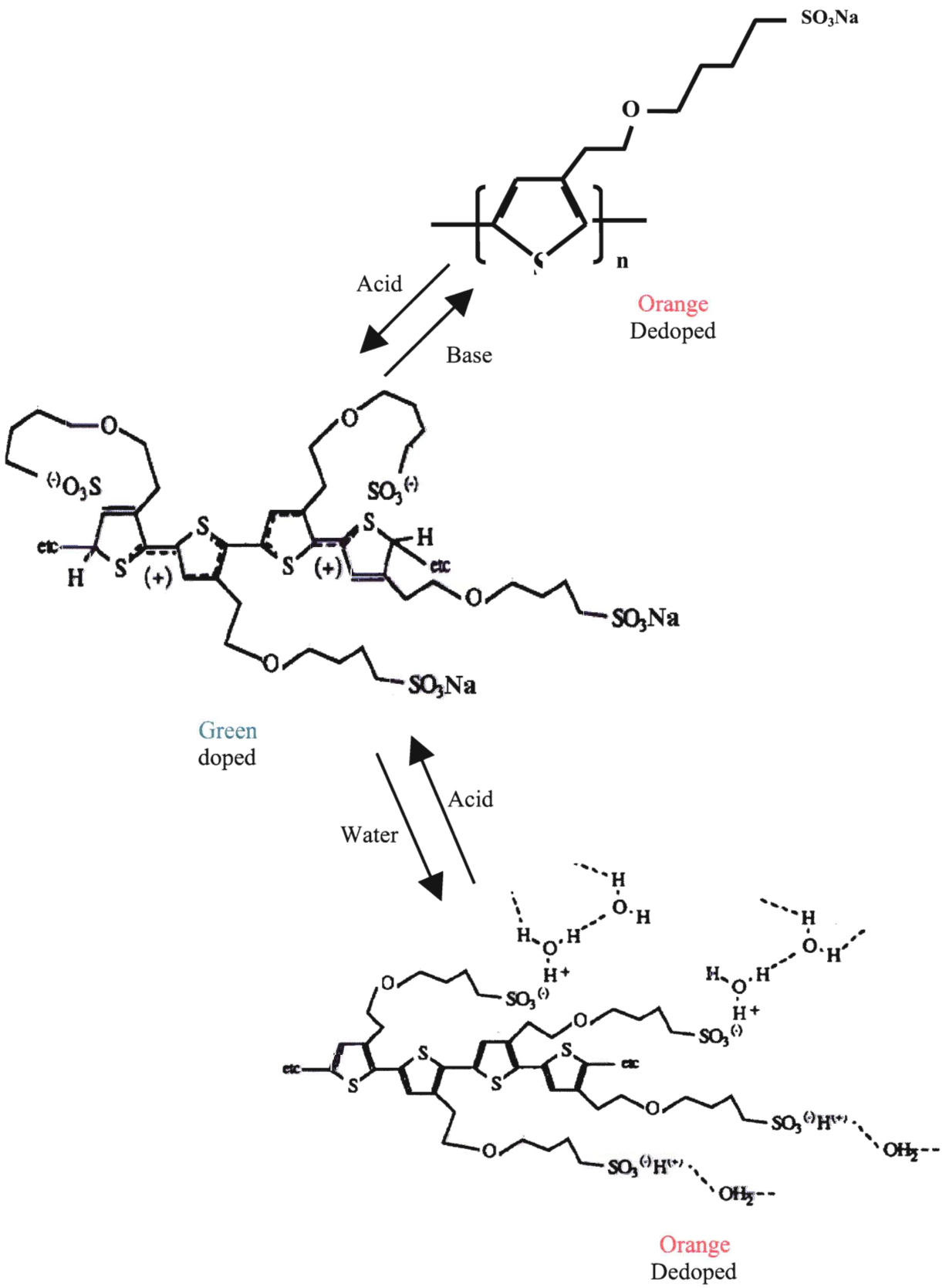

Figure 23 Self doping and dedoping mechanisms

Patil et al.[121, 123] and Ikenoue et al.[122, 124] have reported that the self-doped polymers with high π-system electrons, such as P3-TPSH, are reversibly electrochromic from orange to green in conjunction with water absorption/removal and the redox process. In their experiments, the orange color of the P3-TPSH film was regenerated by exposing P3-BTSH film to water vapor. In addition, the thorough removal of water from the film by thionyl chloride and concentrated sulfuric acid[123] reversed the process and turned the film green. The polymeric acid is very hygroscopic and thus the film will absorb the vapor (H_2O) from the air to form a layer of water that coats the surface[124].

A similar phenomenon has been observed in the doped acidic PTEBS films from both PTEBSNa and PTEBSH. Due to the incorporation of H^+ from H_2O into the polymer side anion, the polymer was dedoped with color converting from green to orange. When exposed to HCl vapor, the film was again doped by the acid, which accounts for the regeneration of green. Attempts to keep the green film from being dedoped by water vapor in the air under vacuum at 80°C were successful although, efforts to dehydrate the orange film by utilizing the same vacuum condition failed. However, HCl vapor can be used to dehydrate the films and remove sodium by cation exchange and acid doping. In the PTEBSH solution, the color change from green to orange with the water content has also been observed. PTEBSH was also obtained via cation-exchange treatment from the sodium salt form using Amberjet 1200(H) ion exchange resin. Following the removal of sodium, the original orange solutions turned green. However, it changed back to orange when diluted with DI water or staying in the air for a few days. The reason for the appearance change with water treatment can be explained by the mechanism discussed in

the film above. However, Figure 18 shows that the absorption in red-IR band has completely disappeared in the solution after being settled in the air for a few days while those in the film remained as shown in Figure 20. One possible reason is that the film absorbed the water vapor and formed a layer that prevents the incorporation of more water inside. Therefore, the inner part of the film is still doped by the HCl causing the higher absorption in the red-IR band.

3.2 TiO_2

Titanium Dioxide (TiO_2 or titania) is inexpensive, chemically inert and non-hazardous. It has found application in pigments, photocatalysis, oxygen sensors and antimicrobial coatings and has three crystal structures: rutile, anatase and brookite[125]. In this work, we used nanoparticle titania with an average particle size of about 30 nm as the electron acceptor material. The titania is degussa P25 powder consisting of 70% anatase and 30% rutile. TiO_2 powder is first suspended in deionized water or acetic acid (pH 3-4) and then sonicated to form a homogenous suspension. The TiO_2 films are made by spin coating onto the fluorine doped tin dioxide (FTO) twice at 2000 rpm to a thickness of about 1.5 μm. The films are then sintered at 500 °C for one hour. This high temperature treatment of the TiO_2 film has two effects. First, it enhances the electronic contact between the TiO_2 particles and FTO electrode. Second, it results in a porous nanocrystalline network of interconnected TiO_2 particles[126].

Figure 22 shows the Scanning Electron Micrograph (SEM) of the porous nanocrystalline TiO_2 film at a magnification of 100,000X. As is shown in Figure 22, the pure TiO_2 film is made of loosely packed particles. The average particle size is ~30 nm

with a distribution range from ~20 nm to ~50 nm. The film has a high porosity with an average pore size of 50 nm. The pore size ranges from ~20 nm to ~100 nm. The high porosity enhances the surface area of titania film by around 1000 times[127]. Figure 22 shows the absorption spectrum of a thin TiO_2 film, in which no light absorption is observed in the visible region. The energy band gap of around 3.2 eV for TiO_2 is obtained from the absorption onset (385 nm, shown in Figure 23). This permits the sunlight to pass through and then be absorbed by the polymer. The X-ray diffraction (XRD) pattern of nanocrystalline TiO_2 is shown in Figure 24, and shows that the crystal structure consists of primarily anatase particles. In the charge separating devices such as organic solar cells, it is easier to form highly porous nanostructures with large surface areas from anatase particles and therefore the anatase structure plays a critical role[128]. In solar cells, the TiO_2 acts as electron acceptor and has an electron mobility of 0.1 cm^2/Vs[14]. The energy levels of the conductance and valence bands are – 4.2 eV and – 7.4 eV, respectively.

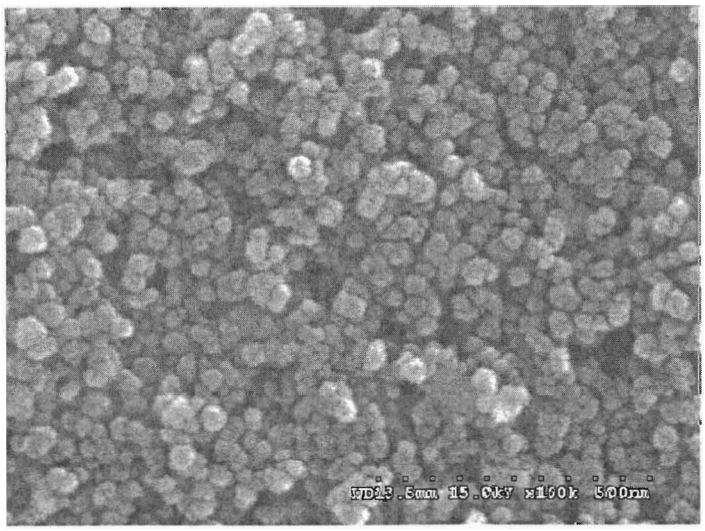

Figure 24 Scanning Electron Micrograph (SEM) of the porous nanocrystalline TiO_2 film at a magnification of 100,000X.

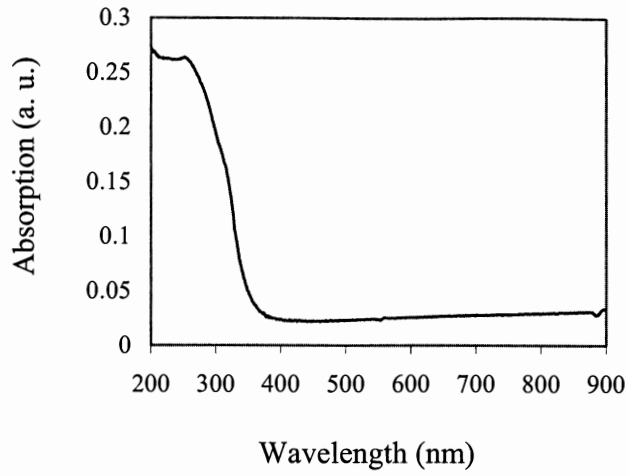

Figure 25 Absorption spectrum for TiO_2 layer

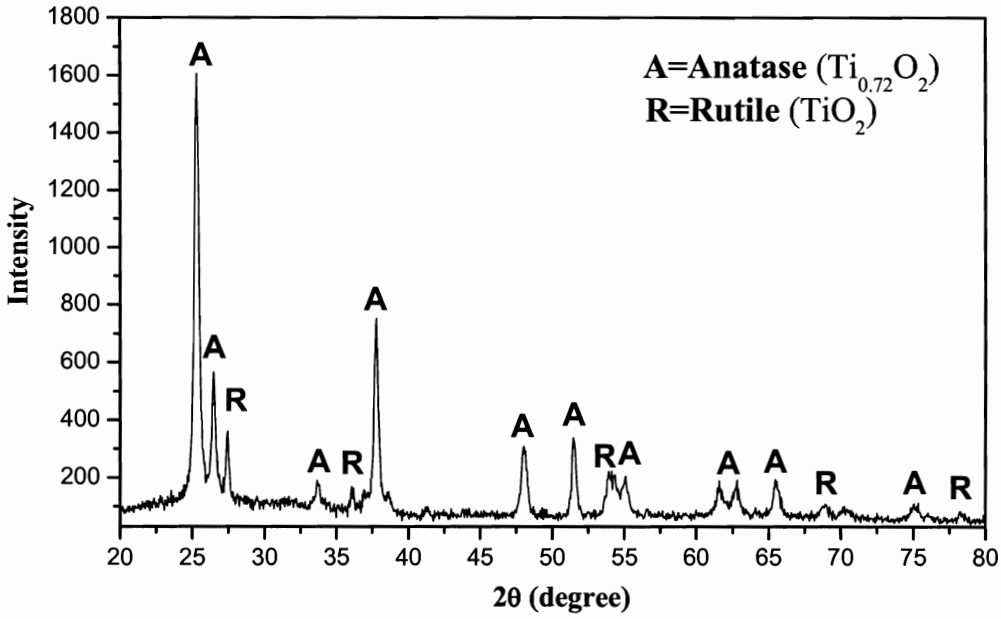

Figure 26 XRD – pattern of sintered nanocrystalline TiO_2

3.3 Electrode Materials

Electrode contacts allow unobstructed charge transport between the photovoltaic cells and an external load. The contacts must not cause a loss of the majority charge carriers in the adjacent semiconductor material. The work functions of the electrode materials are very important in organic photovoltaic devices because in conjunction with the LUMO/HOMO of a polymer and the Fermi level of a semiconductor nanomaterial, they determine whether the electrode contact is an ohmic or a Schottky contact. Generally, an electrode material with a small work function forms an ohmic contact to a p-type semiconductor such as polymers (donor). On the other hand, an electrode material with a large work function makes ohmic contact to an n-type semiconductor such as nanomaterials (acceptor).

In organic photovoltaics, the top electrodes are usually metals including calcium (Ca), Indium (In), silver (Ag), aluminum (Al), chromium (Cr), copper (Cu), gold (Au), and platinum (Pt) etc. The work functions of the typical metals are shown in Table 6.

Table 6 Work functions (eV) of commonly used top electrode materials

	Ca	In	Ag	Al	Cr	Cu	Au	Pt
Work function /eV	2.87	4.12	4.26	4.28	4.5	4.65	5.1/5.2	5.65

The metalization techniques include e-beam evaporation[129], thermal evaporation[26] and sputter coating[14-16, 18]. Krebs et al.[129] reported that the direct aluminum cathode deposition onto the active layer by e-beam evaporation led to devices with very poor performance. However, the thermal evaporation of the aluminum improved the photovoltaic efficiency by an order of magnitude for the solar cells with a

configuration of ITO/MEH-PPV/C_{60}/Al. The thicknesses of the top electrodes range from 10 nm to 200 nm[18, 29, 72, 130, 131].

The bottom electrode is transparent and is deposited onto a glass or plastic substrate. Indium tin oxide (ITO) and fluorine doped tin dioxide (FTO) are commonly used as the transparent conducting oxide (TCO) and both of them are commercially available.

Table 7 Work functions (eV) of commonly used bottom electrode materials

	FTO	ITO
Work function /eV	4.4	4.4-4.7

ITO coated glasses are widely used in organic light emitting diodes (OLEDs) and organic photovoltaics (OPV). The ITO substrates have low resistance (R_s = 8 – 12 ohms)[17, 26], high work function (4.4 – 4.7 eV)[132, 133] and high transmittance of more than 80% in visible spectrum[134]. ITO surface quality such as surface defects and traps, carbon contamination, and surface dipoles affects solar cell performance significantly[2]. Various surface treatment techniques, such as plasma pretreatment[135, 136], soaking the ITO in acids or bases [137] and UV ozone treatment[138], have been reported to improve the interfaces for the solar cell performance. In addition, the sides of the ITO substrates need to be etched off in acids such as HCl and HF to prevent the shorting between the top electrodes and ITO[139].

However, the indium tin oxide (ITO) coated glass that is widely used for polymer-based solar cells is expensive. In addition, the indium diffuses into the polymer easily and its work function can change depending upon the cleaning process[140]. Fluorine tin

oxide (FTO), a less expensive alternative with lower work function, is extensively being used as the electrode in dye sensitized TiO_2 solar cells[68, 141]. In addition, polymer LEDs using FTO and other TCOs as the bottom electrode have been reported as alternatives to ITO [140, 142]. FTO coated glass has recently been explored in polymer based solar cells[14-16, 18, 80].

Details of the comparison of fluorine tin oxide and indium tin oxide as the transparent electrode for P3OT/TiO_2 Solar Cells was demonstrated by Qiao et al[17]. The experimental results showed that FTO is a better electrode than ITO in the P3OT/TiO_2 composite solar cells when we use a high work function metal such as gold as the back electrode. A higher open circuit voltage of 0.65V has been obtained for FTO devices. The MIM model can be used in explaining the origin of higher V_{OC} in FTO devices (as discussed in Chapter 8). In addition, this may lead to lower cost processing for organic polymer solar cells.

Interfacial layers have been used between the active layers and the electrodes to improve the efficiencies of polymer solar cells. The use of LiF as an interface layer between the photoactive material and an aluminum electrode has been reported to reduce the interface barrier and improve the energy conversion efficiencies in MDMV-PPV/fullerene solar cells[143, 144] by improving the contact between the active layer and the top electrodes. For the bottom electrode such as ITO, PEDOT:PSS (work function: 5.1 – 5.2 eV) has been investigated to minimize the ITO roughness, prevent the degradation of the polymer, and subsequently improve the electric contact to the polymer[145].

In this work, Fluorine doped tin dioxide (FTO) coated glass squares (2.5 cm x 2.5 cm) were used as bottom electrode. The FTO coated glass is purchased from Hartford Glass Co. Inc. and has a resistance of 12.5-14.5 ohms/square and layer thickness of 400 nm. The substrates were cleaned in ultrasonic baths first with acetone and then with deionized water. Sputter coated gold is used as the top electrode with a thickness of 50 nm.

Chapter 4 PTEBS/TiO_2 Bilayer Solar Cells

In order to determine whether or not the PTEBS polymer has the photovoltaic characteristics required for solar cell applications, the first configuration of PTEBS/nanocrystalline TiO_2 photovoltaic devices investigated is a bilayer structure consisting of two distinct layers: a PTEBS polymer layer (donor) and a TiO_2 layer (acceptor). The cells were made using a modified doctor blade technique. The polymer was dropped onto a TiO_2 nanocrystalline film and then a clean glass rod was repeatedly swept across the polymer as it dried on a heating plate at about 50 °C. The devices showed an open circuit voltage of 0.81 V, a short circuit current density of 0.35 mA/cm^2, a fill factor of 0.4, and an energy conversion efficiency of 0.13%. The water-soluble polythiophene showed significant photovoltaic behavior and the potential for use in solar cells.

4.1 The bilayer configuration

In photoconducting polymers including PTEBS, photo-generated excitons are strongly bound and resist dissociation into separate charges. Furthermore, these materials generally suffer from low charge mobility and short exciton diffusion lengths[67]. Therefore, the performance of the solar cells made from homogenous polymer layers has been limited. This problem has been resolved in part by first making a porous TiO_2 layer and building a bilayer heterojunction structure. The TiO_2 layer has a binary function in the devices. First, it provides a highly porous TiO_2 nanocrystalline film that helps to form a good thin film of PTEBS by compensating for the effects of low viscosity and

high surface force. Second, it generates sites for phase separation between the polymer and TiO_2. In the first phase of this research, we fabricated bilayer heterojunction solar cells using a water-soluble thiophene polymer (Sodium poly[2-(3-thienyl)-ethoxy-4-butylsulfonate]) [PTEBS] as the electron donor and TiO_2 as the electron acceptor. The device configuration was Glass/FTO/TiO_2/PTEBS/Au and is shown in Figure 25.

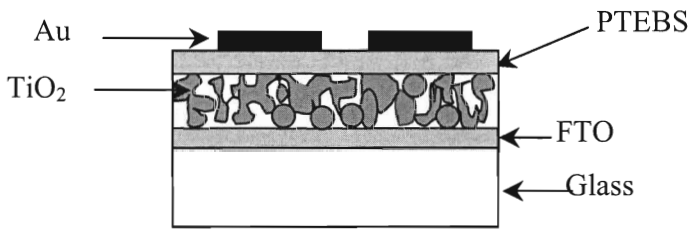

Figure 27 Schematic of Glass/FTO/ TiO_2/polymer/Au solar cells

4.2 Device fabrication

To make the TiO_2 films, an anatase TiO_2 powder was first suspended in acetic acid (pH 3-4) and then stirred and heated for three hours. The TiO_2 films were made by spin coating onto the FTO twice at 2000 rpm. In our experiments, devices made with a single TiO_2 layer tended to develop shorts between the electrodes and therefore two layers of TiO_2 were deposited to prevent shunting. The TiO_2 was then sintered at 500 °C for one hour. This high temperature treatment of the TiO_2 film has two effects. First, it enhances the electronic contact between the TiO_2 particles and FTO electrode. Second, it results in a porous nanocrystalline network of interconnected TiO_2 particles[126].

Arango et al. used atomic force microscopy (AFM) of sintered nanocrystalline TiO_2 layers to show that their films had an average particle size of 80 nm and pore diameters of more than 20 nm[67]. This pore diameter is large enough for the polymer to penetrate into the film. In our work, SEM was used to reveal a TiO_2 nanocrystalline film made of loosely packed anatase particles (see Figure 26). The average particle size is ~30 nm with a distribution range from ~20 nm to ~50 nm. The film has high porosity with an average pore size of 50 nm. The pore size ranges from ~10 nm to ~100 nm.

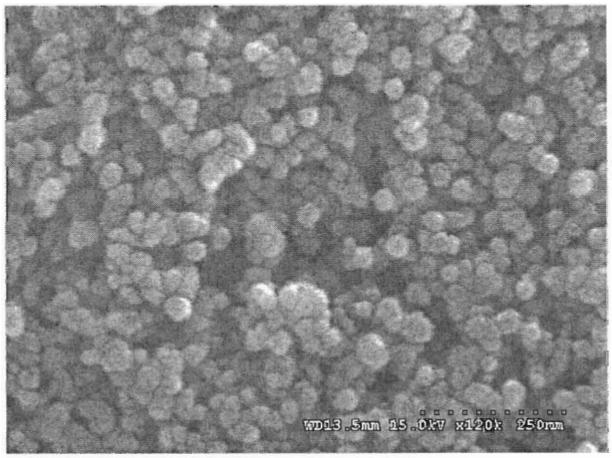

Figure 28 Scanning Electron Micrograph (SEM) of the porous nanocrystalline TiO_2 film at a magnification of 120,000X.

The thiophene polymer (PTEBS) was dissolved in deionized (DI) water to a concentration of 1%. A few drops of dimethylformamide (DMF) were added in order to enhance dissolution. The solution was stirred for two days and then left for 24 hours to allow undissolved particles to settle out.

Spin coating the polymer film is difficult due to the low viscosity of the water solution. Instead, a variation of the doctor blade technique was employed. The TiO_2 coated substrate was placed on a 50 °C heating plate. The polymer solution was dropped onto the TiO_2, and a clean glass rod was swept back and forth across the polymer film until it dried. One of the many benefits of the water-soluble polymer is that this can be done in the open atmosphere without using a fume hood or a glove box. The sample was then further dried in a vacuum oven at 150 °C overnight to remove any remaining water. Finally, a mask was applied to the sample to define a 2 mm × 5 mm device area and 50 nm of gold was sputter coated onto the polymer to serve as the electrode.

4.3 Device characterization

The devices were tested in the dark and under AM1.5 illumination with an intensity of approximately 80 mW/cm^2 through the FTO electrode. The current density-voltage (J-V) curve was measured using a Keithley 236 source generator by varying the voltage from –3 V to 3 V in 0.04 V steps across the FTO and gold electrodes. The device has a rectification ratio of more than one order of magnitude in the dark, indicating diode behavior (Figure 27).

Figure 28 shows the linear current-voltage curve in the light in 4^{th} quadrant. This indicates a short circuit current density of 0.35 mA/cm^2 and an open circuit voltage of 0.81 V. From the curve in Figure 28, we calculated a fill factor (*FF*) of 0.40 and an energy conversion efficiency of 0.13%.

The PTEBS used here is the low MW polymer. As is stated in chapter 3, the HOMO level is estimated to be between -4.7 eV and -5.1 eV. The optical gap of 2 eV results in a LUMO level between -2.7 eV and -3.1 eV.

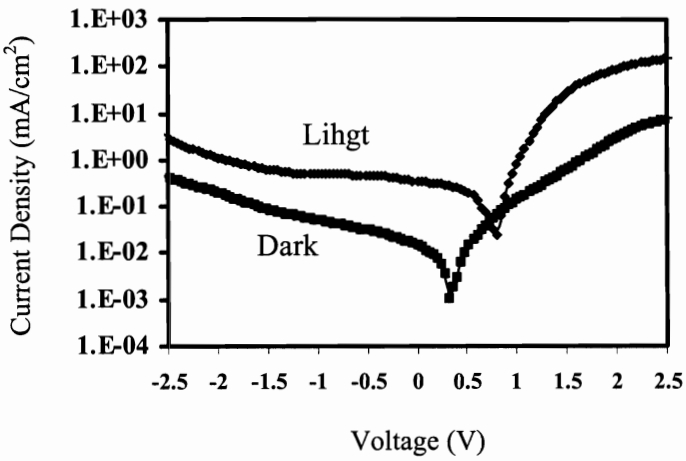

Figure 29 Current density vs applied voltage of the devices tested under AM1.5 illumination on semi-log scale

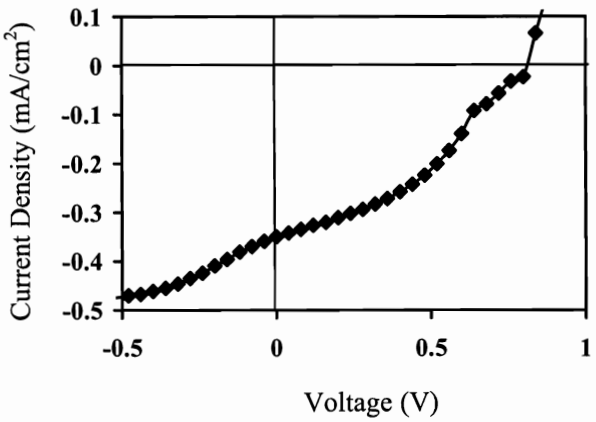

Figure 30 The linear J-V curve in the 4th quadrant under 80 mW/cm^2 AM1.5 illumination.

Interestingly, devices fabricated at room temperature show limited photovoltaic behavior, but devices fabricated on a 50 °C hot plate performed well. This difference is not yet fully understood, but other studies have shown that solvent evaporation rates can have a significant influence on the performance of the devices due to changes in film morphology[66, 146]. Another possibility may be related to the solubility of the TiO_2. Under standard conditions, the slowly evaporating water may interfere with the TiO_2 nanocrystalline network and therefore inhibit the electron transport path in the completed devices. However, at 50 °C, the water evaporates much more quickly and does not have time to destroy the TiO_2 nanocrystalline structure.

Chapter 5 Optimization of bilayer devices

In the previous chapter, a bilayer structure PTEBS/TiO_2 solar cell has been successfully fabricated by using a variation of the doctor blade technique. However, sweeping a glass rod across the polymer solution on top of TiO_2 is hard to control and can easily destroy the TiO_2. Therefore, further research has been done to optimize the bilayer solar cells by altering the TiO_2 thicknesses and investigating different fabrication techniques.

5.1 TiO_2 thickness

The pretreatment and cleaning of the FTO substrates are the same as described in Chapter 4. The basic device configuration is shown in Figure 25.

To make the TiO_2 films, an anatase TiO_2 powder was first suspended in deionized water to a concentration of 30% by weight and then sonicated for three hours. The TiO_2 films were made by spin coating onto the conductive FTO layer of the substrates. The TiO_2 films were then sintered at 500 °C for one hour.

An Ambios XP-1 surface profiler was used to measure the exact film thickness. Part of the TiO_2 film was removed in order to measure the height difference between the top of the film and the substrate. Figure 29 shows the surface scan of a TiO_2 film on a FTO substrate. The film thickness is about 500 nm. The profiler scans at a speed of 0.03 mm/second with a scanning length of 0.5 mm. The typical width of the removed part of the film was 80 μm.

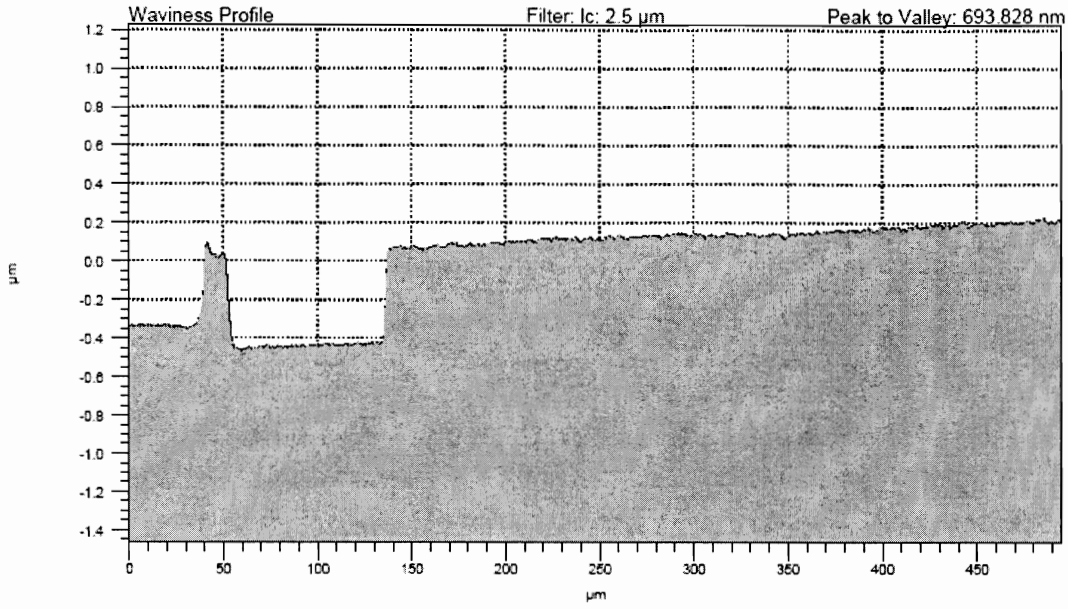

Figure 31 Surface scan of a TiO_2 film on a FTO substrate

The thickness of the TiO_2 layers was altered by changing one of several parameters: spin coating speed, suspension concentration, and number of coats. The top curve in Figure 30 shows the film thickness produced by spin coating a single layer at different speeds. Generally, higher speed gave rise to thinner layers. In each experiment represented in the Figure 30, the samples were spin-coated in two 40 second time steps. The speed of the first time step is given in figure 30. In each case, the second step was performed at 2000 rpm for 40 seconds. As seen in the Figure 30, the film thickness produced by spin coating at less than 700 rpm decreases as the speed becomes lower. In these cases, it is possible that wet solution remained on the substrates before the second step (2000 rpm) took effect. Therefore, the thickness depended more on the second step.

In order to fabricate TiO_2 films thinner than 1 µm, it was necessary to dilute the 30% concentration by adding more DI water. Figure 30 also shows the effect of

suspension concentration. The 30% solution is represented in the top curve (■). This solution was then diluted to less than 20% by weight (▲ in Figure 30) and a new set of experiments was performed. The less concentrated solution resulted in thinner layers.

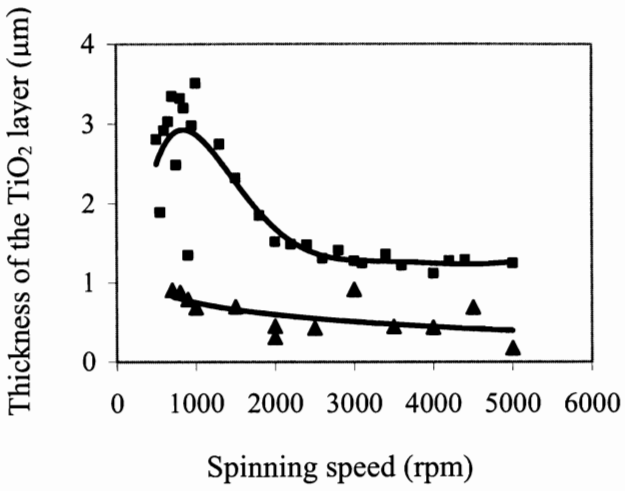

Figure 32 The dependence of the thickness of TiO_2 on the initial spin coating speed from the solution with a concentration of 30% (■ black squares) and less than 20% (▲black triangles).

In order to get the samples thicker than 3.5 μm from the 30% solution, the TiO_2 must be spin coated two or more times. Obviously, increasing the number of coats led to thicker layers. Table 8 shows the spinning methods used to make the exact thickness of TiO_2 layers from different number of coatings with different spinning speed.

Table 8 Spinning methods used to make the exact thickness of TiO_2 layers from different number of coatings with different spinning speed. (Note, (#) means one coating spin-coated at # rpm; ($\#_1/\#_2$) means one coating spin-coated in two 40 second time steps first at $\#_1$ rpm and tthen at $\#_2$ rpm.)

Spinning methods with speed (rpm) from solution of 15 mg TiO_2 / 47 ml DI water	Thickness (μm)
(950) – (950/2000)	4.11
(450/2000) – (450/2000)	4.36
(450/1500) – (500/2000)	4.66
(850) – (850/2000)	4.75
(2000) – (2000) – (4000)	5.46
(1500) – (2000) – (2000)	5.65
(1500) – (1800) – (2000)	6.20
(1500) – (3000) – (3000) – (4000)	6.54
(1500) – (1500) – (3000)	6.87
(1500) – (1800) – (4500)	6.95
(850) – (1000/2000) – (1500/2000)	7.02
(1000) – (1000) – (1000)	7.94
(1000) – (1000) – (1000)	8.08
(950) – (950/2000)	4.11
(450/2000) – (450/2000)	4.36
(450/1500) – (500/2000)	4.66
(850) – (850/2000)	4.75
(2000) – (2000) – (4000)	5.46
(1500) – (2000) – (2000)	5.65
(1500) – (1800) – (2000)	6.20

5.2 Fabrication technique

The concentration of thiophene polymer (PTEBS) dissolved in deionized (DI) water was increased from 10 mg/ml to 15 mg/ml. A few drops of ammonium hydroxide were added in order to enhance dissolution. The solution was stirred for two days before being used. The influence of the solvent on the performance of solar cells has been investigated by several groups[66, 120] and it has been found that by dissolving the polymer in the optimal solvent, extended polymer chains can be formed. When these

solutions are then cast into thin solid films, the chains remain extended. As reported by Shi et al.[120], the effect of the solvent is more pronounced in high concentration solutions than in diluted solutions because of the interchain interactions. However, as stated before, spin coating the polymer film is difficult due to the low viscosity of the water solution. Therefore, using a strong PTEBS solution such as 15 mg/ml concentration, 300 ml of PTEBS solution was evenly drop cast on top of the TiO_2 layer and then dried on a heating plate at 50 °C. The films dried more quickly at temperatures higher than 50 °C but the film uniformity was not as good and the resulting solar cells did not perform as well. Any excess solution was removed with a pipet during the drying process. Normally, a few visible rings formed in the PTEBS film. It was found that the best results were obtained from devices fabricated in the center ring.

5.3 Device characteristics

The devices were tested in the dark and under AM1.5 illumination with an intensity of approximately 80 mW/cm^2 through the FTO electrode. The current density-voltage (J-V) curve was measured using a Keithley 236 source generator by varying the voltage from 0 V to 1.5 V in 0.03 V steps across the FTO and gold electrodes. Samples with thicknesses in the range of 180 nm ~ 8.08 μm have been fabricated to investigate the dependence of the efficiency on the TiO_2 thickness. Energy conversion efficiencies as a function TiO_2 thickness are summarized in Figure 31. There is an increase in the energy conversion efficiency (η) with the thickness, reaching a maximum value of 0.15% at about 4.17 μm. Above this value, efficiency decreases as the thickness continues to increase. Figure 32 shows the linear J-V curve in the 4th quadrant of a 4.17 μm device under 80 mW/cm^2 AM1.5 illumination. This indicates a short circuit current density of

0.15 mA/cm^2 and an open circuit voltage of 0.84 V. From the curve in Figure 32, we calculated a fill factor (*FF*) of 0.91. An energy conversion efficiency of 0.15% has been obtained.

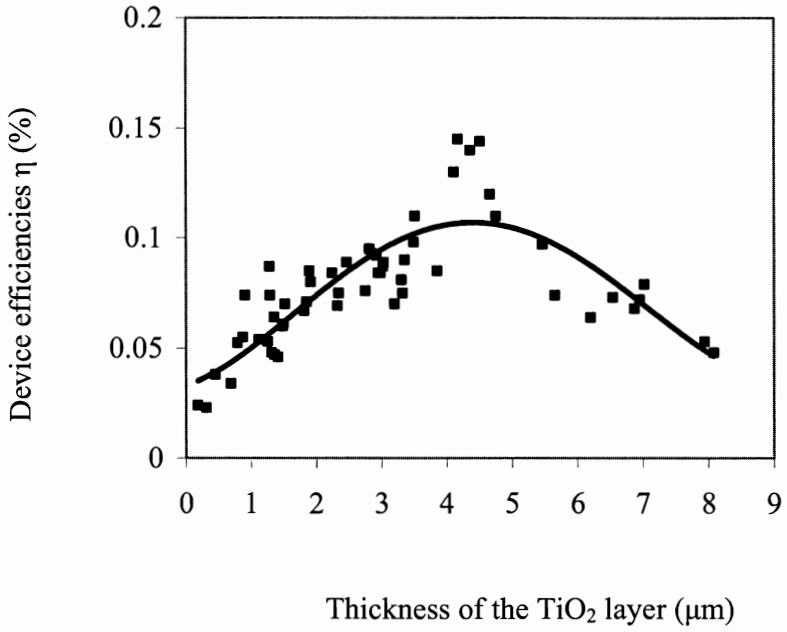

Figure 33 External energy conversion efficiencies versus TiO_2 thickness

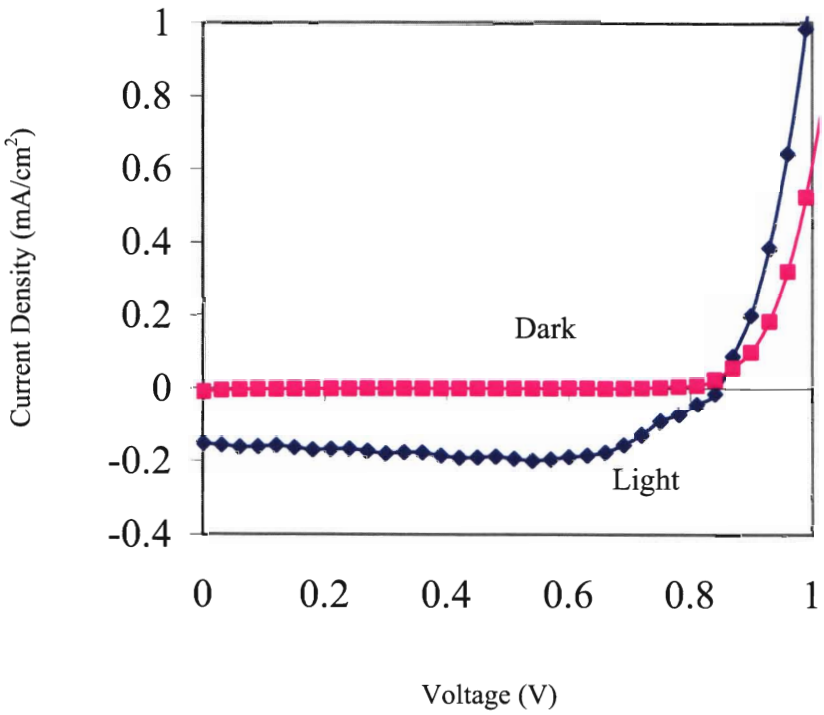

Figure 34 The linear J-V curve in the 4th quadrant in the dark (pink square) and under 80 mW/cm^2 AM1.5 illumination (blue diamond).

For a given TiO_2 layer thickness, there was some variation in efficiency (Figure 31). This may be due to variations in the thickness and film quality of PTEBS film and some initial research on the relation between the photovoltaic results and the thickness of the polymer was also done. It was observed that the amount of polymer dropped on each cell greatly affected both the V_{OC} and the short circuit current density (J_{SC}). Drop casting more than 1000 µl of polymer on the one inch^2 substrates resulted in minimal V_{OC} and J_{SC}. Recombination will be increased (and efficiency decreased) if the polymer layer is too thick. However, the light will not be absorbed completely if the polymer is very thin. Further research needs to be done to give detailed results and find the optimal amount of polymer.

In summary, solar cells with a power conversion efficiency of 0.15% have been fabricated using a water-soluble polythiophene. Very high fill factors (0.91) have also been obtained. The results show that the polymer provides significant photovoltaic response and has the potential to be used as an electron donor in solar cells, replacing solvent-based organic polymers. This may lead to lower costs and environmentally friendly processing for organic polymer solar cells.

Chapter 6 PTEBS/TiO_2 Bulk Heterojunction Solar Cells

This chapter describes the characteristics of PTEBS:TiO_2 composites and their application in solar cells. We observed that the absorption spectrum of the PTEBS:TiO_2 composite is a superposition of the absorption of PTEBS and TiO_2 and that aggregates in polymer films lead to a redshift in the absorption spectrum. Photoluminescence (PL) quenching indicates that the exciton dissociation and charge separation occurs successfully at the PTEBS:TiO_2 (1:1 by weight) interface. Scanning Electron Micrograph (SEM) images show how the PTEBS and TiO_2 are interconnected and form paths to the electrodes to improve charge transport. This enhances the possibility that the separated charges will reach the electrodes before recombining. The devices achieve an energy conversion efficiency of $\eta = 0.056\%$, a short circuit current of $J_{SC} = 0.16$ mA/cm^2, an open circuit voltage of $V_{OC} = 0.85$ V and a fill factor of $ff = 0.33$ under the illumination of 80 mw/cm^2.

6.1 Introduction

As described in Chapter 2, interpenetrating network composites of phase separated electron donors and acceptors have been developed as an approach to overcome the limitations to the MIM and bilayer devices. It has been discovered that charge separation tends to occur at a material interface[28], and therefore nanocrystals can be

blended with the polymers to form heterojunctions[147, 148]. The charge transfer is energetically favorable if the polymer and nanocrystals have different electron affinities[69]. Normally, the nanocrystals serve as the electrons acceptors due to their higher electron affinity while the polymers act as electron donors[12] because the excited electrons will transfer to the conduction band of the nanocrystals. Semiconductor nanocrystals or quantum dots including TiO_2[67, 68], CdSe[69], CdS[69], carbon fullerenes[73, 74], and carbon nanotubes[70-72] have been reported for photovoltaic applications. The external energy conversion efficiencies of the solar cells made from the composite of conjugated-polymer and semiconductor nanocrystals have increased steadily in the past decade[44] and several groups have achieved 5% using carbon fullerenes[82].

6.2 Preparation of samples

The PTEBS was dissolved in DI water at a concentration of 15mg/ml and a few drops of ammonium hydroxide were added for better dissolution. The solution was stirred for three days on a 40 °C heating plate to increase the solubility of PTEBS. The solution turns orange when PTEBS is satisfactorily dissolved. Two composite solution samples were then prepared by adding TiO_2 to the PTEBS solutions. For the two solutions, the concentration of the TiO_2 relative to the PTEBS was 20 wt% (1 PTEBS:0.2 TiO_2) and 100 wt% (1 PTEBS:1 TiO_2). The solutions were sonicated for 4 hours to disperse the TiO_2 powder and prevent the separated powder from aggregating again. A 300 µl solution of TiO_2/PTEBS was drop cast on FTO substrates (2.5 cm × 2.5 cm) until the whole surface was covered. Subsequently, the substrate with the solution on the

surface was moved onto a heating plate and dried. The drying temperature was kept below 260°C to prevent the PTEBS from decomposing. Both the solution and film samples were prepared in air.

6.3 UV-Visible absorption spectrum

The absorption spectra of TiO_2, PTEBS and a PTEBS:TiO_2 composite (1:1 by weight) were measured with a Lambda 40 spectrometer and are shown in Figure 33. The peak and line shape of the absorption in the composite indicate that it is the superposition of the absorption of PTEBS and TiO_2. For wavelengths lower than 400nm, the absorption of the composite has increased compared to the pure PTEBS and a new peak appears at 310 nm due to absorption by the TiO_2. The line shape for wavelengths longer than 400 nm is similar to that of PTEBS, implying that absorption in this range is mainly due to the π-π^* absorption of polymer. This means that no significant ground-state charge transfer or electronic interaction occurs between the two materials in the composite film under steady-state illumination at low intensities[105]. When illuminated in the white light, the photoinduced electrons are expected to transfer from the excited states of PTEBS to the conduction band of TiO_2. This can be demonstrated by the quenching of the photoluminescence in the composite films and will be discussed in the next section.

Figure 33 reveals that with addition of TiO_2, the absorption peak of PTEBS shifts to shorter wavelengths–a shift of 25 nm from 415 nm for pure PTEBS to 390 nm for PTEBS:TiO_2 composite. This can be explained in two ways. First, the absorption edge of TiO_2 around 400 nm increased the composite absorption and shifted the peak. The second may be that the TiO_2 prevents the formation of polymer aggregates in the

composite films. Van Hal et al.[22] reported that increasing the amount of TiO_2 from 1% to 50% in MDMO-PPV solutions caused the shifting of the absorption maximum to shorter wavelengths. Shi et al.[120] has also reported that polymers tend to form aggregates in solutions and solid-state films at high concentration. They observed that MEH-PPV solutions at concentrations of more than 1% lead to the development of strong aggregates in solid-state films. It is generally agreed that aggregates in polymer films lead to a redshift in both absorption and emission spectra[149].

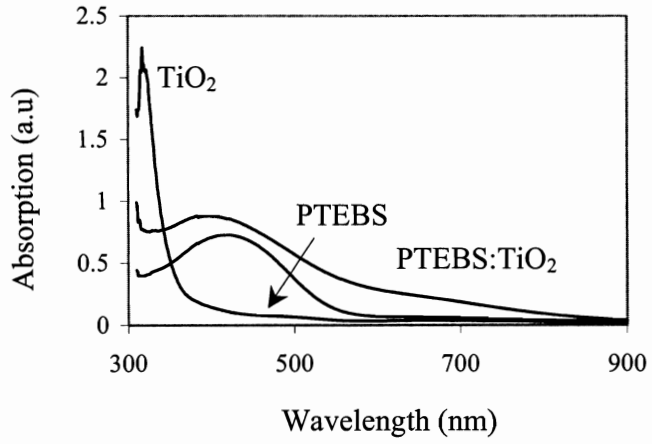

Figure 35 Absorption spectra of PTEBS, TiO_2 and 1:1 (by weight) PTEBS:TiO_2 composite on a FTO glass substrate.

6.4 Photoluminescence spectra

Charge transfer is an important factor for good performance in solar cells and photoinduced charge transfer across the donor-acceptor junctions in composites offers a molecular approach to improving the solar cell efficiency[69]. Photoluminescence (PL) spectroscopy is one method for investigating the efficiency of the exciton dissociation

and separation that occurs at the material interfaces in interdiffused polymer-nanocrystal composites. Because the diffusion range of singlet excitons of most conjugated polymers is approximately 5 ~ 15 nm and their radiative decays take place in the time of 100 ~1000 picoseconds, a large area of nanosize interface in bulk heterojunction needs to be created so that the charge separation occurs faster than the radiative decay[12]. It has been shown[69] that the concentration of the nanocrystals affects the PL spectra and intensity. Photoluminescence occurs as a result of radiative decay. Its efficiency (ϕ) is determined by the fraction of absorbed photos (η) that produce singlet excitons and the probability (ε) that these singlets decay to the ground state via the radiative emission[105]. The expression is defined as:

$$\phi = \eta \cdot \varepsilon$$

Upon the incorporation of nanocrystals, either η or ε decreases due to the ultrafast electron transfer from the HOMO of polymer to the conduction band of the nanocrystals. This has been verified using a microwave conductivity technique[104]. Therefore, PL quenching occurring in the composite is caused by the existence and distribution of nanocrystals in the polymer matrix.

In addition, Salafsky[105] reported that the degree of the photoluminescent quenching is an indication of how well the nanocrystals are mixed in the polymer and the quality of polymer-nanocrystal interface. He presented a simple model explaining that the PL quenching caused by the dissociation of singlet excitons could be expressed as[105]

$$\Gamma = \eta \cdot \kappa$$

where Γ is the possibility of charge separation events of an absorbed photon, η is the possibility of an absorbed photon resulting a state able to produce a singlet exciton and κ is the efficiency of singlet exciton dissociation. Provided that the nonradiative decay caused by conformational defects in the polymer chains is negligible, all the absorbed photons take part in either PL or charge separation.

The PL intensity for the PTEBS/TiO_2 composites was first measured using a 50 mW, 325 nm HeCd laser with spot diameter of 4 mm. Figure 34 shows the PL of three different film samples. The first film was prepared from pure PTEBS, the second from a composite of 20% TiO_2 by weight of PTEBS and the third from a composite of 100% TiO_2 by weight of PTEBS. All of the samples were on glass substrates coated with FTO. The laser was directly incident on the films and the PL was collected from the same side. To simplify the comparison, all the three films are approximately 10 um thick, which is thick enough to absorb nearly all of the light from the excitation laser.

As shown in Figure 34, there is a significant quenching of the fluorescence in the composites as compared to the pure PTEBS. The PL is quenched by a factor of about 5 with the 20% TiO_2. As the concentration of TiO_2 increases to 100%, the PL is further quenched to a factor of about 7. To verify that the quenching resulted from the addition of TiO_2 (and not simply because TiO_2 also has the absorption at 325 nm), we conducted a second set of experiments with a different excitation wavelength where the TiO_2 absorption is negligible. Seven films with different TiO_2 concentrations of 50%, 60%, 70%, 80%, 90%, 110% and 120 % (relative to the PTEBS) have been made. The photoluminescence was measured with Cary Eclipse fluorescence spectrophotometer and is shown in Figure 35. The excitation wavelength is at 430 nm and the scanned

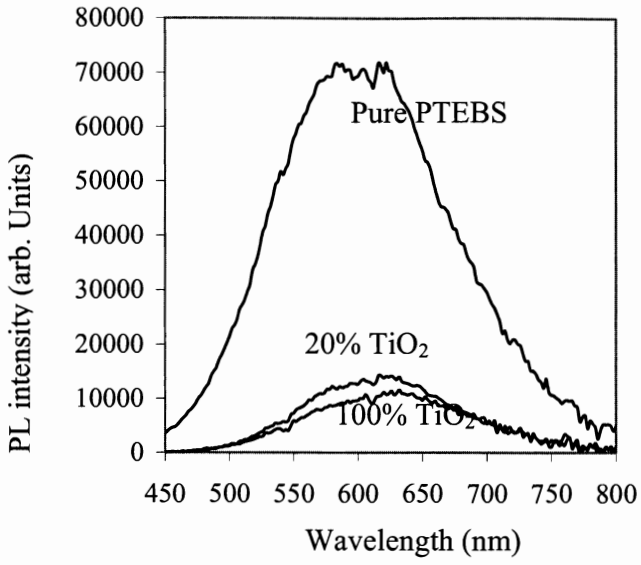

Figure 36 The photoluminescence spectra excited at 325 nm from PTEBS:TiO_2 films for 0%, 20% and 100% TiO_2.

photoluminescence is from 450 nm to 800 nm. Figure 35 shows that the photoluminescence of the samples with TiO_2 concentrations between 50% and 120% has been quenched compared to that of the pure PTEBS. Interestingly, a peak appears at the wavelength of around 588 nm on the fluorescence spectrum. A possible reason for this maybe that the interfaces between the sample and the air and between the sample and the substrate form a cavity making the fluorescence travel through the film and causing stimulated emission. The photoluminescence of solutions with different TiO_2 concentrations was also investigated and the peak was not found, as seen in Figure 36. In addition, the quenching in the solutions is not as significant as that observed in the films. This is easily understood because the TiO_2 nanoparticles in solution are not in close

physical contact with the PTEBS. Other properties such as the scattering by nanoparticle distribution in the solution can also reduce the photoluminescence intensities. Therefore, it is possible that charge transfer from PTEBS to TiO_2 plays a very small role in thequenching of photoluminescence in the solutions.

In the polymer-TiO_2 bulk structures, PL quenching implies that the excitons dissociate and separate successfully at the interface of PTEBS (donor) and TiO_2 (acceptor). The polymer phase in the composites is continuous and forms favorable paths for holes throughout the film. However, charge transfer to the electrodes is still inhibited due to the limited paths for the separated electrons in the composite. This is because only some of the TiO_2 nanocrystals are in physical contact with each other[105], leading to discontinuous paths for electrons. Recombination still occurs when the electrons leave the TiO_2 and re-enter the polymer[69]. As more TiO_2 is added to the polymer, more of the TiO_2 nanocrystals are in physical contact with each other and the PL is the quenched further as charge transfer improves.

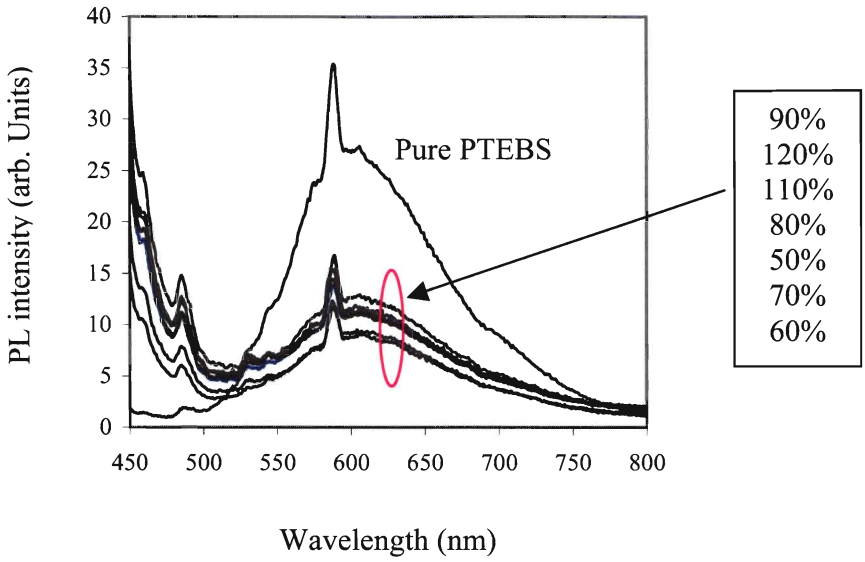

Figure 37 The photoluminescence spectra excited at 430 nm from pure PTEBS and composite PTEBS:TiO_2 films (In the red circle, from bottom to top are 90%, 120%, 110%, 80%, 50%, 70%, 60%).

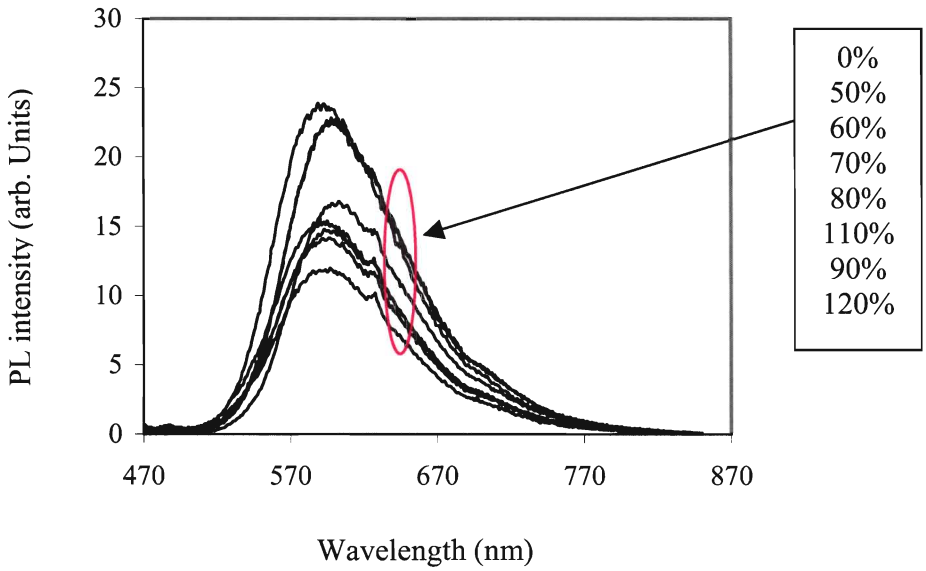

Figure 38 The photoluminescence spectra excited at 460 nm from pure PTEBS and composite PTEBS:TiO_2 solutions (In the red circle, from bottom to top are 120%, 90%, 110%, 80%, 70%, 60%, 50% and pure PTEBS solution).

6.5 Scanning electron micrograph (SEM)

The morphology of the samples was studied using a LEO 440 e-beam writer. Scanning Electron Micrograph (SEM) images of a 20% (1:0.2) composite of PTEBS:TiO_2 and a 100% (1:1) composite of PTEBS:TiO_2 are shown in Figure 37. In the 20% film (Figure 37a), the TiO_2 nanocrystals agglomerated together and formed areas of densely packed TiO_2 bounded by regions of PTEBS. The size of the agglomerates ranges from a few hundred nanometers to micrometers.

Figure 37b shows the image from the 1:1 composite of PTEBS:TiO_2 at a magnification of 500X. Two morphology structures have been demonstrated. From the amplified images at a magnification of 15000X, it can be seen that the structures in Figure 37c and Figure 37d are different. The explanation may be that, as compared to the 1:0.2 PTEBS:TiO_2 composite, part of TiO_2 in the 1:1 composite fully agglomerated on the top and formed crystals as the solution was drop cast and dried on the heating plate.

As the percentage of TiO_2 increases, the size of the TiO_2 agglomerates increases and it is believed that more highly interpenetrated networks of TiO_2 are produced at higher concentrations. These networks form good paths for electrons and may help explain why the solar cells made using the 1:1 ratio of PTEBS to TiO_2 worked much better than the others. These results are consistent with those from CdSe and MEH-PPV composites verified using transmission electron microscopy (TEM)[69].

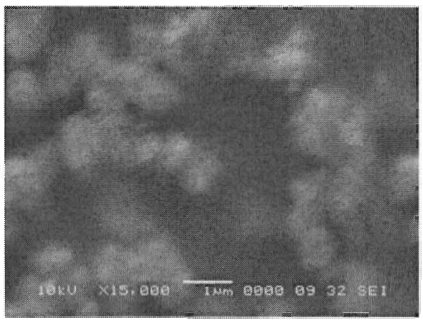

Figure 37a 20% TiO_2

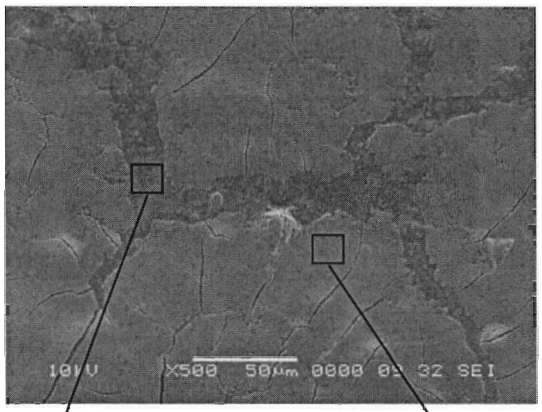

Figure 37b 100% TiO_2

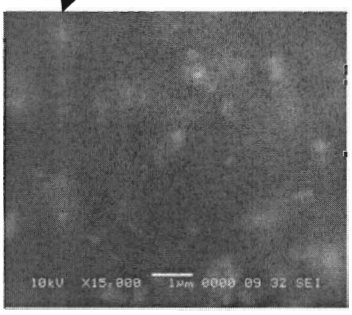

Figure 37c

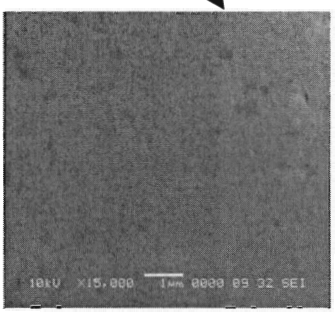

Figure 37d

Figure 39 SEM images of films from (a) pure PTEBS; (b) pure TiO_2; (c) PTEBS:TiO_2 (1:0.2); (d) PTEBS:TiO_2 (1:1); (e), (f) amplified SEM for PTEBS:TiO_2 (1:1).

6.6 Bulk heterojunction solar cells

A Glass/FTO/TiO_2:PTEBS/Au photovoltaic device structure was tested and is shown schematically in Figure 38. The active layer is composed of an interpenetrating network of nanocrystalline TiO_2 and PTEBS (a bulk heterojunction). The gold electrode was then sputter coated. The current density-voltage (J-V) characteristics of the solar cells made from 1:1 PTEBS:TiO_2 composite were tested using a Keithley 236 Source Generator by sourcing the voltage from – 2 to + 2 V in 0.1V steps both in the dark and under illumination. A solar simulator was used as the visible light source to measure the efficiency. The devices were illuminated from the glass side due to the high transparency of the glass coated with FTO at the intensity of approximately 300 mW/cm^2 measured using Spectra-Physics Model 407A power meter.

The current density-voltage (J-V) characteristics of the devices are shown in Figure 39. The devices achieve an energy conversion efficiency of $\eta = 0.056\%$, a short circuit current of $J_{SC} = 0.16$ mA/cm^2, an open circuit voltage of $V_{OC} = 0.85$ V and a fill factor of $ff = 0.33$. However, the solar cell performance is not stable. Of the cells that produced a notable voltage, it was interesting that the voltage slowly increased with time, as if electrons and holes were being slowly built up on the surface of the cell.

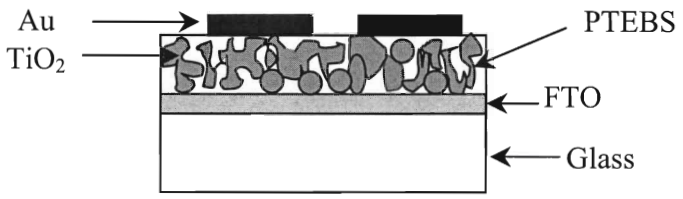

Figure 40 Schematic of Glass/FTO/ TiO_2:PTEBS/Au solar cells.

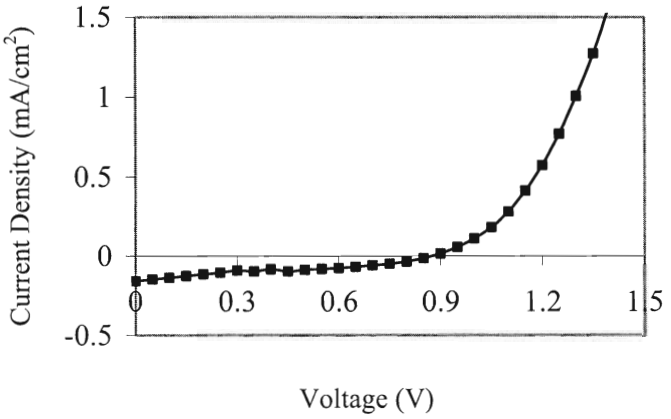

Figure 41 The linear current density–voltage (J-V) curve under the illumination of 80 mW/cm^2.

The bulk heterojunction device performance we achieved above is not as good as those from bilayer cells, which can be explained by a number of reasons. The water solution of PTEBS is not viscous enough to form a homogeneous film on a smooth FTO substrate. In addition, the TiO_2 was sintered at a temperature less than 260 °C because

PTEBS will decompose if the temperature is higher than 260 ^{o} C. Furthermore, due to the PTEBS addition to TiO_2 solution, part of the TiO_2 nanoparticles were not in contact to form continuous path for electron transport. Efforts in improving the fabrication process to overcome the ugly PTEBS film formation on smooth FTO has been done and will be presented in the next chapter.

Chapter 7 Hybrid of bilayer and heterojunction PTEBS/TiO_2 solar cells

The hybrid of a bilayer and a bulk heterojunction structure seems to be a solution to the difficulty of formation of PTEBS on a smooth substrate. A thin buffer layer of pure TiO_2 is first deposited onto clean FTO glass, followed by the drop casting of a blended layer of PTEBS and TiO_2. The "rough" TiO_2 surface will help to form a blended coating and also serve as a hole blocking layer.

7.1 Absorption depth

The absorption depth can be measured using the transmittance spectrum. Figure 40 shows the transmittance spectra from 23 nm, 83 nm and 550 nm thick PTEBS films. At the wavelength of 422 nm, the transmissions are 86%, 72% and 5%, respectively. If we neglect the reflectance, this means about 95% of the 422 nm light can be absorbed at the thickness of 550nm. A thickness of around 550 nm was used to make solar cells in our experiments. Clearly, optimization of the device thickness requires accounting for not only absorption and but also other factors such as carrier recombination and carrier mobility and future designs will include these parameters.

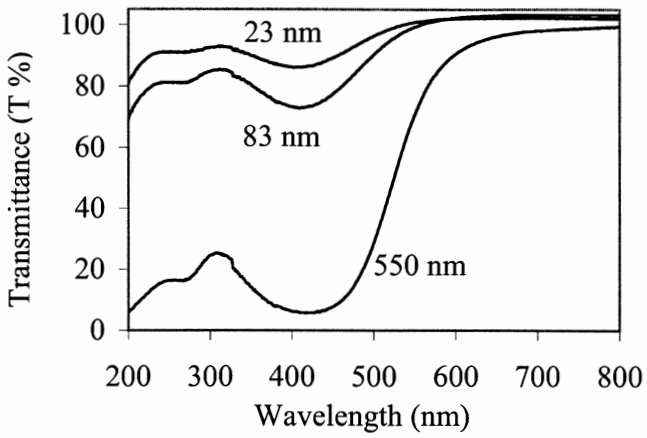

Figure 42 The transmittance of PTEBS films with thickness of 23 nm, 83 nm and 550 nm

7.2 Scanning electron micrograph (SEM)

SEM was performed with a Hitachi S - 4300. Scanning Electron Micrograph (SEM) images of a pure TiO_2 layer, a TiO_2 layer covered with a thin layer of PTEBS and a TiO_2 layer covered with a thick layer of PTEBS are shown in Figures 41 (a), (b), and (c), respectively. As shown in Chapter 3, the pure TiO_2 film is made of loosely packed anatase particles. The average particle size is ~30 nm with a distribution range from ~20 nm to ~50 nm. The film has high porosity with an average pore size of 50 nm. The pore size ranges from ~10 nm to ~100 nm. When a thin film of PTEBS was applied on the top of the pure TiO_2 film, the SEM images appear similar to those of the pure TiO_2 film, as is shown in Figure 41 (b). However, as shown in Figure 41 (c), after a thick PTEBS film was formed on the pure TiO_2 film, the pores of TiO_2 were filled with PTEBS, indicating that PTEBS penetrates into the TiO_2 films. This is in agreement with the results from other research groups[106, 107, 111]. This tells us that the PTEBS penetrates into the nanopores of the TiO_2 films.

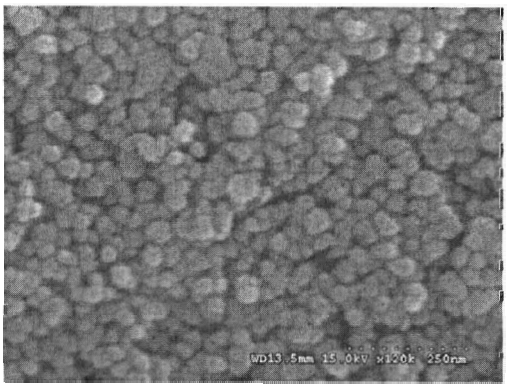

(a)

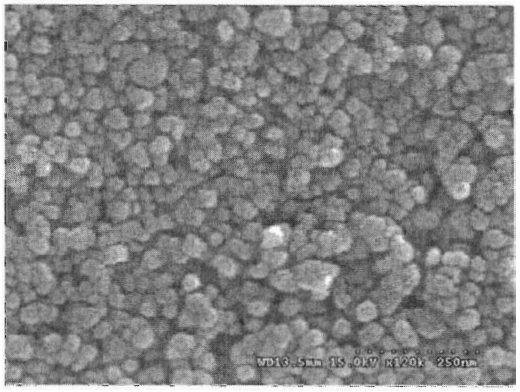

(b)

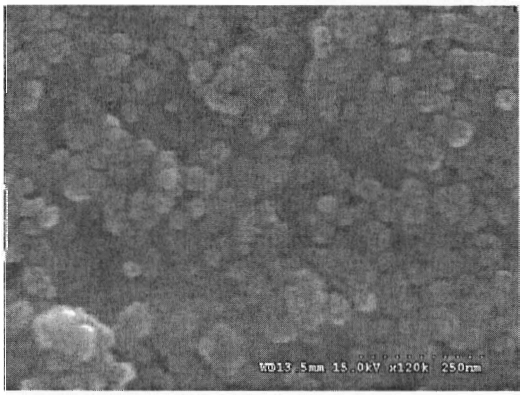

(c)

Figure 43 Scanning Electron Micrograph (SEM) of the porous nanocrystalline TiO_2 film at a magnification of 120,000X. (a) pure TiO_2 layer; (b) TiO_2 layer covered with a thin layer of PTEBS; (c) TiO_2 layer covered with a thick layer of PTEBS.

7.3 Devices and results

Previous chapters have reported on solar cells made using PTEBS in bilayer[18] and bulk heterojunction[14] structures. Contrary to what might be expected, the bilayer devices have yielded higher efficiency. In addition, it is challenging to form uniform thin films of PTEBS or of PTEBS:TiO_2 blends on smooth Fluorinated Tin Oxide (FTO) substrates using the spin coating technique. To resolve these issues, a new combined bilayer/bulk heterojunction device configuration has been developed. In this arrangement (Figure 42), a buffer layer of TiO_2 was deposited on the FTO glass before depositing the PTEBS:TiO_2 blend. Compared to the results[14] we reported previously, the device characteristics have improved significantly. As is revealed from the current density – voltage curve (Figure 43), the open circuit voltage is 1 V and the short circuit current is 0.165 mA/cm^2. The fill factor is 0.84. By calculation from $\eta = (FF \cdot V_{OC} \cdot I_{SC}) / P_{light}$, an external energy conversion efficiency of 0.17% has been achieved.

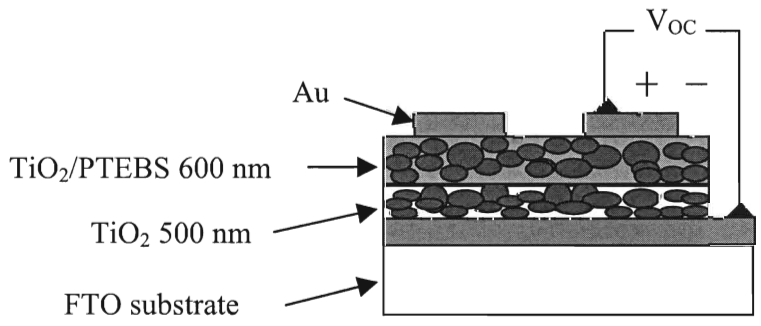

Figure 44 Schematic of Glass/FTO/ TiO_2/PTEBS : TiO_2/Au solar cells.

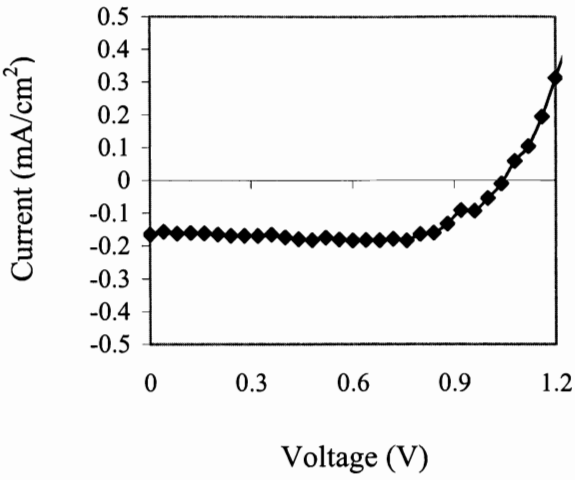

Figure 45 Linear J-V curve under 80 mW/cm^2 illumination.

Chapter 8 Discussion and Analysis

The open circuit voltage, short circuit current, fill factor and energy conversion efficiency are four main parameters for solar cells. These parameters are dependent on not only the material properties, but the device structure as well. In this chapter, the origin of the open circuit voltage and the equivalent circuit have been described and compared with our experimental results.

8.1 Open circuit voltage (V_{OC})

The built-in potential of the thin film photovoltaics is an essential parameter and it has an effect on charge dissociation, charge transport and collection. The built-in potential can be estimated by the open circuit voltage, which underestimates the built-in potential at room temperature and comes close to the correct value at low temperatures[150].

Although the exact origin of the open circuit voltage in bilayer PTEBS / TiO_2 devices is not fully understood, the author has demonstrated[17] that V_{OC} can be estimated by the difference of the work functions of the electrodes in a bilayer P3OT / TiO_2 solar cell. This same estimate may be applied here in a PTEBS / TiO_2 solar cell. In the early research in bilayer PTEBS / TiO_2 solar cells, the highest V_{OC} achieved was 0.84 V. This value nearly matches the difference between the work function of gold ((5.2 eV) (or the HOMO of PTEBS) and the work function of FTO (4.4 eV)[151] (Figure 44a).

In a TiO_2/polymer solar cell, TiO_2 is an n-type semiconductor material and the conjugated polymers including polyaniline, polypyrrole, and several derivatives of polythiophenes and PPV are p-type semiconductor materials. In our devices, the low work function electrode (FTO) serves as anode and the high work function electrode (gold) is cathode. Therefore, as is shown in Figure 44 (b), FTO forms an ohmic contact to TiO_2, and gold also makes an ohmic contact to PTEBS if its HOMO is between 5.2 eV and 5.3 eV. Otherwise, for the HOMO to be between 5.1 eV and 5.2 eV, the gold contact will be a Schottky contact, which is not shown in Figure 44. Similar open circuit voltages have been found in the bulk heterojunction devices.

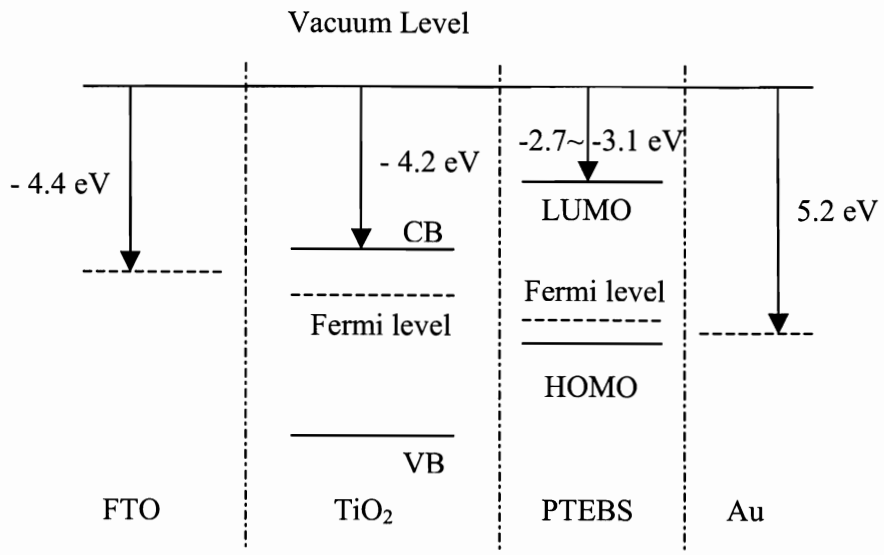

(a) Before making contact

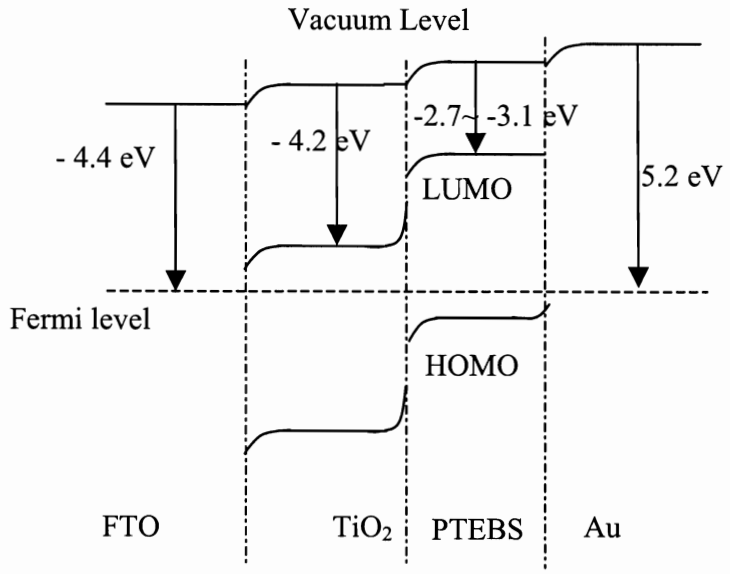

(b) In contact

Figure 46 Schematic energy diagram of an Ohmic contact between FTO and TiO_2 before making contact (a) and in contact (b), CB: conduction band, VB: valence band. The work functions of FTO, TiO_2, gold are 4.4 eV, 4.2 eV and 5.2 eV, respectively.

As noted above, the work function of the gold contact (5.2 eV) [17] is very close to the HOMO level of the polymer and the work function of the FTO (4.4 eV)[151] is close to the conduction band energy of the TiO_2 (CB: 4.2 eV)[65] (Figure 44 a). This makes it difficult to ascertain the influence of the polymer and the TiO_2 on the V_{OC}. In fact, as the research went on, open circuit voltages as high as 1 V were achieved in both the bilayer and bulk heterojunction solar cells. This value is closer to the difference between the conduction band of TiO_2 and the HOMO of PTEBS (instead of the difference between the work functions of the FTO (4.4 eV) and the gold (5.2 eV).

In agreement with this, Brabec et al.[150] investigated the correlation between the open circuit voltage and electron acceptor materials with different acceptor strengths and top electrode materials with different work functions in bulk heterojunction devices. Their results showed that the open circuit voltage of the donor (MDMO-PPV) – acceptor (PCBM) bulk heterojunction devices is determined by the difference between the HOMO level of the donor and the LUMO level of the acceptor. Additional study with PTEBS/TiO_2 devices may be necessary to separate the influences of the electrode materials and the donor acceptor materials on open circuit voltage.

8.2 Equivalent Circuit

In order to better understand our devices, an equivalent circuit analysis has been performed. By using studying this circuit, the influence of the shunt resistance and series resistance on device parameters (open circuit voltage, short circuit current, and fill factor) can be determined.

Figure 45 shows a widely used model for an equivalent circuit of a solar cell. Generally, series resistance results from the limited conductivity of the semiconductor material, the contact resistance between the semiconducting materials and the adjacent electrodes, and the connecting resistance between the electrodes and the external circuit. Shunt resistance (R_{sh}) may be related to the device structure and morphology. For example, shunt resistance will be lowered by the leakage current through the pinholes in the film. The pinholes are correlated to the surface roughness and the debris on the surface or in the film. Recombination of charge carriers in the devices also decreases the shunt resistance when the active films are very thick and the distribution of the nanoparticles in the films is not perfect. Shunt resistance (R_{sh}) and series resistance (R_s) are important for high fill factors.

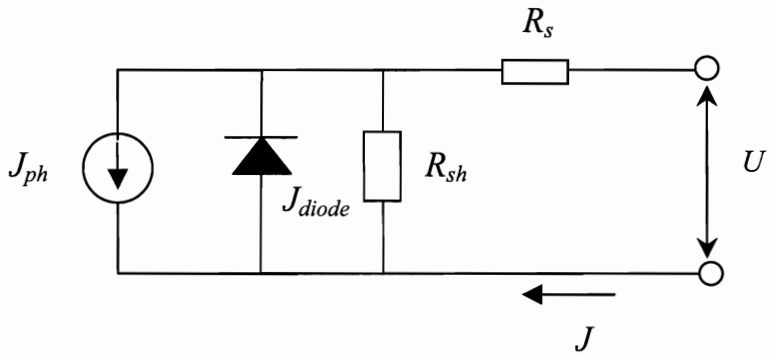

Figure 47 Equivalent circuit for a solar cells

The current-voltage characteristics of a realistic solar cell are then given by:

$$J = J_0\left(\exp(\frac{q}{nkT}(U - JR_sA)) - 1\right) + \frac{U - JR_sA}{R_{sh}A} - J_{ph} \qquad (8.1)$$

The first term is for a diode as described by the Shockley equation, where J_0 is the saturation current of the diode, q is the elementary charge, n is the diode ideality factor, k is the Boltzman constant and T is the temperature. The second term is the current through the shunt resistance R_{sh}. The third term is the photo-generated current (J_{ph}), which is the activity of the solar cells under the illumination. Ideally, R_s and R_{sh} should be 0 Ω and + ∞, respectively.

8.2.1 Influence of shunt resistance

The effect of shunt resistance on the device parameters is analyzed in this section and compared to our experimental results. To simplify the analysis, the series resistance is assumed to be zero.

Figure 46 shows the effect of shunt resistance on open circuit voltage and fill factor as the shunt resistance is varied from 2000 Ω to 10 MΩ. As can be seen, V_{OC} decreases as the shunt resistance decreases. In addition, it can be seen that a low shunt resistance will influence the fill factor by shifting the maximum power point (Figure 46). However, Figure 46 reveals that the short circuit currents do not change with shunt resistance, which means that the influence of R_{sh} on short circuit current is typically negligible.

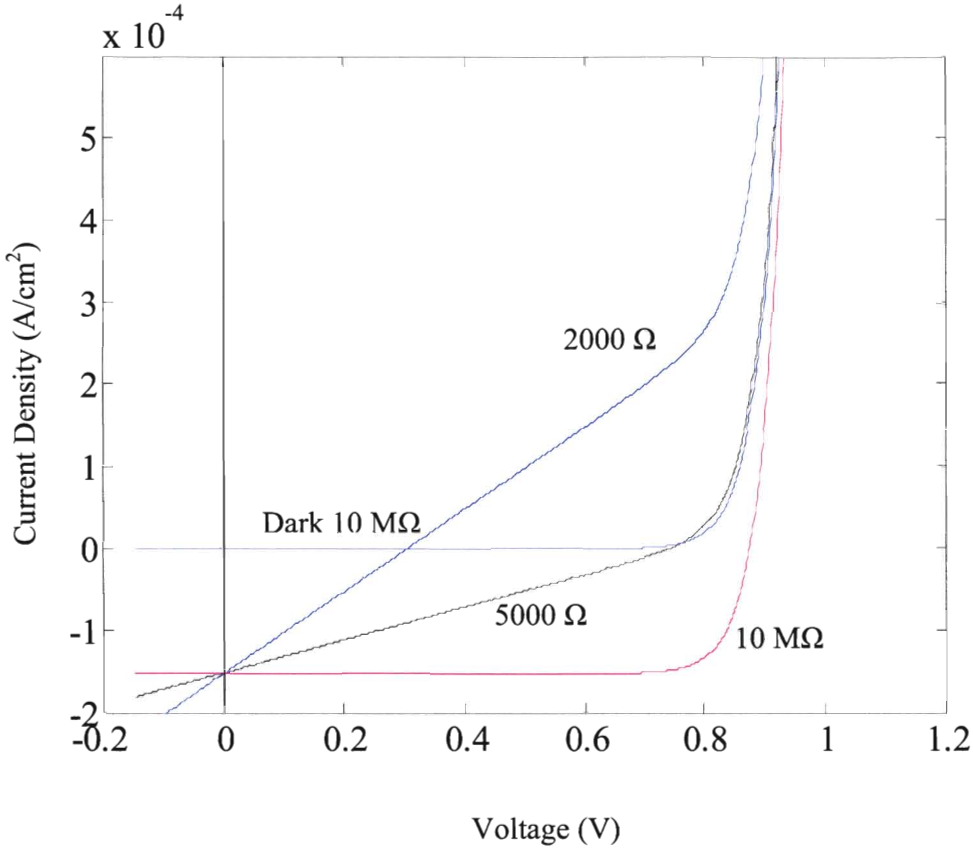

Figure 48 Effect of R_{sh} on the J-V characteristics of a bilayer PTEBS/TiO2 solar cell when $R_s = 0\ \Omega$ and $J_{ph} = 0.152$ mA/cm^2

In Figure 47, the experimental J-V data from a bilayer device has been matched to the model. As can be seen, a shunt resistance value of $R_{sh} = 10$ MΩ provides a good fit to our data implying that this is close to the value of shunt resistance in our solar cells.

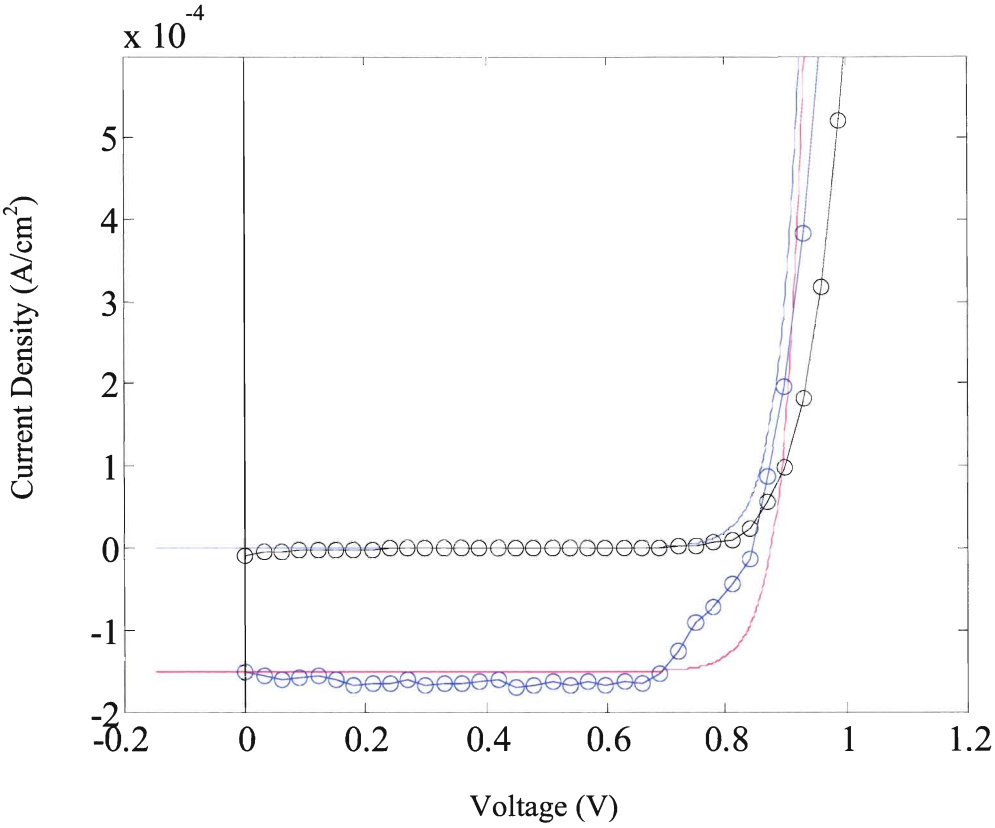

Figure 49 The comparison of experimental results and the modeling at R_{sh} = 10 MΩ. Blue circles: the experimental J-V curve data under the illumination of 80 mW/cm^2; black circle: experimental J-V data in the dark; Red line: J-V curve from modeling at R_{sh} = 10 MΩ in the light; Blue line: J-V curve from modeling at R_{sh} = 10 MΩ in the dark.

8.2.2 Influence of series resistance

The effect of series resistance on the device parameters is analyzed in this section and compared to our experimental results. To simplify the analysis, the shunt resistance is assumed to be infinity.

Figure 48 shows the effect of series resistance on open circuit voltage and fill factor as the shunt resistance is varied from 10 Ω to 10 kΩ. As can be seen, J_{SC} decreases as the series resistance increases. In addition, it can be seen that a high serial resistance

will influence the fill factor by shifting up the maximum power point (Figure 48). However, Figure 48 reveals that the open circuit voltage does not change with the series resistance, which means that the influence of R_s on open circuit voltage is typically negligible.

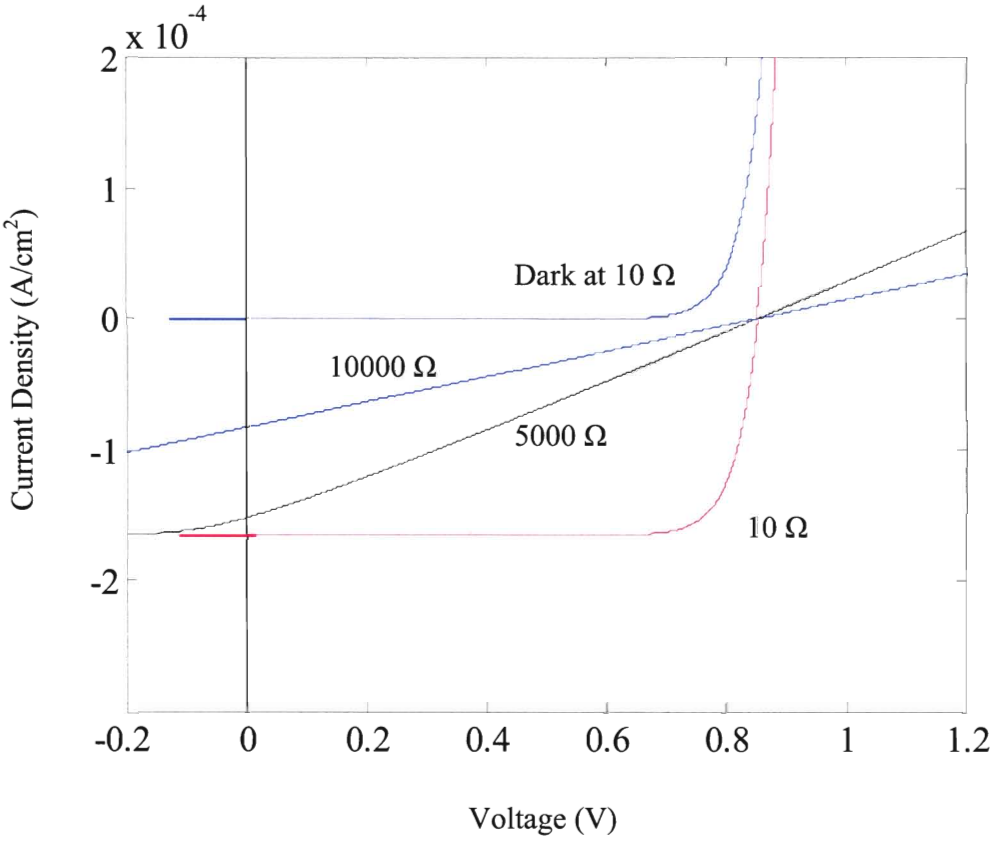

Figure 50 Effect of R_s on the J-V characteristics of a bilayer PTEBS/TiO2 solar cell when R_{sh} =+ ∞ and J_{ph} = 0.152 mA/cm^2

In Figure 49, the experimental J-V data from a bilayer device has been matched to the model. As can be seen, a series resistance value of R_s = 10 Ω provides a good fit to our data implying that this is close to the value of series resistance in our solar cells.

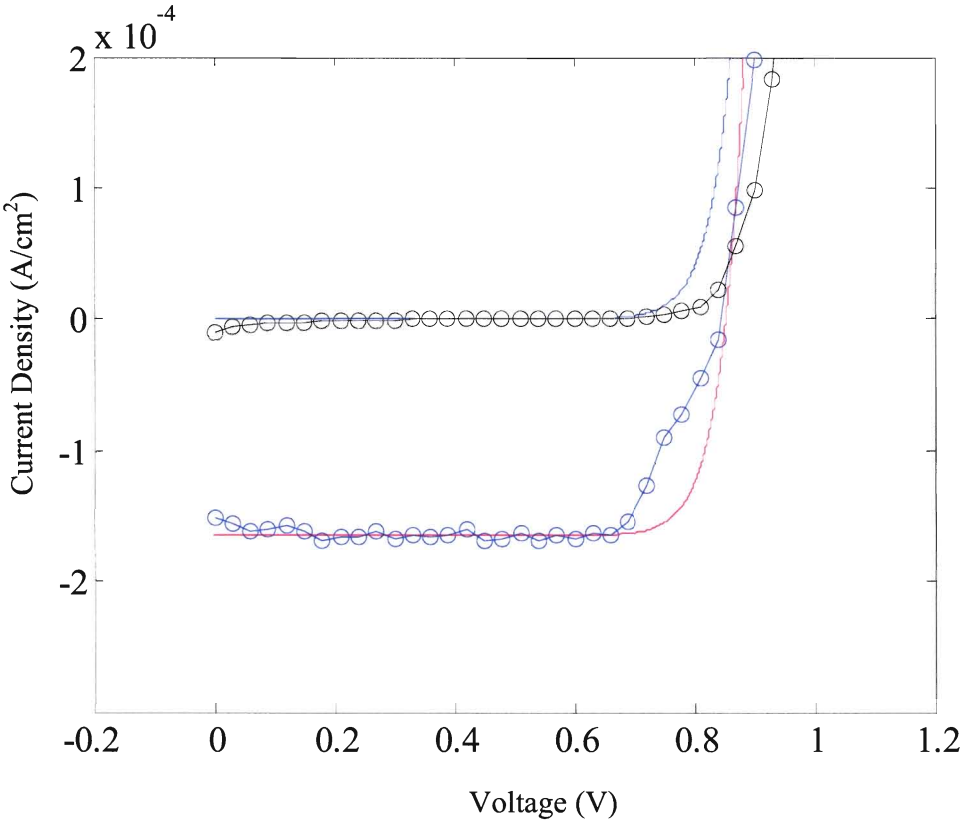

Figure 51 The comparison of experimental results and the modeling at R_s = 10 Ω. Green circle: the experimental J-V curve data under the illumination of 80 mW/cm^2; black circle: experimental J-V data in the dark; Red line: J-V curve from modeling at R_s = 10 Ω in the light; Blue line: J-V curve from modeling at R_{sh} = 10 Ω in the dark.

8.2.3 J-V characteristics of PTEBS/TiO_2 devices

From the two previous sections, it has been determined that for the bilayer structure PTEBS/TiO_2 devices, an R_s of around 10 Ω (assume R_{sh} = + ∞) and an R_{sh} of around 10 MΩ (assume R_s = 0 Ω) provide a good fit.

It has been observed that the blended PTEBS/TiO_2 devices produced lower fill factors than the devices based on the bilayer or hybrid of bilayer and bulk heterojunction. This may be due to the poor contact between the FTO substrates and PTEBS/TiO_2 films

and between the PTEBS/TiO_2 film and the gold electrode. All these bad contacts will increase the series resistance. In addition, the nanoparticle TiO_2 tends to accumulate during the drying process, leading to uneven distribution of TiO_2 in PTEBS film and consequently increase the possibility of recombination.

This is overcome, in part, by the implementation of the bilayer and bulk heterojunction hybrid. The TiO_2 makes an ohmic contact with the FTO and the polymer in the PTEBS/TiO_2 blend can make an ohmic contact to the gold. As demonstrated above, it results in a low series resistance and a high shunt resistance and subsequently very high fill factors. Further analysis would benefit from detailed numerical modeling.

Yoo et al.[152] has reported modeling of solar cell parameters with the following equations, which also supports what has been described above,

The dependences of FF on R_s and R_{sh} can be described as:

$$FF = FF_0\left(1-\frac{R_s}{V_{oc}/(J_{sc}A)}\right) \qquad (8.2)$$

$$FF = FF_0\left\{1-\frac{v_{oc}+0.72}{v_{oc}}\frac{FF_0}{R_{sh}/\left[V_{oc}/(J_{sc}A)\right]}\right\} \qquad (8.3)$$

Where $FF_0 = \frac{v_{oc}-\ln(v_{oc}+0.72)}{v_{oc}+1}$.

From the equation (8.2) describing the relationship between FF and R_s as shown above, we can conclude that FF decreases as R_s increases. In addition, in the equation (8.3), it can be derived that FF increases as R_{sh} increases.

Chapter 9 Conclusions and future studies

9.1 Conclusion

In this work, a green organic solar cell based on water-soluble PTEBS and nanocrystalline TiO_2 was studied. This is the first time that water-soluble polymer has been used for photovoltaics and the polymer offers many advantages. The polymer has a strong absorption band in the visible region and dissolving the polymer in acid yields another absorption peak opening the possibility for increased performance.

Because the polymer is water-soluble and TiO_2 is generally deposited from a water suspension, the two can be blended for simultaneous deposition. In addition, solvent evaporation rates have been shown to have an effect on morphology and the evaporation of water can be carefully controlled using heat.

Water is obviously non-toxic. This eliminates the need for expensive waste disposal and in turn lowers the cost of these devices. In the lab, it is not necessary to work with a fume hood or a glove box.

In this work, optical and semiconducting properties of PTEBS were initially explored. UV-Vis absorption revealed that PTEBS absorbs the light effectively in the visible part of solar spectrum with a peak at around 430 nm and an onset at 560 nm. The band gap of PTEBS was calculated as 2.2 eV. Electrochemical experiments showed that HOMO level of PTEBS was between –5.0 ~ -5.3 eV. With HOMO level and band gap, LUMO level was expected between –2.8 ~ -3.1 eV. TiO_2 was also characterized by UV-Vis absorption and SEM. The bottom electrode has also been studied in polymer/TiO2 solar cells. FTO showed better photovoltaic parameters than ITO in P3OT/TiO_2 devices.

Bilayer heterojunction PTEBS/TiO_2 solar cells were first developed. Devices were fabricated by doctor blading a layer of PTEBS onto a sintered TiO_2 nanocrystalline film. The concentration of PTEBS in water was 10 mg/ml. FTO and gold were used as bottom and top electrodes, respectively. The devices showed an open circuit voltage of 0.81 V, a short circuit current density of 0.35 mA/cm^2, a fill factor of 0.4, and an energy conversion efficiency of 0.13%. The water-soluble polythiophene showed significant photovoltaic behavior and the potential for use in solar cells.

Because doctor blading PTEBS on TiO_2 films is hard to control and it will remove part of the TiO_2 on the surface, a new fabrication method is needed. The concentration of PTEBS was increased to 15 mg/ml. The PTEBS films were fabricated by drop casting and a pipette was used to remove any extra solution. In addition, the thickness of TiO_2 was optimized. Fill factor and open circuit voltage were increased although the energy conversion efficiency was improved slightly.

In order to further improve the charge separation and transport, a bulk heterojunction PTEBS/TiO_2 solar cell was developed. The PTEBS was first dissolved in DI water and then nanoparticle TiO_2 powder was added and sonicated. Devices were made by drop casting the blended solution on a FTO substrate. The devices achieve an energy conversion efficiency of $\eta = 0.056\%$, a short circuit current of $J_{SC} = 0.16$ mA/cm^2, an open circuit voltage of $V_{OC} = 0.85$ V and a fill factor of $ff = 0.33$. The results were not promising. One of the reasons is that the water solution of PTEBS is not viscous enough to form a homogeneous film on a smooth FTO substrate. Therefore, a new bilayer and bulk heterojunction hybrid structure was investigated. The buffer layer provided a rough surface, which helped to form a uniform film. The initial layer of TiO_2

also acts as a hole blocking layer. An external energy conversion efficiency of 0.17% was achieved.

The open circuit voltage has been determined by the difference of the conductance band of TiO_2 and the work function of gold electrode. In addition, the equivalent circuit analysis has predicted the low series resistance and large shunt resistance for our bilayer cells and bilayer and bulk heterojunction hybrid cells. This results in high fill factors.

9.2 Future studies

In order to better understand the fundamental electronic transport physics in polymer films and polymer/metal oxide composite films, the hole mobility and the singlet exciton diffusion length need to be studied more carefully. Future experiments to measure these properties will be conducted. In addition, devices will be optimized to improve the performance.

9.2.1 Mobility measurements

Following exciton separation at the polymer/oxide (donor/acceptor) interface, the holes must move through the polymer to the cathode. This requires a high hole mobility in the polymer. Solvent based polythiophenes such as P3HT and P3OT have mobilities in the range of 0.01 - 0.001 cm^2-V^{-1}-s^{-1} [52] and it is expected that the mobility of the PTEBS will be of the same order of magnitude. Mobility measurements for PTEBS have not been previously reported. One of the future studies is to measure the hole mobility of the PTEBS polymer film.

The Hall effect is a commonly used technique to measure the mobilities of high mobility materials. But for low mobility materials such as polymers, it is very difficult to use the Hall effect for measurement[153]. Several techniques such as Time-of-flight (TOF) measurement[103, 154-161], field-effect transistor (FET) mesurement[162], space-charge-limited current (SCLC) [2] measurement and the pulse radiolysis time-resolved microwave conductivity (PR-TRMC)[163] technique are used to measure the charge motion in low mobility materials.

9.2.2 Exciton diffusion length measurement

When light is absorbed in the polymer, it generates an exciton. Generally, this exciton must migrate to the polymer/metal oxide (donor/acceptor) interface in order to separate into an electron-hole pair. If the distance to the interface is greater than the exciton diffusion length, the exciton will recombine and no current will be produced in the device. It is, therefore, important to measure the exciton diffusion length of these materials.

Photoluminescence is a technique that can be used to determine the exciton diffusion length in the polymer[103]. If the exciton generated in the polymer recombines before reaching the TiO_2, it will luminesce. It has been found that this luminescence varies approximately linearly with polymer thickness[103]. The polymer thickness at which complete quenching of the luminescence occurs can be used to estimate the exciton diffusion length. This length is typically 15-20 nm for conducting polymers and the value for PTEBS is expected to comparable.

9.2.3 Device optimization

9.2.3.1 Devices from basic solutions

Controlling or altering the PTEBS thickness will further optimize bilayer heterojunctions. At present time, the PTEBS layer was just drop cast and a pipette was used to remove any extra solution during the drying process. Therefore, it is hard to measure and control a consistent thickness. A new film making technique is still desired.

Some of future work will be done to improve the devices from the bilayer and bulk heterojunction hybrid. In the initial work, a nanoparticle TiO_2 with a average size of 30 nm was used to make the buffer layer and the film is 500 nm. As an alternative, a thinner buffer layer from a dense TiO_2 will be investigated.

9.2.3.2 Devices from acidic solutions

Bilayer, bulk heterojunction, and bilayer and bulk heterojuction hybrid devices from acidic solutions of PTEBS will also be made. In addition, a tandem structure including one of layer of basic solution and one layer of acidic solution will also be a direction for future work. As is discussed in Chapter 3, the films from acidic solutions have an absorption band in the red band of the solar spectrum. This acidic layer will help to increase the efficiency by absorbing the light in the red band.

List of References

List of References

1. James T. McLeskey, J., *Development of the femtosecond energy diffusion sensor for use in the manufacture of amorphous silicon solar cells.* Ph.D. dissertation, 2003.
2. Sun, S.-S. and N.S. Sariciftci, *Organic Photovoltaics: Mechanisms, Materials, and Devices.* 2005.
3. H. Shirakawa, A. G. MacDiarmid, and A.J. Heeger, in *J. Chem. Soc., Chem. Commun.* 1977. p. 578.
4. Beek, W.J.E., M.M. Wienk, and R.A.J. Janssen, *Efficient hybrid solar cells from zinc oxide nanoparticles and a conjugated polymer.* Advanced Materials, 2004. **16**(12): p. 1009-1013.
5. Baigent, D.R., et al., *Conjugated Polymer Light-Emitting-Diodes on Silicon Substrates.* Applied Physics Letters, 1994. **65**(21): p. 2636-2638.
6. Yu, G., K. Pakbaz, and A.J. Heeger, *Semiconducting Polymer Diodes - Large-Size, Low-Cost Photodetectors with Excellent Visible-Ultraviolet Sensitivity.* Applied Physics Letters, 1994. **64**(25): p. 3422-3424.
7. Sirringhaus, H., et al., *Mobility enhancement in conjugated polymer field-effect transistors through chain alignment in a liquid-crystalline phase.* Applied Physics Letters, 2000. **77**(3): p. 406-408.
8. Baraton, M.I., et al., *Investigation of the TiO2/PPV nanocomposite for gas sensing applications.* Nanotechnology, 1998. **9**(4): p. 356-359.
9. Kymakis, E. and G.A.J. Amaratunga, *Single-wall carbon nanotube/conjugated polymer photovoltaic devices.* Applied Physics Letters, 2002. **80**(1): p. 112-114.
10. Shaheen, S.E., et al., *Fabrication of bulk heterojunction plastic solar cells by screen printing.* Applied Physics Letters, 2001. **79**(18): p. 2996-2998.
11. Brabec, C.J., *Organic photovoltaics: technology and market.* Solar Energy Materials and Solar Cells, 2004. **83**(2-3): p. 273-292.
12. Greenham, N.C., X. Peng, and A.P. Alivisatos. *A CdSe nanocrystal/MEH-PPV polymer composite photovoltaics.* in *Proceedings of Future Generation Photovoltaic Technologies: First NREL Conference.* 1997.
13. Arango, A.C., S.A. Carter, and P.J. Brock, *Charge transfer in photovoltaics consisting of interpenetrating networks of conjugated polymer and TiO2 nanoparticles.* Applied Physics Letters, 1999. **74**(12): p. 1698-1700.
14. Qiao, Q., et al., *Characteristics of Water Souble Polythiophene:TiO(2) Composite and its Application in Photovoltaics.* J. Appl. Phys., 2005. **98**(10): p. 094906.
15. Qiao, Q., J. Beck, and J. James T. McLeskey. *Photovoltaic devices from self-doped polymers.* in *Organic Photovoltaics VI.* 2005: SPIE.
16. Qiao, Q., et al., *Optimization of Photovoltaic Devices from Layered PTEBS and Nanocrystalline TiO[sub 2].* ECS Transactions, 2006. **1**(33): p. 1-6.
17. Qiao, Q., et al., *A comparison of fluorine tin oxide and indium tin oxide as the transparent electrode for P3OT/TiO2 solar cells.* Solar Energy Materials and Solar Cells, 2006. **90**(7-8): p. 1034-1040.
18. Qiao, Q. and J.T. McLeskey, *Water-soluble polythiophene/nanocrystalline TiO[sub 2] solar cells.* Applied Physics Letters, 2005. **86**(15): p. 153501.
19. Huynh, W.U., J.J. Dittmer, and A.P. Alivisatos, *Hybrid Nanorod-Polymer Solar Cells.* Science, 2002. **295**: p. 2425-2427.

20. Breeze, A.J., et al., *Charge transport in TiO2/MEH-PPV polymer photovoltaics.* Physical Review B, 2001. **6412**(12): p. art. no.-125205.
21. Kwong, C.Y., et al., *Influence of solvent on film morphology and device performance of poly(3-hexylthiophene):TiO2 nanocomposite solar cells.* Chemical Physics Letters, 2004. **384**(4-6): p. 372-375.
22. van Hal, P.A., et al., *Photoinduced electron transfer and photovoltaic response of a MDMO-PPV : TiO2 bulk-heterojunction.* Advanced Materials, 2003. **15**(2): p. 118-121.
23. *http://solardat.uoregon.edu/SolarRadiationBasics.html.*
24. Malliaras, G.G., et al., *Photovoltaic measurement of the built-in potential in organic light emitting diodes and photodiodes.* Journal of Applied Physics, 1998. **84**(3): p. 1583-1587.
25. Alam, M.M. and S.A. Jenekhe, *Efficient solar cells from layered nanostructures of donor and acceptor conjugated polymers.* Chemistry of Materials, 2004. **16**(23): p. 4647-4656.
26. Drees, M., *Polymer/fullerene photovoltaic devices - nanoscale control of interface by thermally - controlled interdiffusion.* Ph.D. dissertation, 2003.
27. Jenekhe, S.A. and S.J. Yi, *Efficient photovoltaic cells from semiconducting polymer heterojunctions.* Applied Physics Letters, 2000. **77**(17): p. 2635-2637.
28. Yu, G. and A.J. Heeger, *Charge Separation and Photovoltaic Conversion in Polymer Composites with Internal Donor-Acceptor Heterojunctions.* Journal of Applied Physics, 1995. **78**(7): p. 4510-4515.
29. Breeze, A.J., et al., *Charge transport in TiO[sub 2]/MEH-PPV polymer photovoltaics.* Physical Review B (Condensed Matter and Materials Physics), 2001. **64**(12): p. 125205.
30. Becker, H., et al., *PL and EL quenching due to thin metal films in conjugated polymers and polymer LEDs.* Synthetic Metals, 1997. **85**(1-3): p. 1289-1290.
31. Martens, T., et al., *Disclosure of the nanostructure of MDMO-PPV:PCBM bulk hetero-junction organic solar cells by a combination of SPM and TEM.* Synthetic Metals, 2003. **138**(1-2): p. 243-247.
32. Bettignies, R.d., et al. *Study of P3HT:PCBM bulk heterojunction solar cells: influence of components ratio and of the nature of electrodes on performances and lifetime.* in *Organic Photovoltaics VI.* 2005: SPIE.
33. Tan, S.X., et al., *Property influence of polyanilines on photovoltaic behaviors of dye-sensitized solar cells.* Langmuir, 2004. **20**(7): p. 2934-2937.
34. Wallace, G.G., et al., *Conjugated polymers: new materials for photovoltaics.* Chemical Innovation, 2000. **30**(1): p. 14.
35. Wang, X.J., et al., *Infrared photocurrent spectral response from plastic solar cell with low-band-gap polyfluorene and fullerene derivative.* Applied Physics Letters, 2004. **85**(21): p. 5081-5083.
36. Campos, L.M., et al., *Extended photocurrent spectrum of a low band gap polymer in a bulk heterojunction solar cell.* Chemistry of Materials, 2005. **17**(16): p. 4031-4033.
37. Sharma, G.D., S.G. Sangodkar, and M.S. Roy, *Study on electrical and photoelectrical behaviour of undoped and doped furazano[3,4-b]piperazine (FP) thin-film devices.* Synthetic Metals, 1995. **75**(3): p. 201-207.

38. Brabec, C.J., et al., *A low-bandgap semiconducting polymer for photovoltaic devices and infrared emitting diodes.* Advanced Functional Materials, 2002. **12**(10): p. 709-712.
39. Wienk, M.M., et al., *Low-band gap poly(di-2-thienylthienopyrazine): fullerene solar cells.* Applied Physics Letters, 2006. **88**(15).
40. Wang, X.J., et al., *Enhanced photocurrent spectral response in low-bandgap polyfluorene and C-70-derivative-based solar cells.* Advanced Functional Materials, 2005. **15**(10): p. 1665-1670.
41. Zhang, F.L., et al., *Polymer solar cells based on a low-bandgap fluorene copolymer and a fullerene derivative with photocurrent extended to 850 nm.* Advanced Functional Materials, 2005. **15**(5): p. 745-750.
42. Kymakis, E., I. Alexandrou, and G.A.J. Amaratunga, *High open-circuit voltage photovoltaic devices from carbon-nanotube-polymer composites.* Journal of Applied Physics, 2003. **93**(3): p. 1764-1768.
43. Brabec, C.J., et al., *Organic Photovoltaics: Concepts and Realization.* Springer Series in Materials Science, ed. R. Hull, R.M.J. Osgood, and J. Parisi. Vol. 60. 2003, New York: Springer-Verlag.
44. Kwong, C.Y., et al., *Poly(3-hexylthiophene): TiO2 nanocomposites for solar cell applications.* Nanotechnology, 2004. **15**(9): p. 1156-1161.
45. Dhanabalan, A., et al., *Synthesis and characterization of a low bandgap conjugated polymer for bulk heterojunction photovoltaic cells.* Advanced Functional Materials, 2001. **11**(4): p. 255-262.
46. Wienk, M.M., M.P. Struijk, and R.A.J. Janssen, *Low band gap polymer bulk heterojunction solar cells.* Chemical Physics Letters, 2006. **422**(4-6): p. 488-491.
47. Chandross, M., et al., *Excitons in Poly(Para-Phenylenevinylene).* Physical Review B, 1994. **50**(19): p. 14702-14705.
48. Marks, R.N., et al., *The Photovoltaic Response in Poly(P-Phenylene Vinylene) Thin-Film Devices.* Journal of Physics-Condensed Matter, 1994. **6**(7): p. 1379-1394.
49. Lee, C.H., et al., *Picosecond Transient Photoconductivity in Poly(P-Phenylenevinylene).* Physical Review B, 1994. **49**(4): p. 2396-2407.
50. Marks, R.N., et al., *The Photovoltaic Response in Poly(P-Phenylene Vinylene) Thin-Film Devices*, in *Journal of Physics-Condensed Matter*. 1994. p. 1379-1394.
51. Barth, S. and H. Bassler, *Intrinsic photoconduction in PPV-type conjugated polymers.* Physical Review Letters, 1997. **79**(22): p. 4445-4448.
52. Zen, A., et al., *Comparative study of the field-effect mobility of a copolymer and a binary blend based on poly(3-alkylthiophene)s.* Chemistry of Materials, 2005. **17**(4): p. 781-786.
53. Dennler, G., et al., *A new encapsulation solution for flexible organic solar cells.* Thin Solid Films, 2006. **511**: p. 349-353.
54. Too, C.O., et al., *Photovoltaic devices based on polythiophenes and substituted polythiophenes.* Synthetic Metals, 2001. **123**(1): p. 53-60.
55. Janietz, S., S. Anlauf, and A. Wedel, *New n-type rigid rod full aromatic poly(l,3,4-oxadiazole)s and their application in organic devices.* Synthetic Metals, 2001. **122**(1): p. 11-14.

56. Huang, W., et al., *A novel series of p-n diblock light-emitting copolymers based on oligothiophenes and 1,4-bis(oxadiazolyl)-2,5-dialkyloxybenzene.* Macromolecules, 1999. **32**(1): p. 118-126.
57. Weinberger, B.R., M. Akhtar, and S.C. Gau, *Polyacetylene Photo-Voltaic Devices.* Synthetic Metals, 1982. **4**(3): p. 187-197.
58. Glenis, S., et al., *Electrochemically grown polythiophene and poly(3-methylthiophene) organic photovoltaic cells.* Thin Solid Films, 1984. **111**(2): p. 93-103.
59. Markvart, T. and L. Castaner, *Practical Handbook of Photovoltaics: Fundamentals and Applications*. 2003: Elsevier Advanced Technology.
60. Theander, M., et al., *Photoluminescence quenching at a polythiophene/C-60 heterojunction.* Physical Review B, 2000. **61**(19): p. 12957-12963.
61. Arango, A.C., et al., *Efficient titanium oxide/conjugated polymer photovoltaics for solar energy conversion.* Advanced Materials, 2000. **12**(22): p. 1689-1692.
62. Choong, V., et al., *Dramatic photoluminescence quenching of phenylene vinylene oligomer thin films upon submonolayer Ca deposition.* Applied Physics Letters, 1996. **69**(10): p. 1492-1494.
63. Tang, C.W., *Two-layer organic photovoltaic cell.* Applied Physics Letters, 1986. **48**(2): p. 183-185.
64. Granstrom, M., et al., *Laminated fabrication of polymeric photovoltaic diodes*, in *Nature*. 1998. p. 257-260.
65. Breeze, A.J., et al., *Charge transport in TiO[sub 2]/MEH-PPV polymer photovoltaics*, in *Physical Review B (Condensed Matter and Materials Physics)*. 2001, APS. p. 125205.
66. Kwong, C.Y., et al., *Influence of solvent on film morphology and device performance of poly(3-hexylthiophene):TiO2 nanocomposite solar cells*, in *Chemical Physics Letters*. 2004. p. 372-375.
67. Arango, A.C., S.A. Carter, and P.J. Brock, *Charge transfer in photovoltaics consisting of interpenetrating networks of conjugated polymer and TiO2 nanoparticles*, in *Applied Physics Letters*. 1999. p. 1698-1700.
68. Oregan, B. and M. Gratzel, *A Low-Cost, High-Efficiency Solar-Cell Based on Dye-Sensitized Colloidal Tio2 Films.* Nature, 1991. **353**(6346): p. 737-740.
69. Huynh, W.U., X.G. Peng, and A.P. Alivisatos, *CdSe nanocrystal rods/poly(3-hexylthiophene) composite photovoltaic devices.* Advanced Materials, 1999. **11**(11): p. 923-927.
70. Kymakis, E. and G.A.J. Amaratunga, *Photovoltaic cells based on dye-sensitisation of single-wall carbon nanotubes in a polymer matrix.* Solar Energy Materials and Solar Cells, 2003. **80**(4): p. 465-472.
71. Lee, S.B., et al., *Electrical and optical properties of conducting plymer-C60-carbon nanotube system.* Synthetic Metals, 2001. **121**: p. 1591-1592.
72. Ago, H., et al., *Composites of carbon nanotubes and conjugated polymers for photovoltaic devices.* Advanced Materials, 1999. **11**(15): p. 1281-1285.
73. Piok, T., et al., *Photocarrier generation quantum yield for ionically self-assembled monolayers.* Synthetic Metals, 2001. **121**: p. 1589-1590.
74. Yu, G., et al., *Polymer Photovoltaic Cells - Enhanced Efficiencies Via a Network of Internal Donor-Acceptor Heterojunctions.* Science, 1995. **270**(5243): p. 1789-1791.

75. Sariciftci, N.S., et al., *Semiconducting polymer-buckminsterfullerene heterojunctions: Diodes, photodiodes, and photovoltaic cells.* Applied Physics Letters, 1993. **62**(6): p. 585-587.
76. Petritsch, K., et al., *Dye-based donor/acceptor solar cells.* Solar Energy Materials and Solar Cells, 2000. **61**(1): p. 63-72.
77. Cyr, P.W., et al., *Quantum dots in a metallopolymer host: studies of composites of polyferrocenes and CdSe nanocrystals.* Journal of Materials Chemistry, 2003. **13**(9): p. 2213-2219.
78. Halls, J.J.M., et al., *Efficient Photodiodes from Interpenetrating Polymer Networks.* Nature, 1995. **376**(6540): p. 498-500.
79. Huynh, W.U., et al., *Charge transport in hybrid nanorod-polymer composite photovoltaic cells.* Physical Review B, 2003. **67**(11).
80. Rud, J.A., et al., *Water soluble polymer/carbon nanotube bulk heterojunction solar cells.* Journal of Materials Science, 2005. **40**(6): p. 1455-1458.
81. Lee, k., et al., *New architecture for thermally stable high efficiency polymer solar cells*, in *Proceedings of SPIE - The International Society for Optical Engineering.* 2005. p. 59380B.
82. Ma, W.L., et al., *Thermally stable, efficient polymer solar cells with nanoscale control of the interpenetrating network morphology.* Advanced Functional Materials, 2005. **15**(10): p. 1617-1622.
83. Beek, W.J.E., et al. *Hybrid ZnO:polymer bulk heterojunction solar cells from a ZnO precursor.* in *Organic Photovoltaics VI.* 2005: SPIE.
84. Beek, W.J.E., M.M. Wienk, and R.A.J. Janssen. *Hybrid bulk heterojunction solar cells: blends of ZnO semiconducting nanoparticles and conjugated polymers.* in *Organic Photovoltaics VI.* 2005: SPIE.
85. Aernouts, T., et al., *Extraction of bulk and contact components of the series resistance in organic bulk donor-acceptor-heterojunctions.* Thin Solid Films, 2002. **403-404**: p. 297-301.
86. Konkin, A.L., et al., *LESR study on PPV-PPE/PCBM composites for organic photovoltaics.* Synthetic Metals. **In Press, Corrected Proof**.
87. Krebs, F.C., et al., *Lifetimes of organic photovoltaics: photochemistry, atmosphere effects and barrier layers in ITO-MEHPPV:PCBM-aluminium devices.* Solar Energy Materials and Solar Cells. **In Press, Corrected Proof**.
88. Melzer, C., et al., *Hole transport in poly(phenylene vinylene)/methanofullerene bulk-heterojunction solar cells.* Advanced Functional Materials, 2004. **14**(9): p. 865-870.
89. Mihailetchi, V.D., et al., *Electron transport in a methanofullerene.* Advanced Functional Materials, 2003. **13**(1): p. 43-46.
90. Munters, T., et al., *A comparison between state-of-the-art 'gilch' and 'sulphinyl' synthesised MDMO-PPV/PCBM bulk hetero-junction solar cells.* Thin Solid Films, 2002. **403-404**: p. 247-251.
91. Nelson, J., S.A. Choulis, and J.R. Durrant, *Charge recombination in polymer/fullerene photovoltaic devices.* Thin Solid Films, 2004. **451-452**: p. 508-514.
92. Riedel, I., et al., *Effect of temperature and illumination on the electrical characteristics of polymer-fullerene bulk-heterojunction solar cells.* Advanced Functional Materials, 2004. **14**(1): p. 38-44.

93. Sahin, Y., et al., *Development of air stable polymer solar cells using an inverted gold on top anode structure.* Thin Solid Films. **In Press, Corrected Proof.**
94. Svensson, M., et al., *High-performance polymer solar cells of an alternating polyfluorene copolymer and a fullerene derivative.* Advanced Materials, 2003. **15**(12): p. 988-991.
95. van Duren, J.K.J., et al., *In-situ compositional and structural analysis of plastic solar cells.* Advanced Functional Materials, 2002. **12**(10): p. 665-669.
96. van Duren, J.K.J., et al., *Relating the morphology of poly(p-phenylene vinylene)/methanofullerene blends to solar-cell performance.* Advanced Functional Materials, 2004. **14**(5): p. 425-434.
97. Zhokhavets, U., et al., *Anisotropic optical properties of conjugated polymer and polymer/fullerene films.* Thin Solid Films, 2003. **444**(1-2): p. 215-220.
98. Peiro, A.M., et al. *The effect of zinc oxide nanostructure on the performance of hybrid polymer/zinc oxide solar cells.* in *Organic Photovoltaics VI.* 2005: SPIE.
99. Ohsawa, Y. and T. Saji, *Electrochemical Detection of C60(6-) at Low-Temperature.* Journal of the Chemical Society-Chemical Communications, 1992(10): p. 781-782.
100. Gratzel, M., *Photoelectrochemical cells.* Nature, 2001. **414**(6861): p. 338-344.
101. Greenham, N.C., X. Peng, and A.P. Alivisatos, *Charge separation and transport in conjugated polymer/cadmium selenide nanocrystal composites studied by photoluminescence quenching and photoconductivity.* Synthetic Metals, 1997. **84**(1-3): p. 545-546.
102. Gur, I., et al., *Air-stable all-inorganic nanocrystal solar cells processed from solution.* Science, 2005. **310**(5747): p. 462-465.
103. Ravirajan, P., et al., *The effect of polymer optoelectronic properties on the performance of multilayer hybrid polymer/TiO2 solar cells.* Advanced Functional Materials, 2005. **15**(4): p. 609-618.
104. Salafsky, J.S., W.H. Lubberhuizen, and R.E.I. Schropp, *Photoinduced charge separation and recombination in a conjugated polymer-semiconductor nanocrystal composite.* Chemical Physics Letters, 1998. **290**(4-6): p. 297-303.
105. Salafsky, J.S., *Exciton dissociation, charge transport, and recombination in ultrathin, conjugated polymer-TiO2 nanocrystal intermixed composites.* Physical Review B, 1999. **59**(16): p. 10885-10894.
106. Coakley, K.M., et al., *Infiltrating semiconducting polymers into self-assembled mesoporous titania films for photovoltaic applications.* Advanced Functional Materials, 2003. **13**(4): p. 301-306.
107. Huisman, C.L., A. Goossens, and J. Schoonman, *Aerosol synthesis of anatase titanium dioxide nanoparticles for hybrid solar cells.* Chemistry of Materials, 2003. **15**(24): p. 4617-4624.
108. Huisman, C.L., A. Goossens, and J. Schoonman, *Preparation of a nanostructured composite of titanium dioxide and polythiophene: a new route towards 3D heterojunction solar cells.* Synthetic Metals, 2003. **138**(1-2): p. 237-241.
109. Fan, Q., et al., *A solid state solar cell using sol-gel processed material and a polymer.* Chemical Physics Letters, 2001. **347**(4-6): p. 325-330.
110. Ravirajan, P., et al., *Hybrid nanocrystalline TiO2 solar cells with a fluorene-thiophene copolymer as a sensitizer and hole conductor.* Journal of Applied Physics, 2004. **95**(3): p. 1473-1480.

111. Liu, Y., K.M. Coakley, and M.D. McGehee. *Electropolymerization of conjugated polymers in mesoporous titania for photovoltaic applications.* in *Organic Photovoltaics IV.* 2004: SPIE.
112. Grant, C.D., et al., *Characterization of nanocrystalline and thin film TiO2 solar cells with poly(3-undecyl-2,2 '-bithiophene) as a sensitizer and hold conductor.* Journal of Electroanalytical Chemistry, 2002. **522**(1): p. 40-48.
113. http://www.nanosolar.com/technology.htm.
114. http://www.konarka.com/technology/.
115. Patil, A.O., et al., *Water-Soluble Conducting Polymers.* Journal of the American Chemical Society, 1987. **109**(6): p. 1858-1859.
116. Tran-Van, F., M. Carrier, and C. Chevrot, *Sulfonated polythiophene and poly (3,4-ethylenedioxythiophene) derivatives with cations exchange properties.* Synthetic Metals, 2004. **142**(1-3): p. 251-258.
117. American Dye Source, *Water Soluble Thiophene Polymer,* in *http://www.adsdyes.com/products/pdf/polythiophene/ADS2000P.pdf.* 2002.
118. *Private Communication, Mai Nguyen, American Dye Source.* 2005.
119. Ouyang, J., et al., *On the mechanism of conductivity enhancement in poly(3,4-ethylenedioxythiophene):poly(styrene sulfonate) film through solvent treatment.* Polymer, 2004. **45**(25): p. 8443-8450.
120. Shi, Y., J. Liu, and Y. Yang, *Device performance and polymer morphology in polymer light emitting diodes: The control of thin film morphology and device quantum efficiency.* Journal of Applied Physics, 2000. **87**(9): p. 4254-4263.
121. Patil, A.O., et al., *Self-doped conducting polymers.* Synthetic Metals, 1987. **20**(2): p. 151-159.
122. Ikenoue, Y., et al., *Evaluation of electrochromic fast-switching behavior of self-doped conducting polymer.* Synthetic Metals, 1991. **40**(3): p. 333-340.
123. Patil, A.O., et al., *Water-soluble conducting polymers.* J. Am. Chem. Soc., 1987. **109**: p. 1858 - 1859.
124. Ikenoue, Y., et al., *Electrochemical studies of self-doped conducting polymers: Verification of the 'cation-popping' doping mechanism.* Synthetic Metals, 1989. **30**(3): p. 305-319.
125. http://ruby.colorado.edu/~smyth/min/tio2.html.
126. Longo, C. and M.A. De Paoli, *Dye-sensitized solar cells: A successful combination of materials.* Journal of the Brazilian Chemical Society, 2003. **14**(6): p. 889-901.
127. http://origin.ch.ic.ac.uk/durrant/nanofilms.htm.
128. Hengerer, R., et al., *Structure and stability of the anatase TiO2 (101) and (001) surfaces.* Surface Science, 2000. **460**(1-3): p. 162-169.
129. Krebs, F.C., et al. *Large area polymer solar cells.* in *Organic Photovoltaics VI.* 2005: SPIE.
130. Wong, H.L., et al., *Low-band-gap, sublimable rhenium(I) diimine complex for efficient bulk heterojunction photovoltaic devices.* Applied Physics Letters, 2004. **84**(14): p. 2557-2559.
131. Drees, M., et al., *Creation of a gradient polymer-fullerene interface in photovoltaic devices by thermally controlled interdiffusion.* Applied Physics Letters, 2002. **81**(24): p. 4607-4609.

132. Park, Y., et al., *Work function of indium tin oxide transparent conductor measured by photoelectron spectroscopy.* Applied Physics Letters, 1996. **68**(19): p. 2699-2701.
133. Kim, J.S., et al., *Indium-tin oxide treatments for single- and double-layer polymeric light-emitting diodes: The relation between the anode physical, chemical, and morphological properties and the device performance.* Journal of Applied Physics, 1998. **84**(12): p. 6859-6870.
134. Fang, G.J., D.J. Li, and B.L. Yao, *Magnetron-sputtered AZO thin films on commercial ITO glass for application of a very low resistance transparent electrode.* Journal of Physics D-Applied Physics, 2002. **35**(23): p. 3096-3100.
135. Kim, J.S., R.H. Friend, and F. Cacialli, *Improved operational stability of polyfluorene-based organic light-emitting diodes with plasma-treated indium-tin-oxide anodes.* Applied Physics Letters, 1999. **74**(21): p. 3084-3086.
136. Milliron, D.J., et al., *Surface oxidation activates indium tin oxide for hole injection.* Journal of Applied Physics, 2000. **87**(1): p. 572-576.
137. Nuesch, F., et al., *A photoelectron spectroscopy study on the indium tin oxide treatment by acids and bases.* Applied Physics Letters, 1999. **74**(6): p. 880-882.
138. Djurisic, A.B., et al., *Indium--tin--oxide surface treatments: Influence on the performance of CuPc/C[sub 60] solar cells.* Journal of Applied Physics, 2003. **93**(9): p. 5472-5479.
139. Bashar, S.A., *Study of indium tin oxide (ITO) for novel optoelectronic devices.* Ph.D. dissertation, 1998.
140. Andersson, A., et al., *Fluorine tin oxide as an alternative to indium tin oxide in polymer LEDs.* Advanced Materials, 1998. **10**(11): p. 859-+.
141. Smestad, G., C. Bignozzi, and R. Argazzi, *Testing of Dye-Sensitized Tio2 Solar-Cells .1. Experimental Photocurrent Output and Conversion Efficiencies.* Solar Energy Materials and Solar Cells, 1994. **32**(3): p. 259-272.
142. Cui, J., et al., *Indium tin oxide alternatives - High work function transparent conducting oxides as anodes for organic light-emitting diodes.* Advanced Materials, 2001. **13**(19): p. 1476-+.
143. Brabec, C.J., N.S. Sariciftci, and J.C. Hummelen, *Plastic solar cells.* Advanced Functional Materials, 2001. **11**(1): p. 15-26.
144. Brabec, C.J., et al., *Effect of LiF/metal electrodes on the performance of plastic solar cells.* Applied Physics Letters, 2002. **80**(7): p. 1288-1290.
145. Winder, C., *Sensitization of low bandgap polymer bulk heterojunction solar cells.* Ph.D. dissertation, 2001.
146. Strawhecker, K.E., et al., *The Critical Role of Solvent Evaporation on the Roughness of Spin-Cast Polymer Films.* Macromolecules, 2001. **34**(14): p. 4669-4672.
147. Nozik, A.J., *Quantum Dot Solar Cells.* Physica E, 2002. **14**: p. 115-120.
148. Raffaelle, R.P., et al., *Quantum Dot Solar Cells.* Progress in Photovoltaics: Research and Applications, 2002. **10**: p. 433-439.
149. Blatchford, J.W., et al., *Photoluminescence in pyridine-based polymers: Role of aggregates.* Physical Review B, 1996. **54**(13): p. 9180-9189.
150. Brabec, C.J., et al., *Origin of the Open Circuit Voltage of Plastic Solar Cells.* Advanced Functional Materials, 2001. **11**(5): p. 374-380.
151. Andersson, A., et al., *Fluorine tin oxide as an alternative to indium tin oxide in polymer LEDs.* Advanced Materials, 1998. **10**(11): p. 859-863.

152. Yoo, S., et al. *Modeling of organic photovoltaic cells with large fill factor and high efficiency*. in *Organic Photovoltaics V*. 2004: SPIE.
153. Goodman, A.M., *Electron Hall Effect in Silicon Dioxide.* Physical Review, 1967. **164**(3): p. 1145-&.
154. Choulis, S.A., et al., *Investigation of transport properties in polymer/fullerene blends using time-of-flight photocurrent measurements.* Applied Physics Letters, 2003. **83**(18): p. 3812-3814.
155. Nagase, T. and H. Naito, *Localized-state distributions in molecularly doped polymers determined from time-of-flight transient photocurrent.* Journal of Applied Physics, 2000. **88**(1): p. 252-259.
156. Tseng, H.E., et al., *Measurements of charge mobility and diffusion coefficient of conjugated electroluminescent polymers by time-of-flight method.* Applied Physics Letters, 2004. **84**(9): p. 1456-1458.
157. Chatten, A.J., et al., *Monte Carlo modelling of hole transport in MDMO-PPV: PCBM blends.* Journal of Materials Science, 2005. **40**(6): p. 1393-1398.
158. Pandey, S.S., et al., *Photocarrier transport in regioregular poly(3-octadecylthiophene).* Japanese Journal of Applied Physics Part 1-Regular Papers Short Notes & Review Papers, 2001. **40**(9A): p. 5350-5356.
159. Kaneto, K., S.S. Pandey, and W. Takashima, *Photocarrier transport in nonuniform field based on schottky cell for the time of flight measurement in poly(3-alkylthiopehene) films.* Japanese Journal of Applied Physics Part 1-Regular Papers Short Notes & Review Papers, 2001. **40**(8): p. 4933-4937.
160. Pandey, S.S., et al., *Poly(3-butylthiophene): conjugated polymer with record high TOF mobility.* Synthetic Metals, 2001. **121**(1-3): p. 1561-1562.
161. Pandey, S.S., W. Takashima, and K. Kaneto, *Photocarrier mobility in poly(2-methoxyaniline).* Journal of Applied Polymer Science, 2001. **79**(8): p. 1506-1512.
162. Dimitrakopoulos, C.D. and P.R.L. Malenfant, *Organic thin film transistors for large area electronics.* Advanced Materials, 2002. **14**(2): p. 99-117.
163. Hoofman, R., et al., *Highly mobile electrons and holes on isolated chains of the semiconducting polymer poly(phenylenevinylene).* Nature, 1998. **392**(6671): p. 54-56.

VITA

Qiquan Qiao was born on November 18, 1975 in Anhui, China. In 1999, he received his Bachelor of Engineering from Hefei University of Technology, China. He joined Shanghai Institute of Optics and Fine Mechanics and worked as an optical engineer till 2000. He then enrolled as a graduate student in the same institute and got his Master degree in 2003. He started as a Ph.D. student at Virginia Commonwealth University from August 2003 and obtained his Doctor degree in 2006. He was selected as the recipient of the ASME Solar Energy Division Graduate Student Award in recognition of his excellent academic achievements and research on developing "green" solar PV cells in July 2006.